BOLT BERANEK AND NEWMAN INC

CONSULTING • DEVELOPMENT • RESEARCH

NASA CR-112166

A STUDY OF THE VARIABLE IMPEDANCE SURFACE CONCEPT AS A MEANS FOR REDUCING NOISE FROM JET INTERACTION WITH DEVELOPED LIFT-AUGMENTING FLAPS

Richard E. Hayden
Yoram Kadman
Robert C. Chanaud

Prepared under Contract No. NAS1-9559-18 by

Bolt Beranek and Newman Inc.
50 Moulton Street
Cambridge, Massachusetts 02138

for

NATIONAL AERONAUTICS AND SPACE ADMINISTRATION
Langley Research Center
Hampton, Virginia

NASA CR-112166

A STUDY OF THE VARIABLE IMPEDANCE SURFACE CONCEPT AS A MEANS FOR REDUCING NOISE FROM JET INTERACTION WITH DEPLOYED LIFT-AUGMENTING FLAPS

Richard E. Hayden
Yoram Kadman
Robert C. Chanaud

Prepared under Contract No. NAS1-9559-18 by

Bolt Beranek and Newman Inc.
50 Moulton Street
Cambridge, Massachusetts 02138

for

NATIONAL AERONAUTICS AND SPACE ADMINISTRATION
Langley Research Center
Hampton, Virginia

FOREWORD

The work presented in this report was performed by Bolt Beranek and Newman Inc., Cambridge, Massachusetts, under Contract No. NAS1-9559-18 and administered by the Acoustics Branch, Loads Division, NASA Langley Research Center, Hampton, Virginia. The work was performed between 1 March 1972 and 15 July 1972.

The authors gratefully acknowledge the contributions of their colleagues Anthony Clemente, Russell Leland, Claude Noiseux, John Stanley, and Elaine Ward to various stages of the project. The assistance of Mr. James Hassell of NASA Langley Research Center in test configuration selection is also gratefully acknowledged.

This report has been assigned Bolt Beranek and Newman Inc. Report No. 2399.

ABSTRACT

The feasibility of quieting the externally-blown-flap (EBF) noise sources which are due to interaction of jet exhaust flow with deployed flaps was demonstrated on a 1/15-scale 3-flap EBF model. Sound field characteristics were measured and noise reduction fundamentals were reviewed in terms of source models.

Tests of the 1/15-scale model showed broadband noise reductions of up to 20 dB resulting from combination of variable impedance flap treatment and mesh grids placed in the jet flow upstream of the flaps. Steady-state lift, drag, and pitching moment were measured with and without noise reduction treatment.

TABLE OF CONTENTS

LIST OF FIGURES AND TABLES

LIST OF FIGURES AND TABLES (Cont.)

LIST OF FIGURES AND TABLES (Cont.)

LIST OF FIGURES AND TABLES (Cont.)

LIST OF FIGURES AND TABLES (Cont.)

LIST OF SYMBOLS

a	characteristic radius of a source
A	area
c	isentropic sound speed
C	chord length, or aerodynamic coefficient when subscripted
D	diameter, or drag force
f	frequency (hertz)
F	force
k	wavenumber
ℓ	length scale of an eddy
m or n	number of sources
p	pressure
q	dynamic pressure ($=1/2\ \rho U^2$)
r	generalized radial distance
SPL	sound pressure level (dB re 0.0002 μbar)
u	fluctuating (turbulent) component of velocity
U	mean flow velocity
v	fluctuating (turbulent) component of velocity normal to mean flow direction
W	Span

Greek symbols:

Γ	normalized sound pressure level
η	descriptor of the variation of an aerodynamic parameter with distance from an origin
θ	spherical angle

LIST OF SYMBOLS (Cont.)

λ	acoustic wavelength
Π	sound power
ρ	density of ambient fluid medium
Φ	spectral density
ψ	angle from a reference plane
ω	radian (circular) frequency

Subscripts:

A	aerodynamic
c	convection, or characteristic
D	dipole
I	r.m.s. turbulence intensity, $\sqrt{\overline{(u'/U)^2}}$ or $\sqrt{\overline{(v'/U)^2}}$
LE	leading edge
m	mean
0	of origin, or ambient
p	pressure
ref	reference pressure
ss	steady state
w	wall, or surface
x	pertaining to x-direction
y	pertaining to y-direction

Superscript:

$( )'$	fluctuating (time variant) quantity

A STUDY OF THE VARIABLE IMPEDANCE SURFACE CONCEPT AS A MEANS FOR REDUCING NOISE FROM JET INTERACTION WITH DEPLOYED LIFT-AUGMENTING FLAPS

by Richard E. Hayden
Yoram Kadman
Robert C. Chanaud

Bolt Beranek and Newman Inc.

SUMMARY

A critical unresolved problem associated with the externally-blown-flap (EBF) jet-stream type lift augmentation concept for STOL aircraft is the reduction of noise due to the interaction of the jet exhaust with the deployed flaps during the takeoff and approach phases of flight. The purpose of this study was to investigate the feasibility of using flaps with variable impedance surfaces as a possible means of noise reduction.

Measurements of farfield sound pressure, lift, drag, and moment of the wing/flap system were made for the unmodified flaps and for a number of flap systems modified by the use of variable impedance surfaces. No attempt was made to optimize noise reduction versus aerodynamic performance.

The findings of the feasibility study indicated that substantial reductions of noise due to jet interaction with the flaps may be realized. The configurations examined in this study resulted in some decrease in aerodynamic performance.

In addition to direct treatment of the flaps, it was found that a mesh-like structure properly located in the jet may provide significant additional noise reduction. Broadband reductions on the order of 10 dB were realized using variable impedance treatment of the flaps and further reductions on the order of 10 dB were realized using screens to break up the jet. Lift losses for both the takeoff and approach flap settings were on the order of 10 to 25%. Drag increases were observed to be between 15 and 40% for the approach setting and 40 and 100% for the takeoff setting. In view of the limitations on available materials and the gross nature of the survey, it is thought that these aerodynamic losses may be reduced substantially through optimization studies.

The need for a clear understanding of the relative importance of the various noise source mechanisms in order to optimize noise treatment of specific configurations is well established. A good understanding of source mechanisms tends to minimize the quantity of treatment required and could thus lead to substantial reductions in the aerodynamic penalties associated with use of variable impedance surfaces.

INTRODUCTION

The General Problem

The externally-blown-flap design in its unmodified state is expected to generate noise far in excess of practical goals which have been established for the operation of future commercial transport aircraft. Current estimates of noise from an EBF-type STOL aircraft in approach and takeoff modes place the noise levels between 15 and 30 dB in excess of the design goal. When selecting noise reduction techniques for any aircraft, attention must be focused on minimizing attendant weight, lift, drag, and thrust penalties. To date, noise reduction concepts attempted on the EBF have been largely unsuccessful, or at least unacceptable in terms of total system performance. So far, the "mixer nozzle" noise reduction concept, which attempts to reduce the velocity of the jet interacting with the flaps, has received the most attention. This concept involves substantial weight penalties and in tests reported to date [References 1, 2, 3] has not provided noise reductions at all near the levels required to meet design goals. This report describes an investigation directed at noise reduction based upon a detailed understanding of the source characteristics and, accordingly, concepts for substantial noise reduction.

Method of Attack

Before attempting specific treatments for the EBF, models of each of the potential noise sources were developed and it was shown that virtually all existing experimental data give strong evidence in support of these models. It was also shown that further study is required to rank order the various sources for specific flap/nozzle configurations. With this physical insight into the problem, noise reduction schemes can be investigated on an orderly and rational basis.

The Basic Experimental Configuration

The three-flap configuration tested in this study represents (at 1/15-scale) the configuration currently being considered by NASA. The nozzle used was of the simple convergent type and had an exit diameter of 4.45 cm (1.75 in.) with which exit velocities (of 70°F air) from 0 to 320 m/sec

(0 to 1050 fps) were possible. The orientation of the nozzle relative to the flaps is shown in Figure 1 for the approach and takeoff flap settings. Acoustic measurements were made in an anechoic space in the "flyover" plane, i.e., in a plane through the jet axis and normal to the spanwise direction of the wing. A photograph of the wing/flap segment is shown in Figure 2.

Scope of Report

The remainder of this report presents a discussion of fundamental aspects of sound generation by turbulent flows interacting with flap-like surfaces and the implications of these fundamental concepts in terms of noise reduction. Acoustic and aerodynamic data on the basic three-flap configuration are presented, as are the corresponding data for a number of cases where variable impedance surfaces have been employed for noise reduction purposes.

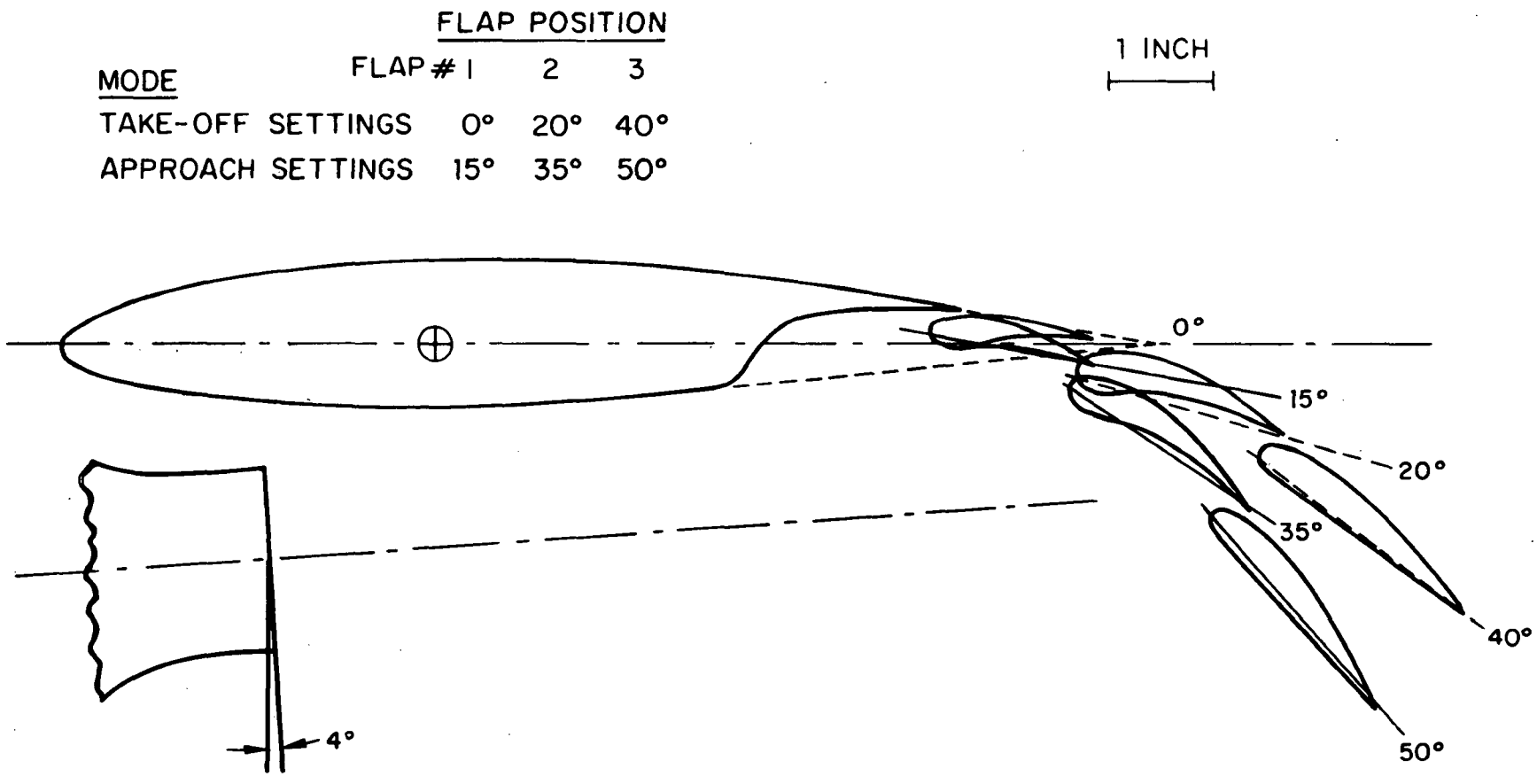

FIG. 1. EXPERIMENTAL CONFIGURATION

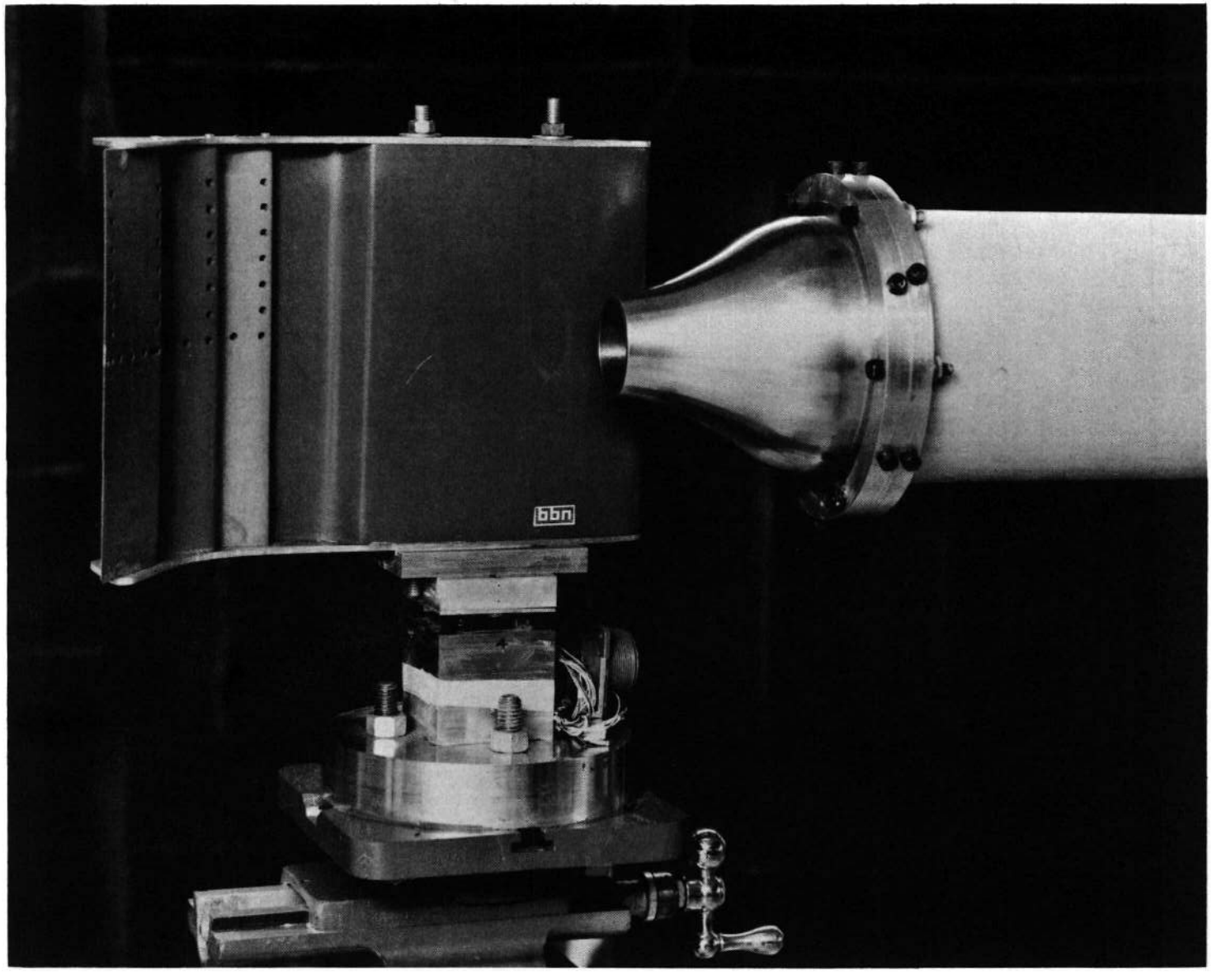

Nozzle dia. = 4.45 cm

FIG. 2. PHOTO OF 3-FLAP EBF SEGMENT ON FORCE BALANCE AND x-y TABLE

FUNDAMENTAL CONCEPTS OF NOISE GENERATION AND REDUCTION

Sources of Noise

When a free jet is directed at flap-like surfaces, noise may arise as a result of:

1. lift and drag fluctuations of the flaps;
2. interaction of turbulence with the leading and trailing edges;
3. direct radiation from the surface boundary layer;
4. vibration of the flap surfaces;
5. jet-like noise from the free shear layer ("mixing" noise).

For the three-flap EBF system, jet velocities between 500 and 900 fps have been considered; it is shown in Figure 3 that when the flap surfaces are introduced into a flow in that Mach-number range, the noise due to the interaction of the flow with the surfaces dominates the total acoustic output of the system. It is useful at this point to attempt to eliminate the secondary sources from the above list so that attention may be focused on the dominant noise producing mechanisms.

Flap vibration is not likely to be a predominant contributor to the sound field; furthermore, due to fatigue life requirements, skin vibration ultimately must be controlled without altering the aerodynamic characteristics of the flaps. Direct sound radiation from the surface turbulent boundary layer is only important on surfaces which are very large with respect to typical acoustic wavelengths, and it is currently thought that sound levels from this source are completely dominated by "edge noise" when a trailing edge is also immersed in the turbulent flow. "Mixing" noise from the free shear layer is obviously insignificant in this case.

Thus, two major source cateogries, (1) and (2) above, remain to be considered in attempting to understand the noise-producing processes associated with the EBF concept.

"Whole body" dipole sources. Impingement of jet turbulence on the flaps causes fluctuating lift and drag forces which act substantially in phase over the entire flap. Sources of lift and drag fluctuations at those frequencies which have acoustic wavelengths much larger than the characteristic dimensions of the source are characterized as point dipoles.

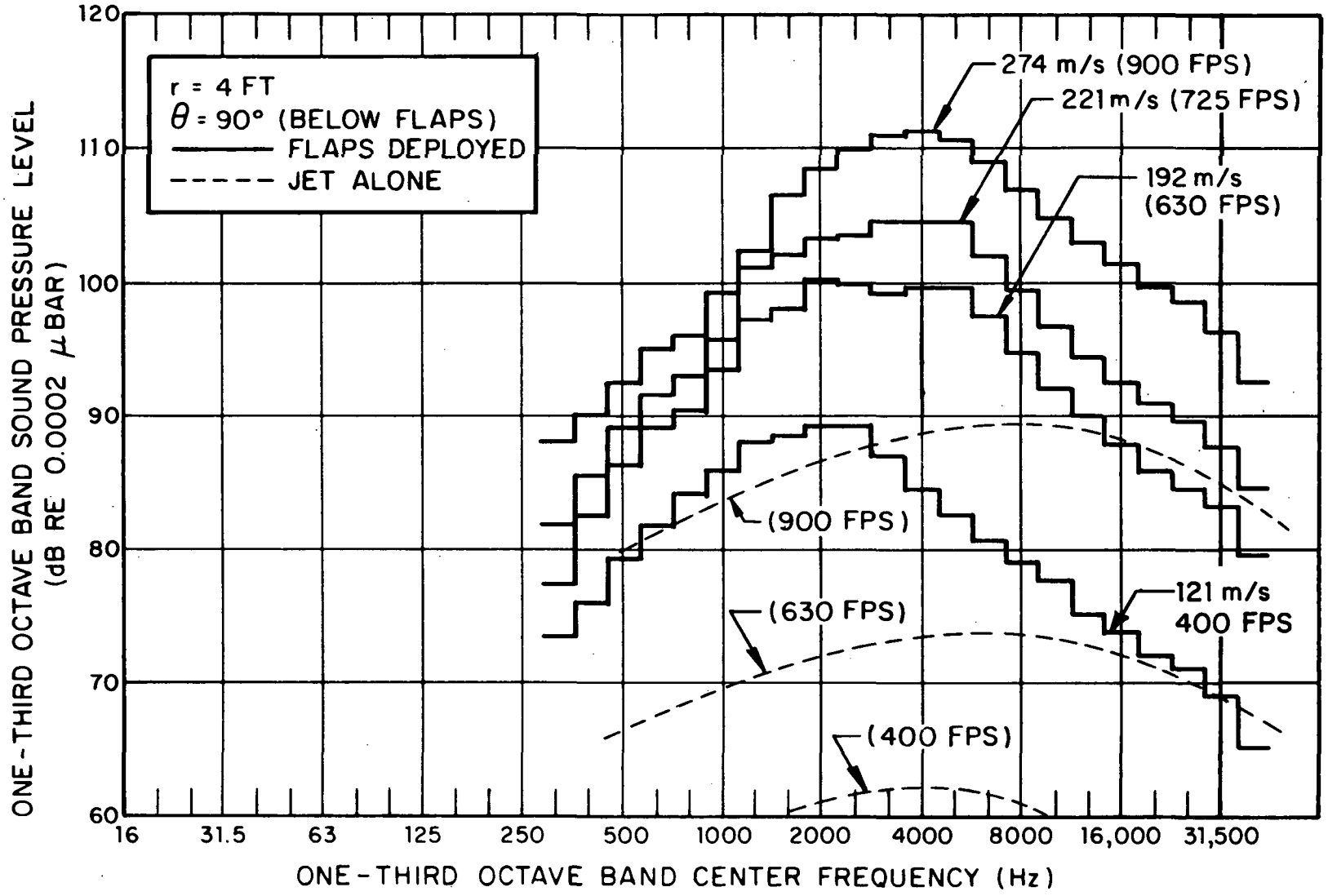

FIG. 3. TYPICAL FAR FIELD SOUND SPECTRA VS. VELOCITY (APPROACH FLAP SETTING).

The sound power Π per unit bandwidth $\Delta\omega=2\pi$ from a point dipole can be described in terms of the fluctuating forces as

$$\frac{\Delta\Pi}{\Delta\omega} = \frac{\Phi_F(\omega)\ \omega^2}{12\pi\rho c_0^3} \tag{1}$$

where Π = the sound power
ω = the radian frequency
$\Phi_F(\omega)$ = the force spectral density
ρ = the ambient density of the medium
c_0 = the isentropic sound speed in the medium.

The aerodynamic forces may be represented in terms of mean flow parameters and fluctuating flow parameters; namely,

$$\begin{aligned} F_A = F_{SS} + F' &= C_A \cdot \tfrac{1}{2}\rho\ (U+u')^2\ \ell_x\ell_y \\ &= C_A \cdot \tfrac{1}{2}\rho \cdot (U^2+2Uu'+\ldots)\ \ell_x\ell_y \end{aligned} \tag{2}$$

where F_{SS} is the steady-state component of the force

F' is the fluctuating component of the force
C_A is a steady-state aerodynamic coefficient
U is the mean axial velocity
u' is the fluctuating velocity component
ℓ_x and ℓ_y are turbulence length scales in the axial and transverse directions respectively.

The fluctuating component is then

$$F' = C_A\ \rho\ (Uu')\ \ell_x\ell_y = C_A\rho U^2\ell_x\ell_y \left(\frac{u'}{U}\right). \tag{3}$$

The frequency spectrum of the forces may be expressed in terms of the turbulence intensity spectral density $\Phi_I(\omega)$,

$$\Phi_F(\omega) = \left[C_A \rho U^2 \ell_x \ell_y\right]^2 \Phi_I(\omega) \propto q^2 \Phi_I(\omega) \left[\ell_x \ell_y\right]^2 \tag{4}$$

Note that for a round subsonic free jet, the length scales ℓ_x and ℓ_y vary with distance from the nozzle exit as does the turbulence intensity (u'/U), and, at a given normalized distance x/D from the nozzle, the turbulence intensity spectrum (with frequency normalized on a Strouhal basis) is essentially invariant with exit velocity. The length scale distributions are also essentially invariant under the same restrictions. Thus, the length scales are directly proportional to D_0, the nozzle exit diameter, over a broad velocity range (i.e., if D_0 is changed, then the length scales ℓ_x and ℓ_y change proportionately).

The characteristic frequency ω_c of the force fluctuations is related to the mean eddy convection velocity U_c and the longitudinal length scales ℓ_x,

$$\omega_c \simeq \frac{U_c}{\ell_x} \propto \frac{U}{D_0} . \tag{5}$$

These simplifications lead to a model based solely on mean flow parameters:

$$\Pi = \frac{\omega^2 F^2}{12\pi\rho c_0^3} \propto \frac{\left(\frac{U}{D_0}\right)^2 (\rho U^2 D_0^2)^2}{\rho c_0^3}$$

i.e.,
$$\Pi \propto \frac{\rho U^6 D_0^2}{c_0^3} \tag{6}$$

This expression exhibits the familiar U^6 velocity dependence and the "area factor" D_0^2.

The expression for farfield sound pressure for a finite ("noncompact") dipole source may be written as:

$$\Phi_p(r,\theta,\psi,\omega) = \frac{\Phi_F(\omega)}{16\pi^2 r^2} \left(\frac{k^2}{1+k^2a^2}\right) \cos^2\theta \qquad (7)$$

where Φ_p is the acoustic pressure spectral density

$k = \frac{\omega}{c_0}$ is the acoustic wavenumber

a is the characteristic source radius which can be taken as 1/2 the flap chord C,

θ, ψ, and r are geometric parameters as given in Fig. 4.

The implications of this expression at large values of k_a in terms of speed dependence of the overall sound level will be discussed in a later section.

Trailing edge wise source. The convection of turbulent boundary layer or wall jet pressure fluctuations past a trailing edge results in the imparting of momentum fluctuations to the fluid medium at the edge. Thus, the edge may be considered to be a pressure release point where the impedance to the hydrodynamic pressure fluctuations in the plane of the surface abruptly changes from infinite to finite (tending toward ρc_0, the characteristic impedance of the medium, as a lower bound). Sources of momentum fluctuations may be appropriately modeled as simple dipole sound sources. Before considering the general distributed source, one might first consider a model for a single correlation area of pressure at the trailing edge of a rigid surface. If the source of the fluctuating force is regarded as a sphere of radius a, exerting a force on the medium along a preferred axis, then the source may be approximated by a point dipole model whose sound power is given by Eq. 1. Of course, replacing the fluid mechanical source with an oscillating sphere does not represent the physical phenomena accurately, but does allow one to visualize qualitative features of this source.

In the edge noise model [References 4, 5, 6] F is again assumed to be proportional to the free-stream dynamic pressure times a correlation area A_c ($F \propto 1/2\rho U^2 A_c$), where A_c is defined as the product of a longitudinal (streamwise) correlation length ℓ_x and a spanwise correlation length ℓ_y. The characteristic frequency of the force (i.e., pressure fluctuations) is usually found to be proportional to U/ℓ_x so that $f\ell_x/U$ = constant.

Thus, the sound power from a single radiating area on a surface near the edge is

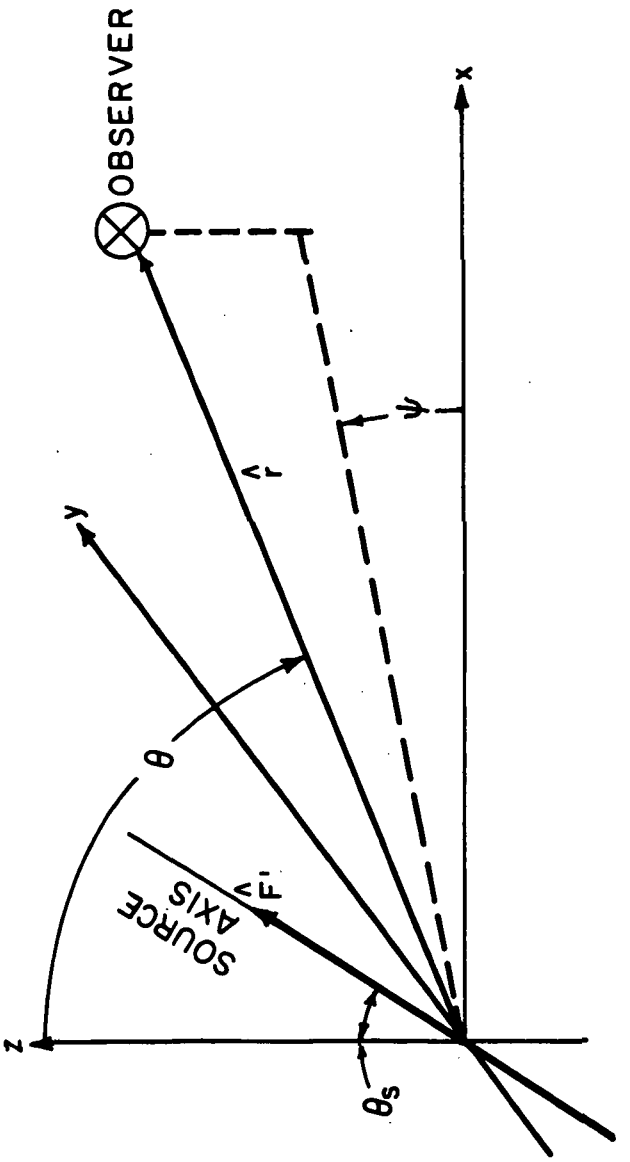

FIG. 4. COORDINATE SYSTEM FOR COMPUTING POINT DIPOLE SOUND FIELD

$$\Pi_D \propto \frac{1}{12\pi\rho c_0^3} \cdot (2\pi U/\ell_x)^2 \cdot (1/2\rho U_m^2 \ell_x \ell_y)^2$$

$$\Pi_D \propto \frac{U_m^6 \rho \ell_y^2}{c_0^3} \quad . \tag{8}$$

This approach may be extended to develop a model for an edge immersed in a large number of such small-scale pressure fluctuations. If, over the edge span W, there are n uncorrelated individual sources, $n = W/\ell_y$, the total power from the edge

$$\Pi_{total} \propto \frac{\rho U_m^6 \ell_y W}{c_0^3} \tag{9}$$

Since it has been shown that the true source can be replaced exactly by the fluctuating wall pressure (by Curle's integral of Ref. 7), the wall pressure can be viewed as representing the "strength" of the sound source. It then follows that the proportionality constant relating the two sides of Eq. 9 would be on the order of $(p_w/q_m)^2$ - the ratio of fluctuating surface pressure to free-stream dynamic pressure. This ratio is known to vary substantially between various classes of viscous flow fields - usually between the orders of 10^{-1} and 10^{-4} for turbulent boundary layers and turbulent wall jets. However, the current state of knowledge of edge noise does not include adequate documentation of the variation in trailing edge noise over a wide range of (p_w/q_m) levels.

The directivity of the trailing edge source is substantially influenced by the presence of the surface. The patterns predicted and observed by Hayden and Chanaud [References 3, 4, 5] are shown in Fig. 5. The same type of directivity was observed in the current study of the corresponding leading edge source in the presence of a semi-infinite surface (Appendix A).

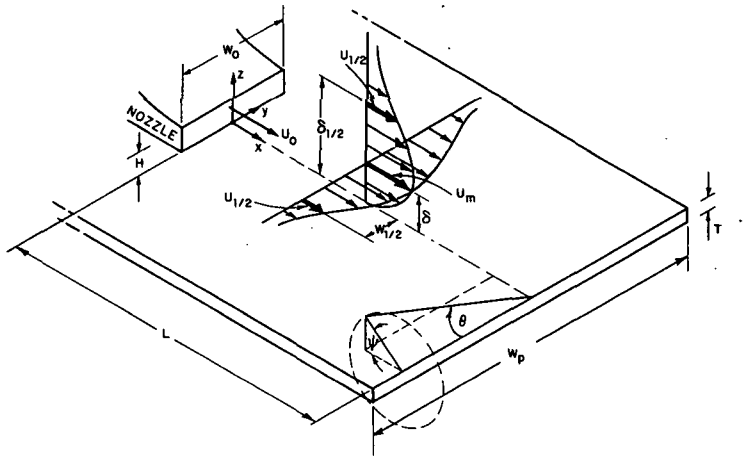

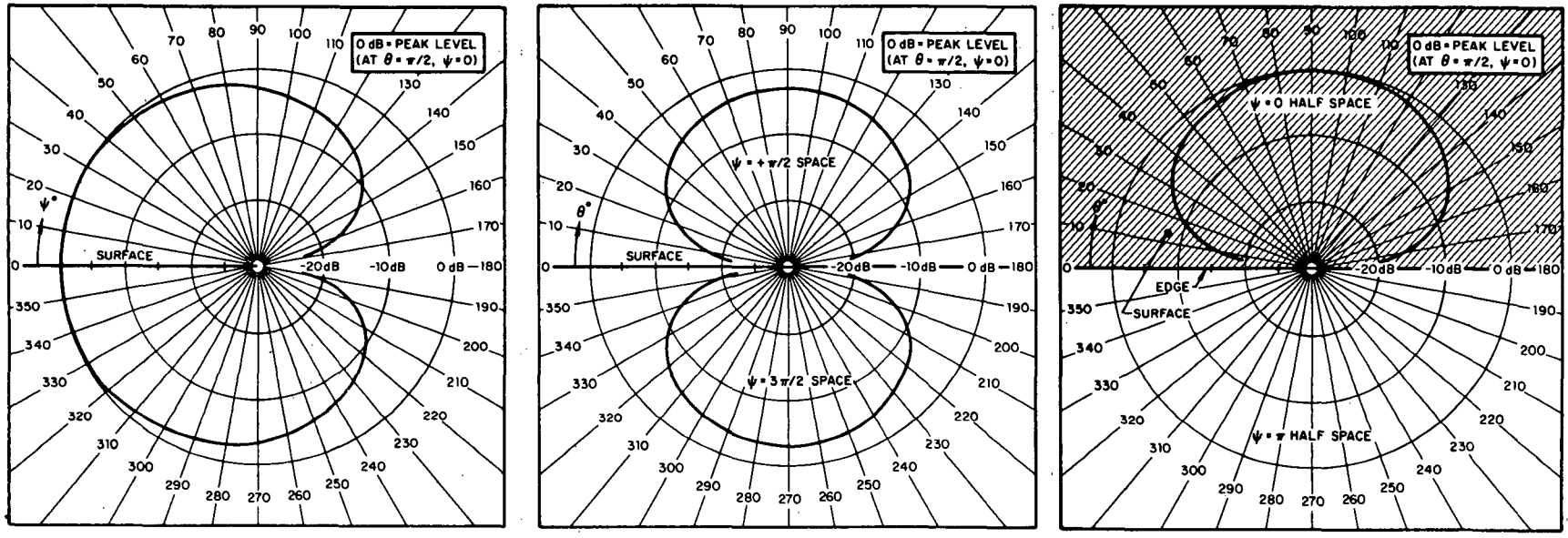

(a) In plane normal to surface and to span

(b) In plane normal to surface and parallel

(c) In plane of the surface

FIG. 5 DIRECTIVITY OF EDGE SOURCES

Leading edge noise source. When a turbulent jet impinges on the leading edge of a flap or plate-like surface whose characteristic dimensions are large with respect to characteristic acoustic wavelengths, the source may be modeled as a distribution of point dipoles in the same manner as the trailing edge source.

As was discussed earlier, in an unmodified free jet, the normalized turbulence intensity spectrum and length scales at a point (or in a plane) are essentially independent of nozzle exit velocity. The leading edge source strength F for a single correlation area is

$$F \propto p_c \, \ell_x \ell_y ,$$

where p_c is a characteristic fluctuating pressure which is related to the inflow parameters* by

$$p_c = C_p \frac{1}{2} \rho \, (U+v')^2 \qquad (10)$$

where C_p is the pressure coefficient and v is the turbulent component normal to the jet axis. Using the simplifications developed previously, the source strength can be written

$$F \propto \rho U^2 \ell_x \ell_y \frac{v'}{U} ; \qquad \Phi_F(\omega) \propto \rho U^2 \ell_x \ell_y \Phi_I(\omega) .$$

Again, the characteristic frequency is

$$\omega_c \propto \frac{U}{\ell_x} .$$

The total leading edge source strength is the sum of the individual source strengths across the leading edge. If the wetted span is W_c, the total sound power is

---

*This gross approach neglects the existence of pressure fluctuations which are already in the jet and convecting with it; however, one may simply account for such pressures once they are known.

$$\Pi \propto \frac{m\omega_c{}^2 F^2}{\rho c^3}$$

where $m \simeq \frac{W_c}{\ell_y}$. Thus

$$\frac{\Delta\Pi}{\Delta\omega} \propto \left(\frac{U}{\ell_x}\right)^2 C_p \rho^2 U^4 \ell_x{}^2 \ell_y{}^2 \frac{W_c}{\ell_y} \cdot \Phi_I(\omega)$$

$$= C_p \rho^2 U^6 \ell_y W_c \Phi_I(\omega) \qquad (11)$$

Since U, ℓ_y, W_c, $\Phi_I(\omega)$ are all proportional to the normalized distance from the nozzle, (x,D_0), and ℓ_y and W_c at any point vary in direct proportion to D_0, the overall leading edge sound power can be expressed as

$$\Pi_{LE} \propto C_p \rho^2 U^6 \left(\frac{x}{D}\right) D_0^2 \eta_1 \left(\frac{x}{D}\right) \eta_2 \left(\frac{x}{D}\right) \eta_3 \left(\frac{x}{D}\right) , \qquad (12)$$

where η_1, η_2, and η_3 are arbitrary descriptors of the variation of W_c, ℓ_y and $\Phi_I(\omega)$ with normalized distance from the nozzle.

Basis for Spectral Normalization of all Flap Noise Data

It has been shown that the overall levels for whole body dipole, leading, and trailing edge sources are all related to U^6, $D_0{}^2$ and ρ and that characteristic frequency distributions (Strouhal spectra), for a given geometry, vary directly with velocity and inversely as the nozzle diameter.*

*It will be shown later that for $k_a >> 1$, the overall levels for the whole body dipole component depend on U^4 instead of U^6.

Thus, the following normalization is suggested:

$$\omega \, \Phi_p(\omega) \Big/ \left(\frac{\rho U^6 D^2}{r^2 c_0^2} \right) = \text{constant},$$

where r is the distance to the observation point. A normalized sound pressure level may thus be defined by the ratio

$$\Gamma = 10 \log \left[\frac{fD/U \cdot \Phi_p \left(\frac{fD}{U} , r_0 \right)}{\frac{\rho^2 U^6 D^2}{r_0^2 c_0^2}} \right] \qquad (13)$$

In terms of easily measurable parameters, the normalized sound pressure level $\Gamma(f_c)$ is

$$\Gamma(f_c) = 1/3 \text{ OB SPL}(f_c, r_0) + 20 \log (p_{ref}) - 10 \log (\rho^2 U^6 D^2) + 10 \log (r_0^2 c_0^2) + 6.3 \text{ dB} \qquad (14)$$

where p_{ref} is the acoustic reference pressure, 1/3 OB SPL (f_c, r_0) is the one-third octave band sound pressure level in dB (re p_{ref}) at a center frequency f_c and an observation radius r_0.

Note that for specific geometries, the above expression must be applied along each specific azimuth with respect to the source orientation, since the source directivity function was not included in the analysis. Such a normalization has been performed on the data shown in Figure 2 - the farfield sound spectra below the wing for the approach setting. The resultant normalized spectrum is shown in Figure 6, where it may be seen that the collapse of data is excellent, which tends to verify the source models proposed earlier.

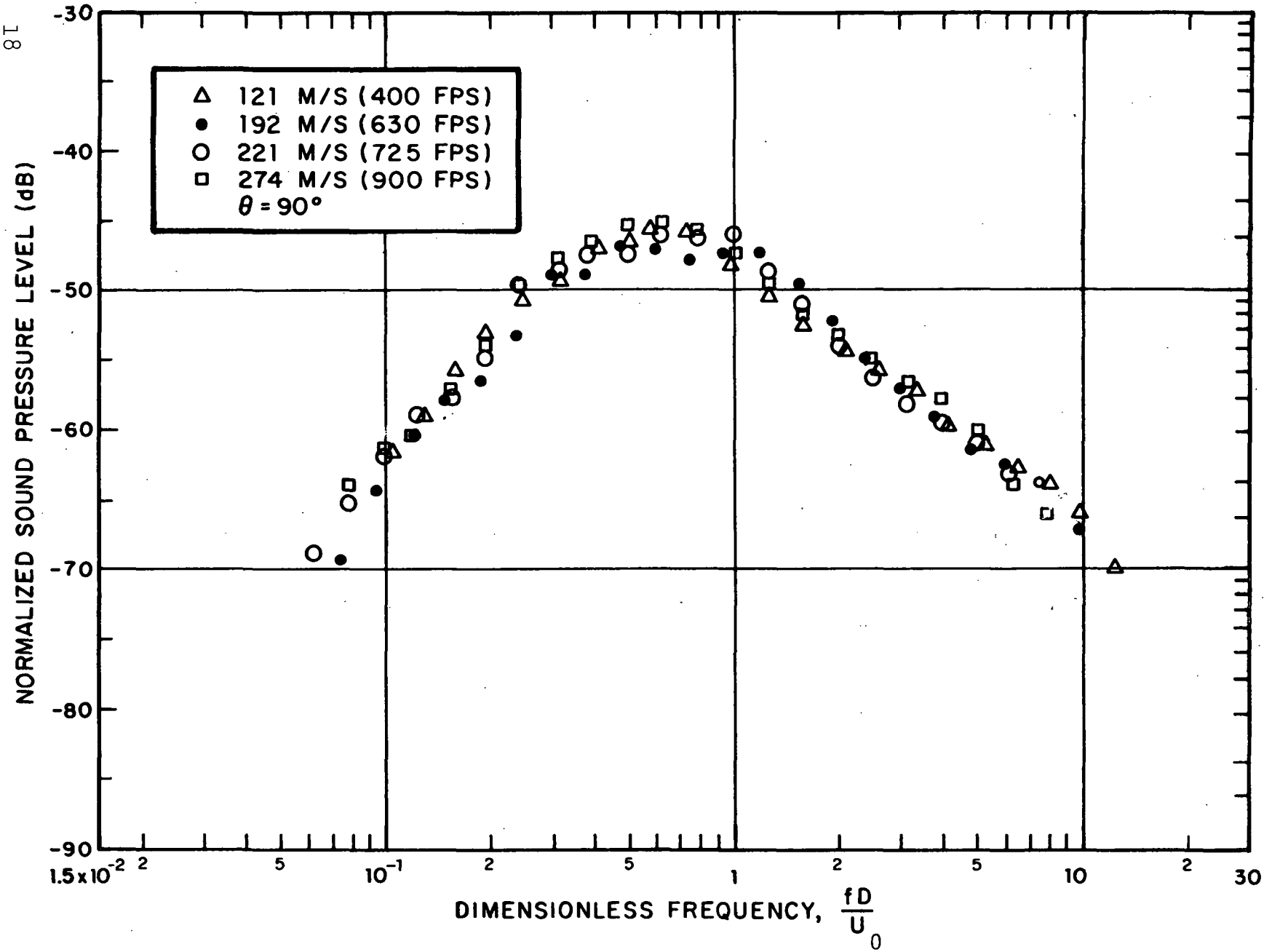

FIG. 6. NORMALIZED SPL SPECTRA FOR DIFFERENT VELOCITIES.

Noise Reduction Concepts

The preceding summary of source characteristics helps to derive suitable noise reduction approaches for the individual sources. The general categories of noise reduction are:

(1) modify mean flow and geometric parameters;
(2) modify fluctuating component of the flow;
(3) modify the acoustic "transduction" process - the specific manner in which pressure or velocity fluctuations are converted into sound.

Specific examples are cited below.

Whole body dipole. It is instructive to return to the expression for sound pressure (Eq. 7) and examine the effect of modification of turbulence parameters on the whole body dipole sound:

$$\Phi_p(r,\theta,\psi,\omega) = \frac{\Phi_F(\omega)}{16\pi^2 r^2} \left[\frac{k^2}{1+k^2\left(\frac{C}{2}\right)^2} \right] \cos^2\theta, \qquad (15)$$

taking $\frac{C}{2}$, half the flap chord, to be the characteristic source radius.

The force spectral density $\Phi_F(\omega)$ is given by the expression (Eq. 4):

$$\Phi_F(\omega) = C_A \rho\, U^2\, \ell_x\, \ell_y\, \Phi_I(\omega). \qquad (16)$$

It must be noted here that C_A, the steady-state aerodynamic coefficient, must be supplemented with an unsteady counterpart, such as a modified Sears function in three dimensions, which gives reduced lift and drag response for decreasing values of ℓ_x/C and ℓ_y/C.

The acoustic wavenumber, $k = \omega/c_0$, may be rewritten as

$$k \approx \frac{U/\ell_x}{c_0}. \qquad (17)$$

Substituting Eqs. 16 and 17 into Eq. 15 results in

$$\Phi_p(r,\theta,\psi,k) \propto \frac{C_A}{r^2}\ \Phi_I(\omega)\ \left(\rho\ U^2\ \ell_x\ \ell_y\right)^2 \left[\frac{\left(\frac{U/\ell_x}{c_0}\right)^2}{1+\left(\frac{U/\ell_x}{c_0}\right)^2\left(\frac{C}{2}\right)^2}\right] \tag{18}$$

It is now evident how the whole body dipole sound will respond to changes in ℓ_x, ℓ_y and $\Phi_I(\omega)$:

1. Decreasing the turbulence intensity $\Phi_I(\omega)$ produces a corresponding drop in sound pressure.
2. Decreasing turbulence scales decreases the rate of increase of sound output with frequency above

$$\omega \cdot \frac{C}{2} = \frac{U}{\ell_x} \cdot \frac{C}{2}\ ,$$

i.e., the rate of sound output eventually becomes dependent only upon the shape of the turbulence spectrum, and not on ω^2 as in the point model. Furthermore, this implies that the speed dependence of the whole body dipole eventually becomes U^4 and not the U^6 associated with point sources ($ka << 1$).

3. Decreasing turbulence scales lowers the "threshold" frequency at which aerodynamic forces begin to decrease due to cancellation effects (Sear's function effect).

Thus, to reduce whole body dipole sound, reduce U, Φ_I, ℓ_x, ℓ_y by proper selection of flap location or by intentional modification of the flow field.

Leading and trailing edge dipoles. The argument presented above can also be applied to the leading and trailing edge sources. However, with these sources, it is possible to modify the physical process by which nonradiating fluid disturbances are converted into sound at the edge. One may modify the local impedance (porosity) of the surface to accomplish this end. Thus, the appropriate noise reduction techniques for the edge sources are:

(1) reduce ℓ_y, the eddy dimension in the spanwise direction;

(2) reduce velocity and turbulence intensity levels (or surface pressure levels for the trailing edge source);

(3) modify the surface impedance locally.

Summary of Noise Reduction Concepts for the EBF

Modify forcing function (flow).

A. Change mean flow parameters
   1. lower U
   2. decrease D
   3. reduce ρ

B. Change unsteady component of flow
   1. reduce overall turbulence levels
   2. reduce length scales

Modify transduction process.

1. Whole body dipole sound. (Can only modify the aerodynamic transfer function by the same process suggested above - produce a large ratio of C/ℓ_x).*

2. Edge sources. Vary edge impedance to create a smooth transition from the rigid surface to the fluid medium.

---

*Whole body forces may originate at the leading and trailing edges as a result of large scale flow disturbances there; thus, treating the leading or trailing edge may reduce the whole body component of the sound field.

SUMMARY OF EXPERIMENTAL OBSERVATIONS ON BASIC THREE-FLAP CONFIGURATION

Acoustic Data

Scaling laws based on mean flow parameters. Measurements of sound radiated from jet interaction with the flaps were taken in an anechoic space in the acoustic and geometric far field of the flaps (kr >> 1 for frequencies above 300 Hz, and kC >> 1 for frequencies above 1000 Hz). The measurement plane was the vertical plane passing through the jet centerline (i.e., the "direct flyover" plane). The spectra showed U^6 speed dependence and linear shifting of frequency with speed, which is consistent with the predictions of the edge dipole models developed earlier. Typical "raw data" are shown in Figure 3 for exit velocities of 121, 192, 221, and 274 m/s (400, 630 725, 900 fps) for the 90° observation position (see Figure 7 for layout). As shown earlier these data may be normalized on the basis of Eq. 14, thus allowing one to predict farfield spectra for a geometrically similar flap system of any scale. Typical normalized sound spectra for the cruise, takeoff and landing flap settings for different observation angles are shown in Figures 8-10 (U_0 between 400 and 900 fps).

Directivity characteristics. As shown in the previous section, the various potential noise sources exhibit different directivity patterns. When these patterns are considered together with the observed directivity of a given flap, they should provide some insight into the predominant noise source(s). However, due to the varying orientations of the various source axes in the 3-flap EBF, this is not a particularly useful diagnostic tool at this stage.

Typical observed directivity patterns are shown in Figures 11-13, again for the cruise, takeoff, and landing settings, respectively. For the cruise setting, the obvious noise source is "trailing edge" noise and the directivity pattern in Figure 11 clearly exhibits the expected cardiod-like pattern associated with this source, with maximum radiation forward of the wing. The directivity patterns for the takeoff and approach flap-settings offer fewer direct clues as to the predominant noise source. However, in all cases, substantial sound is radiated forward and minima are observed in the direction of the trailing edge of the third flap, which again suggests that the trailing edge source may be very significant. More conclusive studies

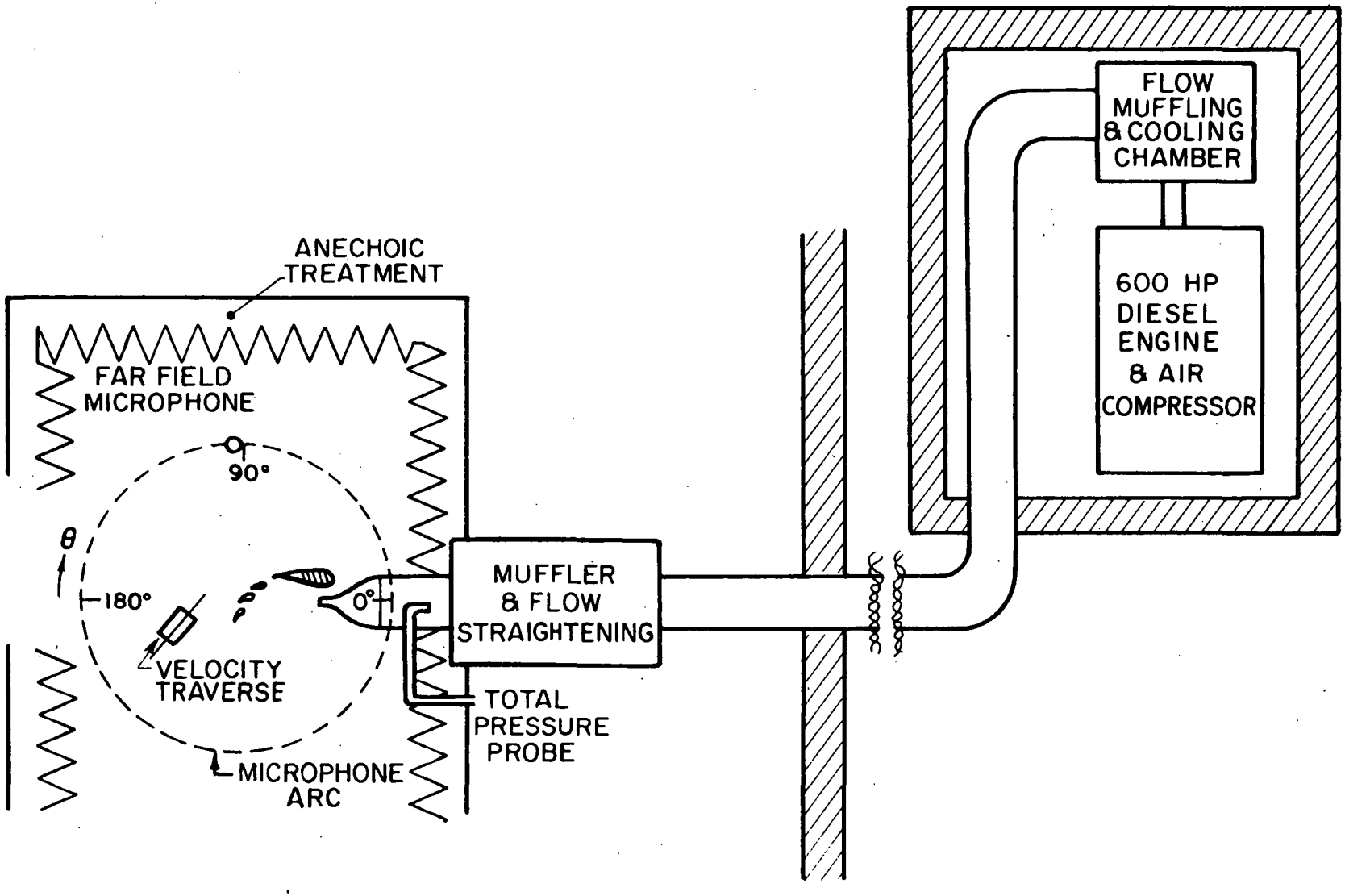

FIG. 7. SCHEMATIC OF LAYOUT FOR ACOUSTIC AND AERODYNAMIC MEASUREMENTS.

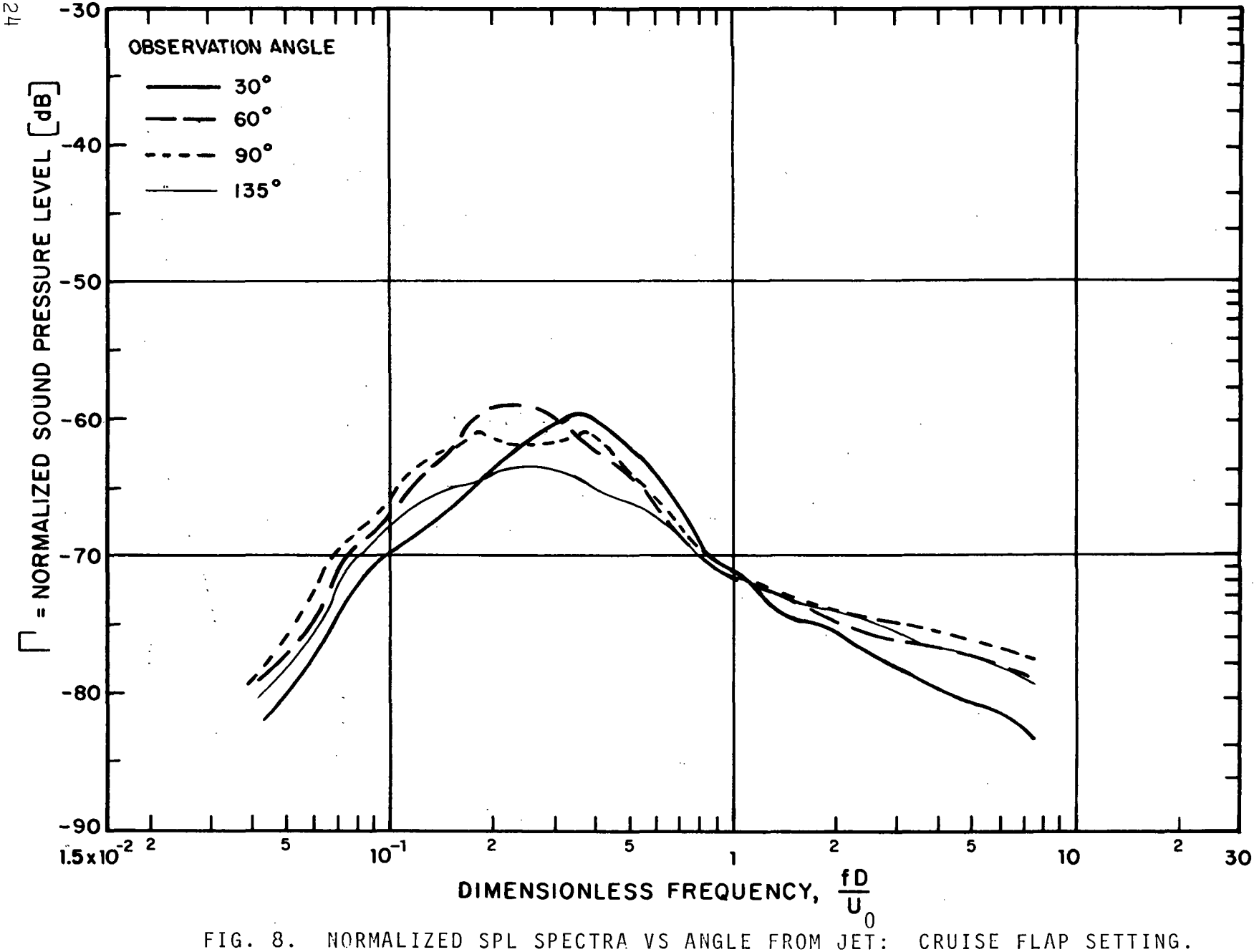

FIG. 8. NORMALIZED SPL SPECTRA VS ANGLE FROM JET: CRUISE FLAP SETTING.

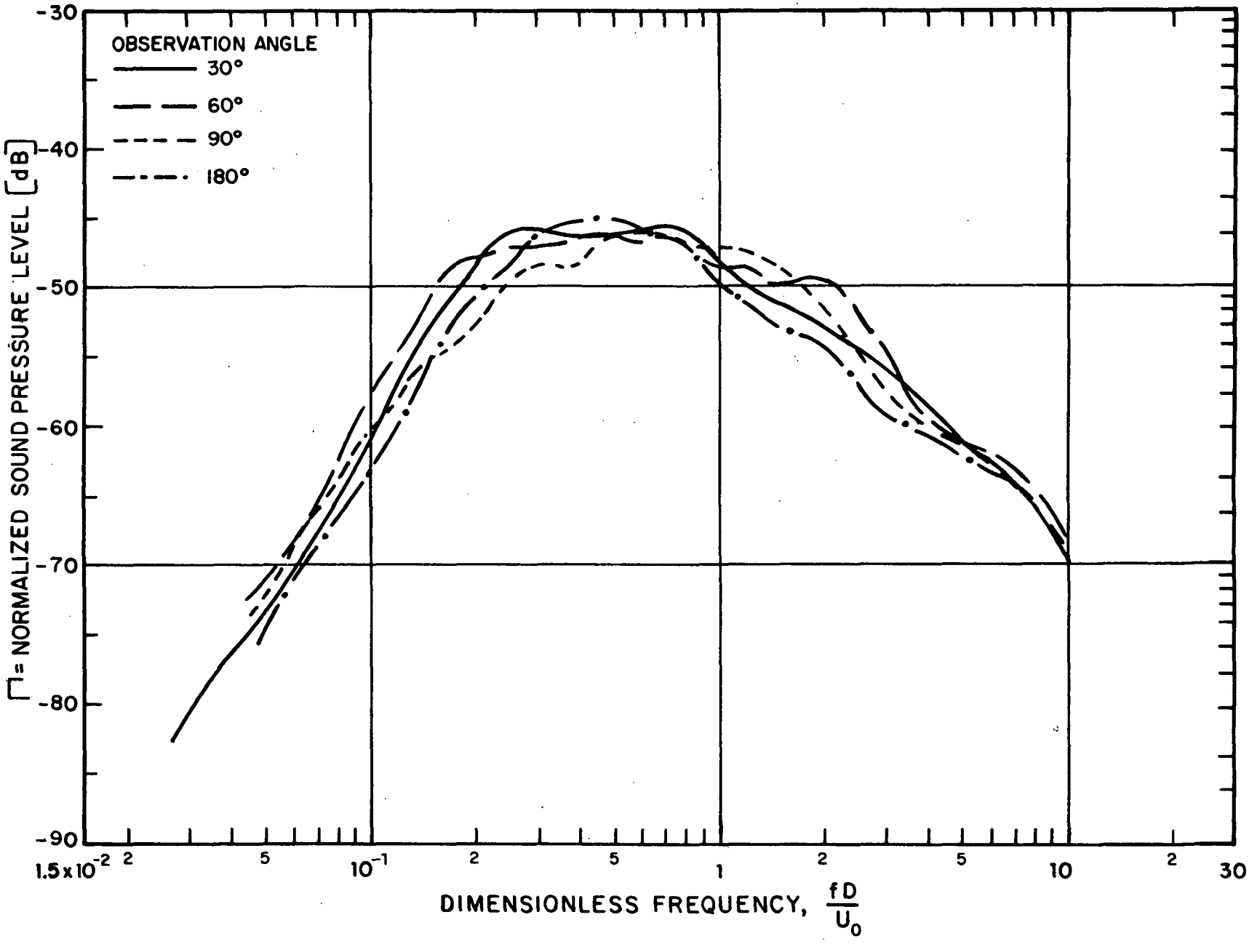

FIG. 9. NORMALIZED SPL SPECTRA vs ANGLE FROM JET: TAKEOFF FLAP SETTING.

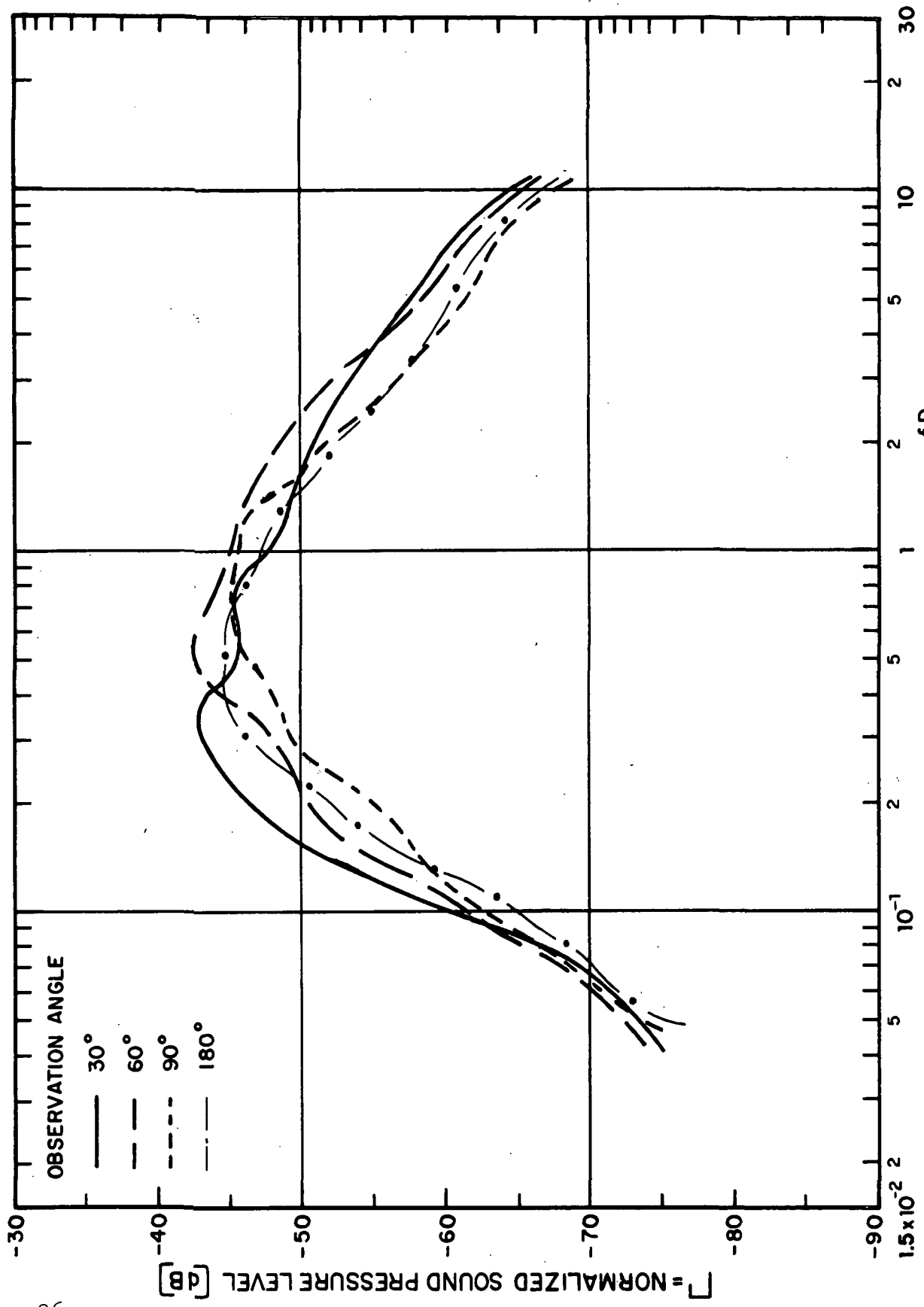

FIG. 10. NORMALIZED SPL SPECTRA VS ANGLE FROM JET: APPROACH FLAP SETTING

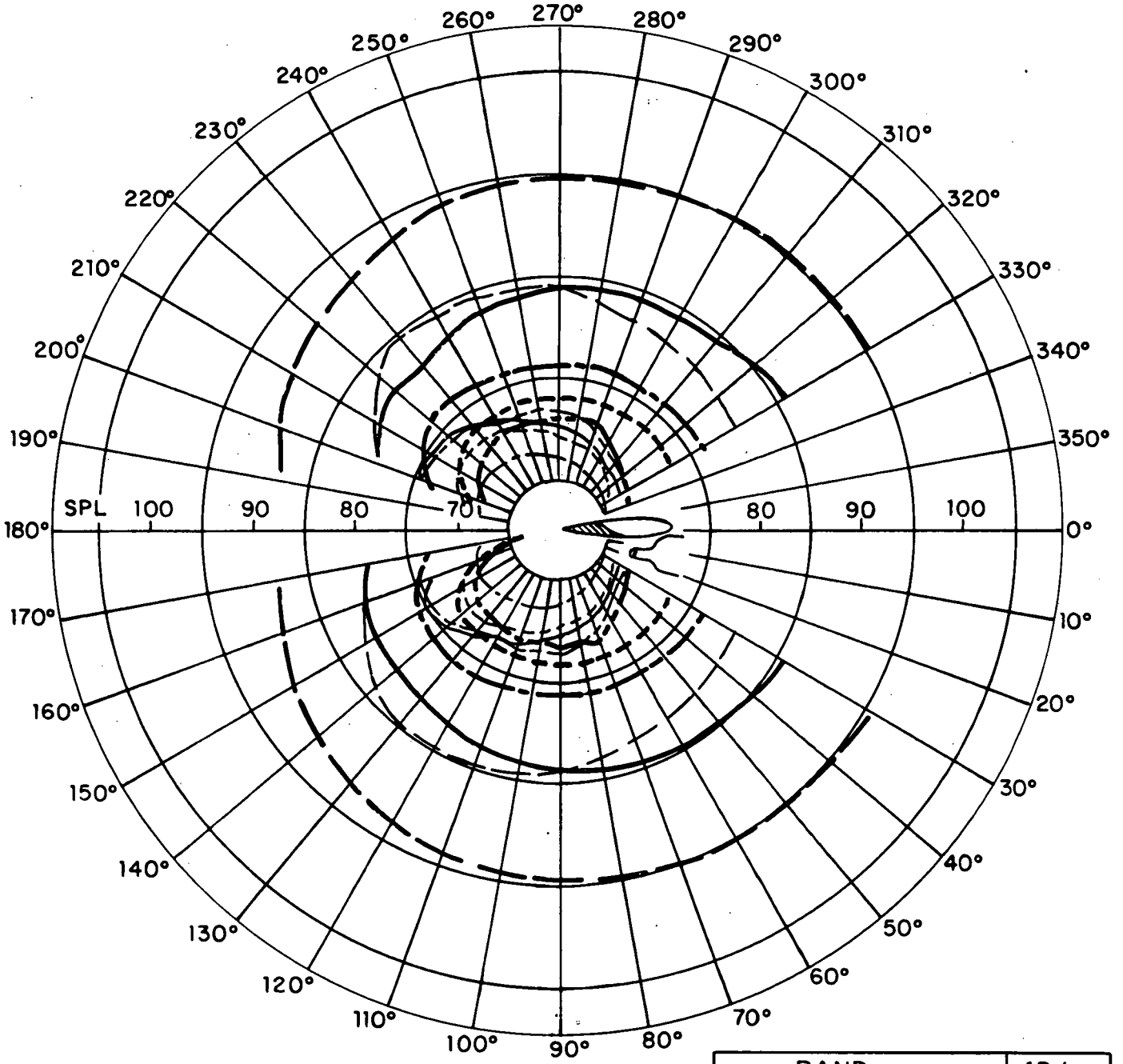

LIGHT LINES = JET ALONE
HEAVY LINES = JET PLUS WING

BAND	fD/u_o
OA SPL	
2 kHz 1/3 O.B.	0.46
4 kHz 1/3 O.B.	0.92
8 kHz 1/3 O.B.	1.84
16 kHz 1/3 O.B.	3.68
u_o = 630 fps	r = 4 ft

FIG. 11. DIRECTIVITY PATTERN: CRUISE FLAP SETTING

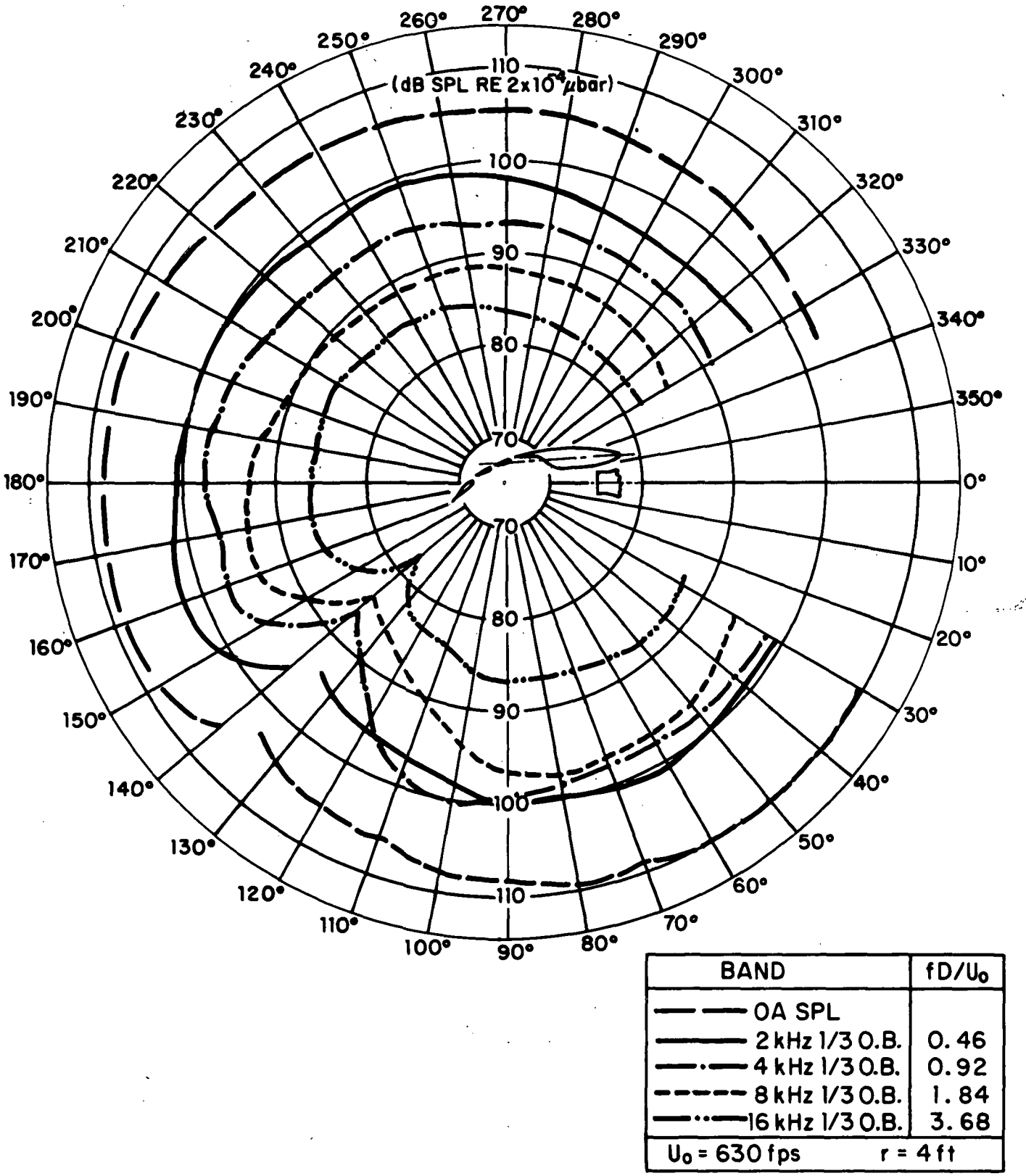

BAND	fD/U_o
OA SPL	
2 kHz 1/3 O.B.	0.46
4 kHz 1/3 O.B.	0.92
8 kHz 1/3 O.B.	1.84
16 kHz 1/3 O.B.	3.68
U_o = 630 fps	r = 4 ft

FIG. 12. DIRECTIVITY PATTERN - TAKEOFF FLAP SETTING.

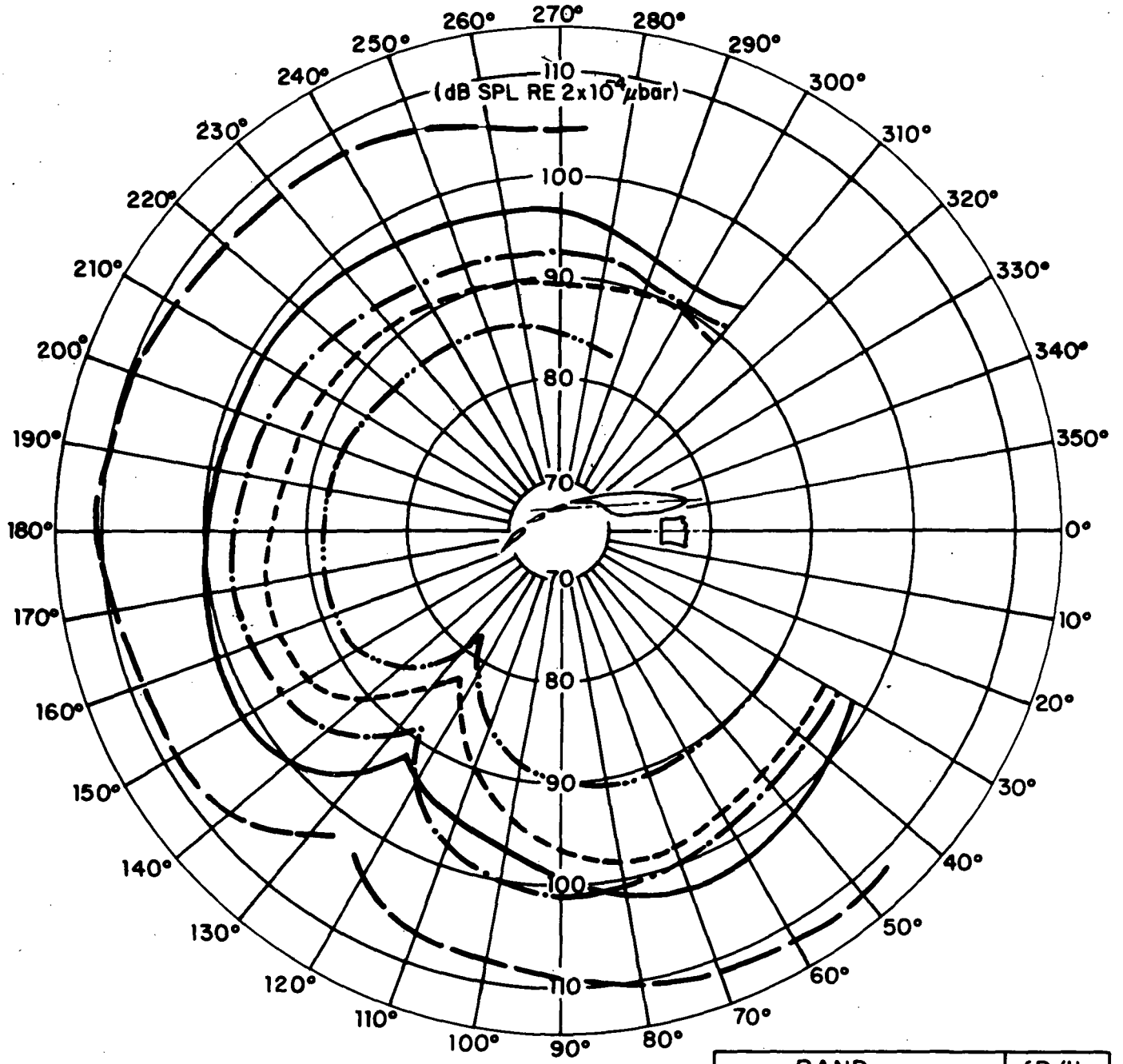

BAND	fD/U₀
OA SPL	
2 kHz 1/3 O.B.	0.46
4 kHz 1/3 O.B.	0.92
8 kHz 1/3 O.B.	1.84
16 kHz 1/3 O.B.	3.68
U_0 = 630 fps	r = 4 ft

FIG. 13. DIRECTIVITY PATTERN - APPROACH FLAP SETTING.

are required to rank order the various sources.

Comparison with earlier NASA data. Although there are no acoustic data on the three-flap EBF with which the current data may be compared, an extrapolation of the current data may be compared with data on a 1/2-scale EBF reported by Dorsch *et al* [Reference 8].

The data on the 1/15-scale three-flap EBF taken in this study were extrapolated using Eq. 15 to full scale, θ=85°, R=500 ft, and an exit velocity of $U_0 \simeq$ 870 fps (corresponding to a pressure ratio of 1.7) for the approach flap setting (15°-35°-50°) and compared with Dorsch's data extrapolated to the same observation point for a two-flap EBF (flap angles of 30 and 60°) in Figure 14. Agreement at the spectral peak is quite good although the three-flap EBF data seem to indicate substantially lower levels at high frequencies. (It has subsequently been learned that the high-frequency hump in the NASA Lewis data is due to valve noise upstream of the nozzle.)

Again, due to configuration differences, comparison of current directivity data with earlier studies is not highly meaningful in terms of checking repeatability. However, as shown in Figures 11-13 and Figure 15, the same general trends are observed in both cases.

Aerodynamic Data

Velocity profiles normal to wing and flap surfaces, surface pressure fluctuations on flaps, and steady-state aerodynamic performance were measured. Velocity profiles and surface pressure data serve to indicate the extent of the aerodynamic sound source region as well as relative source strength on various parts of the flaps. Static lift, drag, and pitching moment serve as a basis for comparison with equivalent data for modified flaps.

Velocity profiles. Figure 16 shows the axial locations of the velocity traverses; in each case the traverse was in a direction normal to the flap chord centerline, with the axial component of velocity being measured. The data for the cruise takeoff and landing settings are shown in Figures 17-19.

Surface oil flow visualization was used to obtain insight into the flow direction on the various flaps for the respective

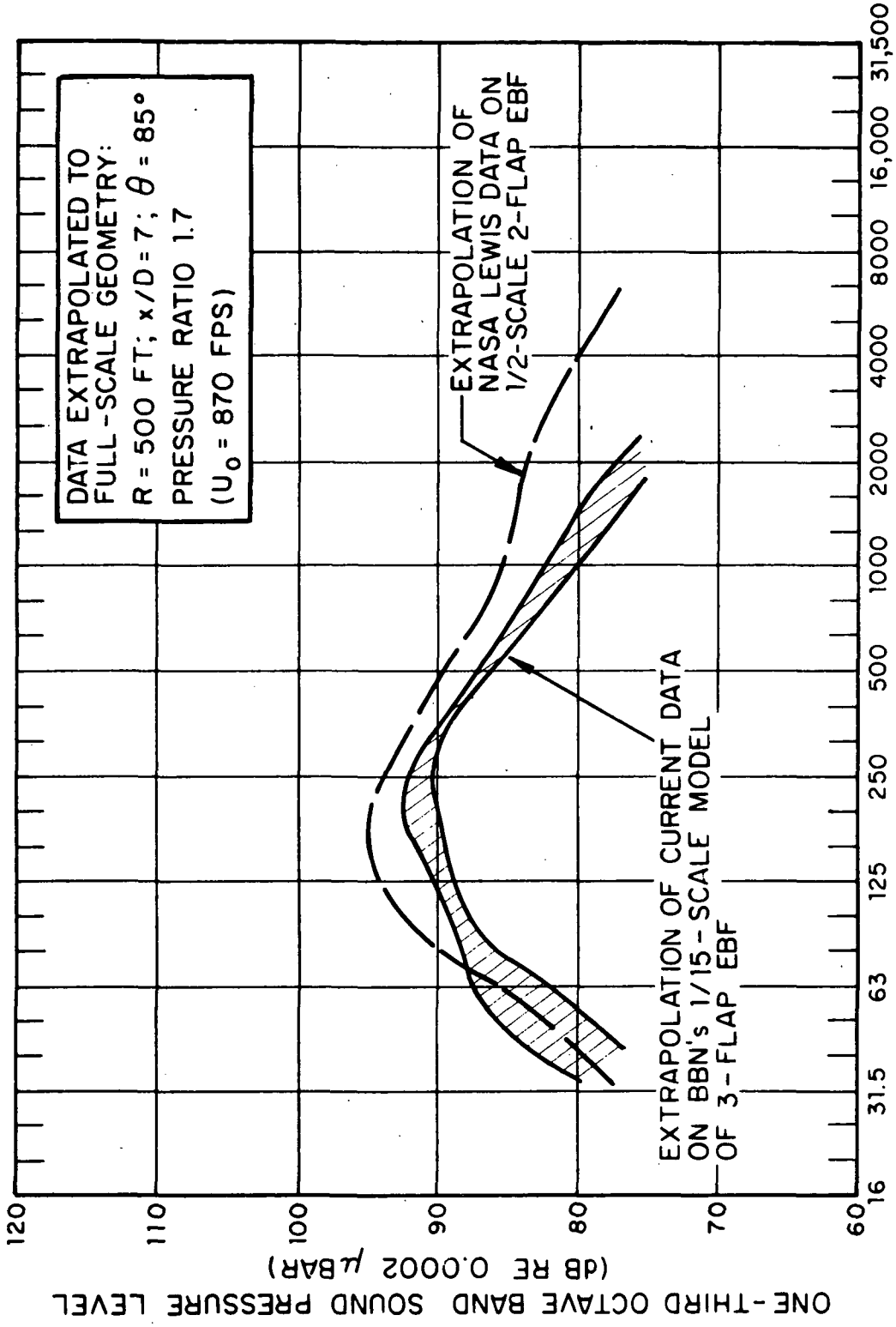

FIG. 14. COMPARISON OF EXTRAPOLATED DATA FROM PRESENT STUDY AND NASA LEWIS STUDY - APPROACH FLAP SETTING.

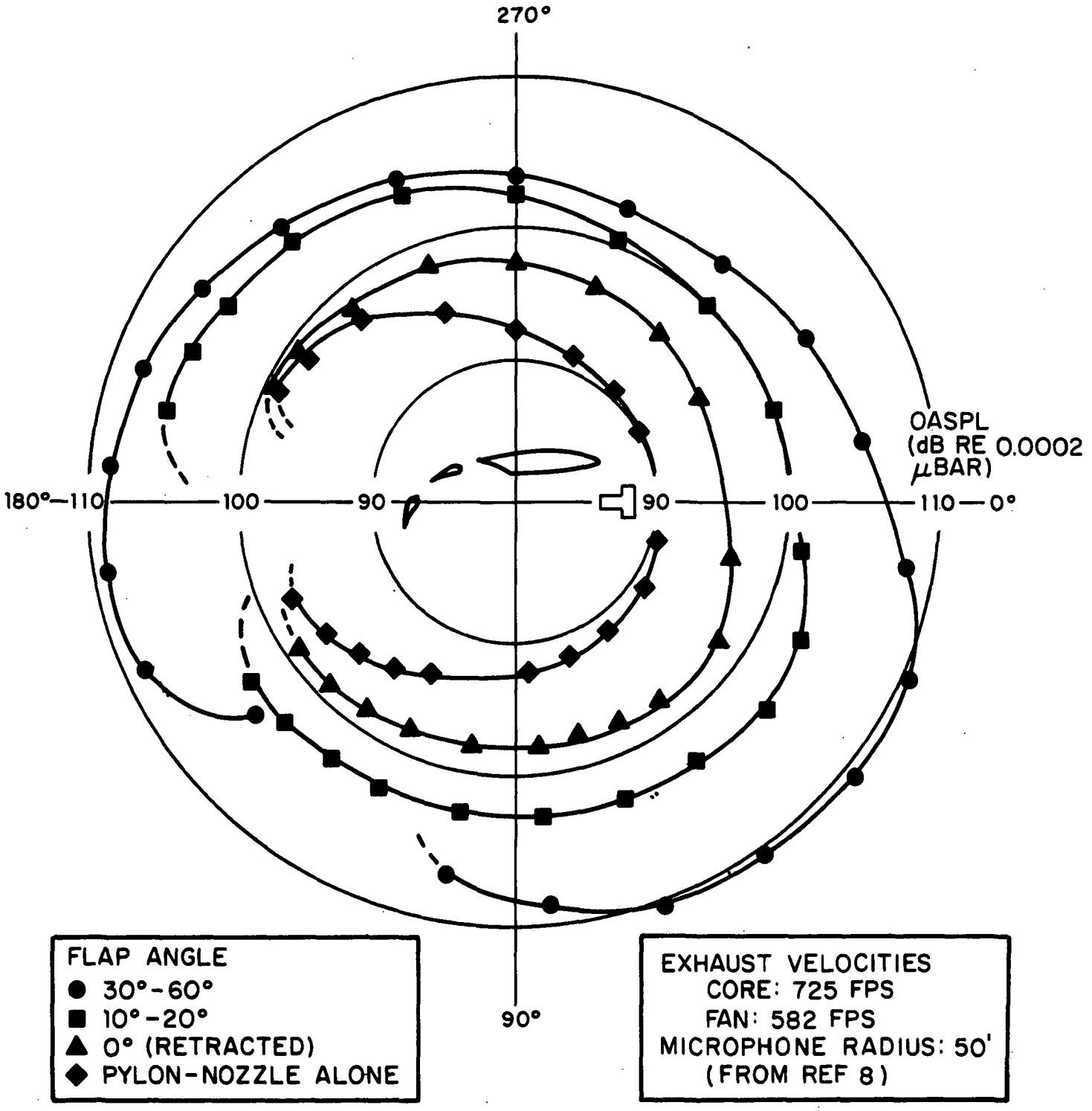

FIG. 15. DIRECTIVITY PATTERNS FROM NASA LEWIS TESTS ON 2-FLAP EBF: 3 DIFFERENT FLAP SETTINGS.

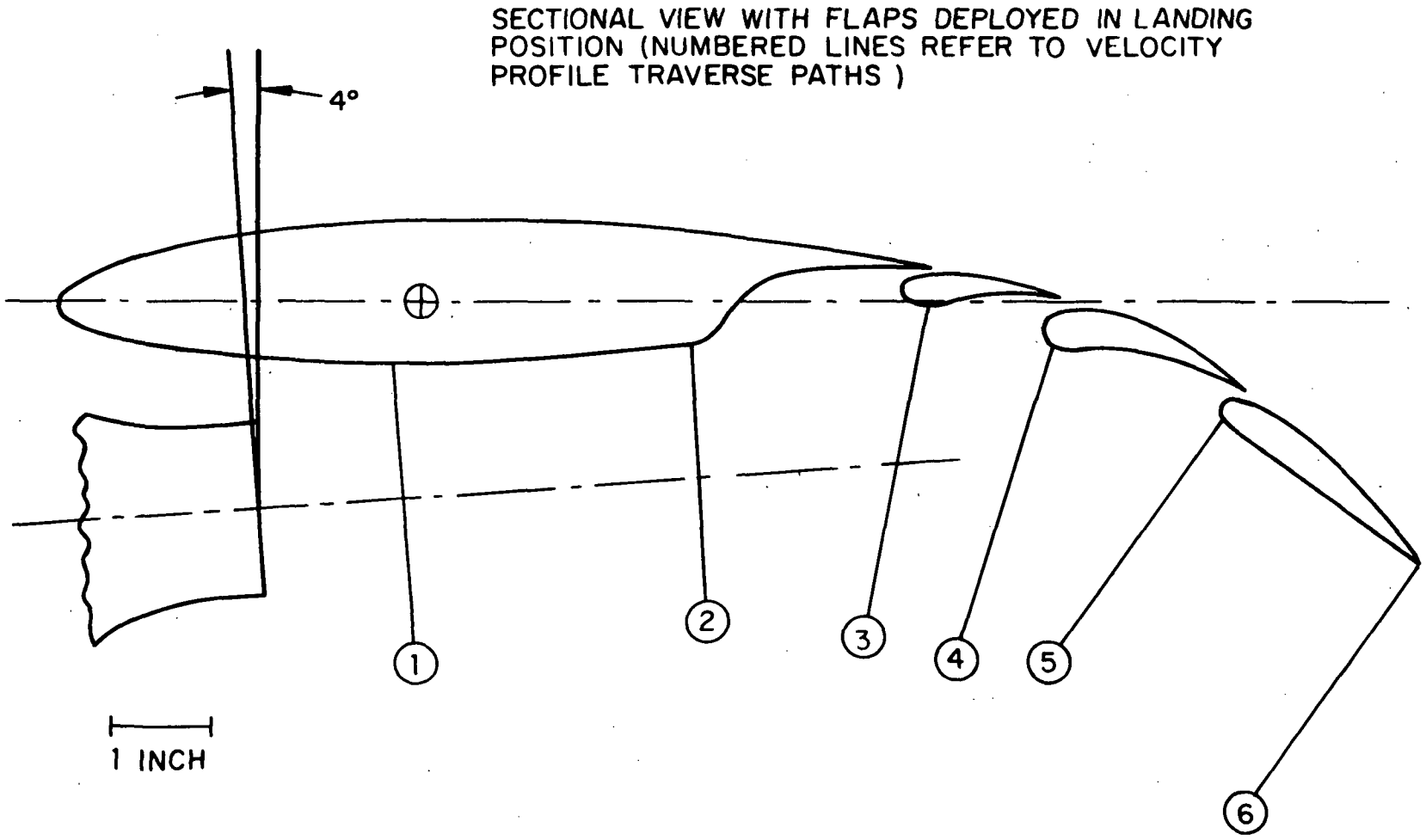

FIG. 16. LOCATION OF VELOCITY TRAVERSES.

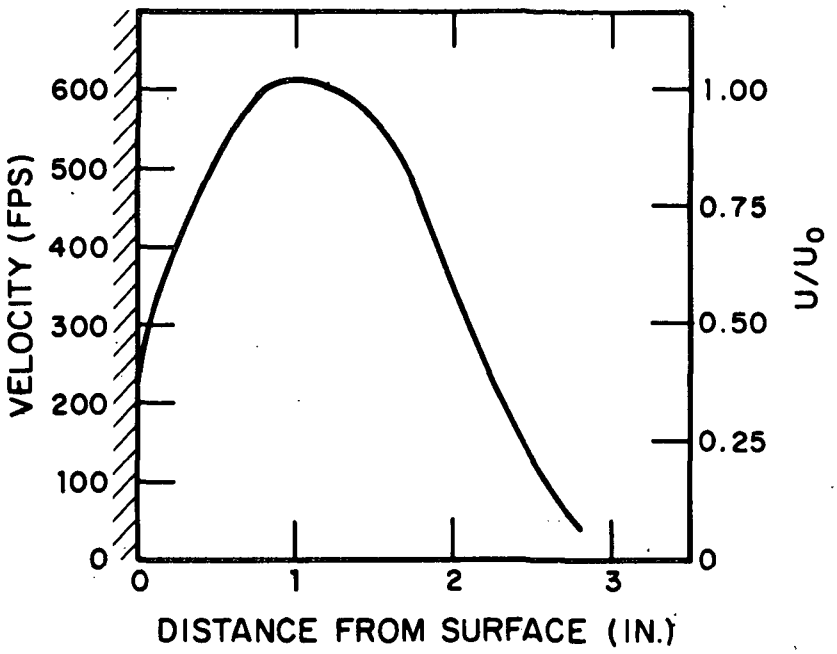

FIG. 17(a). MEASURED VELOCITY PROFILE NORMAL TO SURFACE AT TRAILING EDGE: CRUISE FLAP-SETTING.

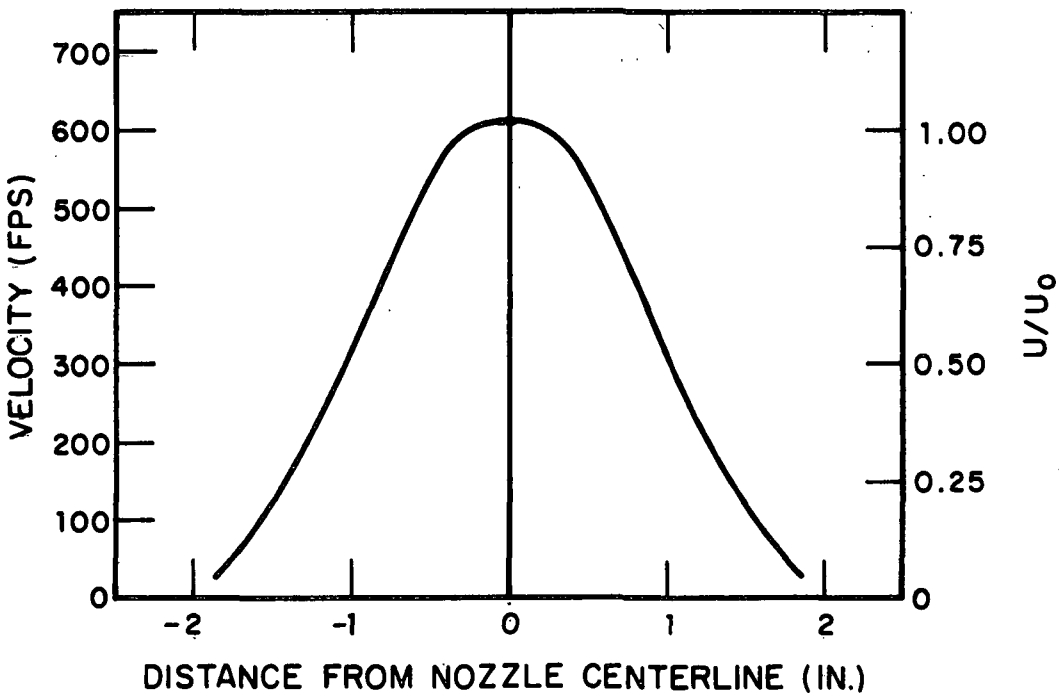

FIG. 17(b). MEASURED AXIAL VELOCITY PROFILE IN SPANWISE DIRECTION AT TRAILING EDGE OF WING: CRUISE SETTING.

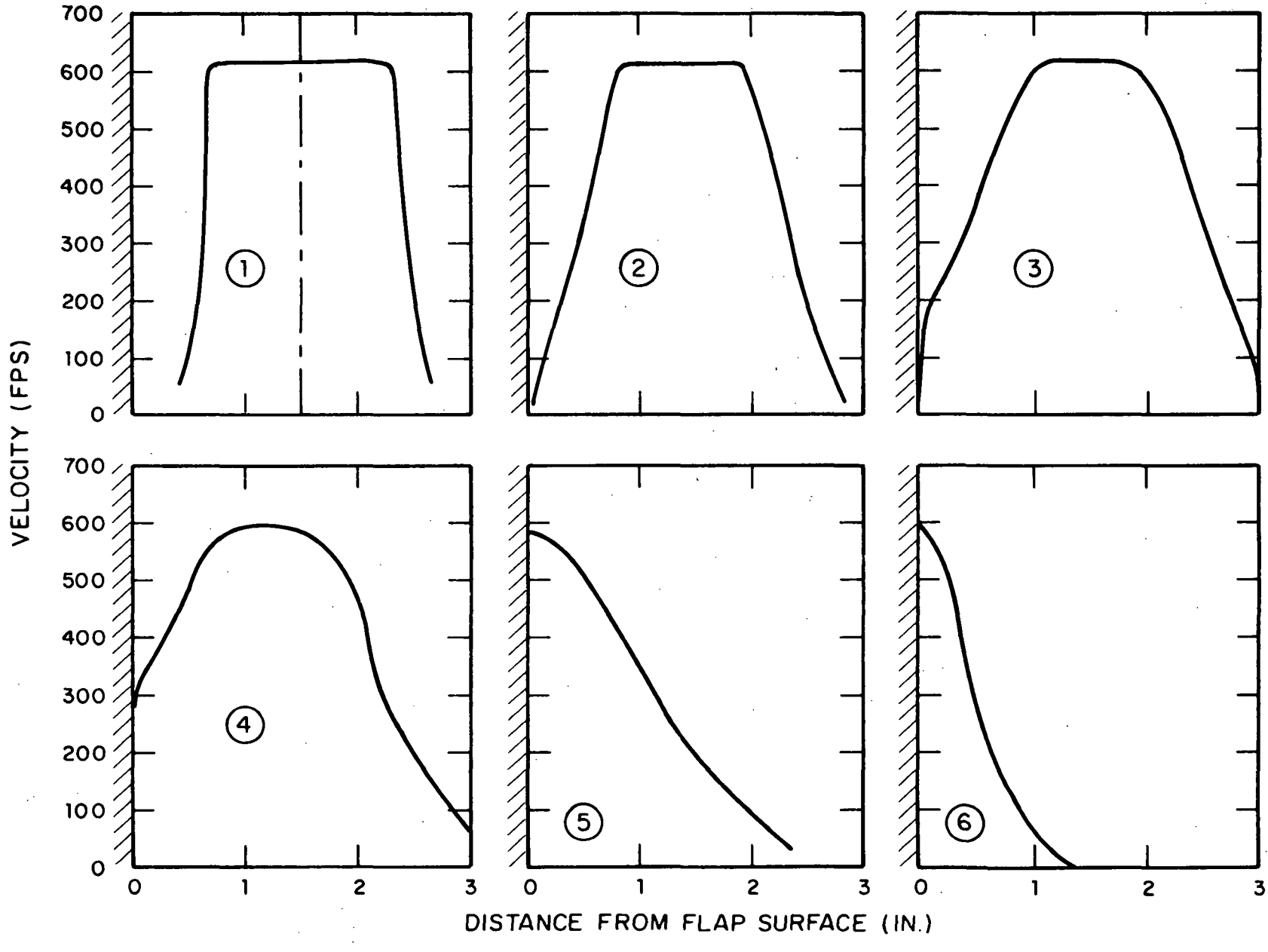

FIG. 18(a). MEASURED PROFILES NORMAL TO LOCAL FLAP SURFACE (TAKEOFF SETTING) (see Fig. 16 for traverse location and orientations).

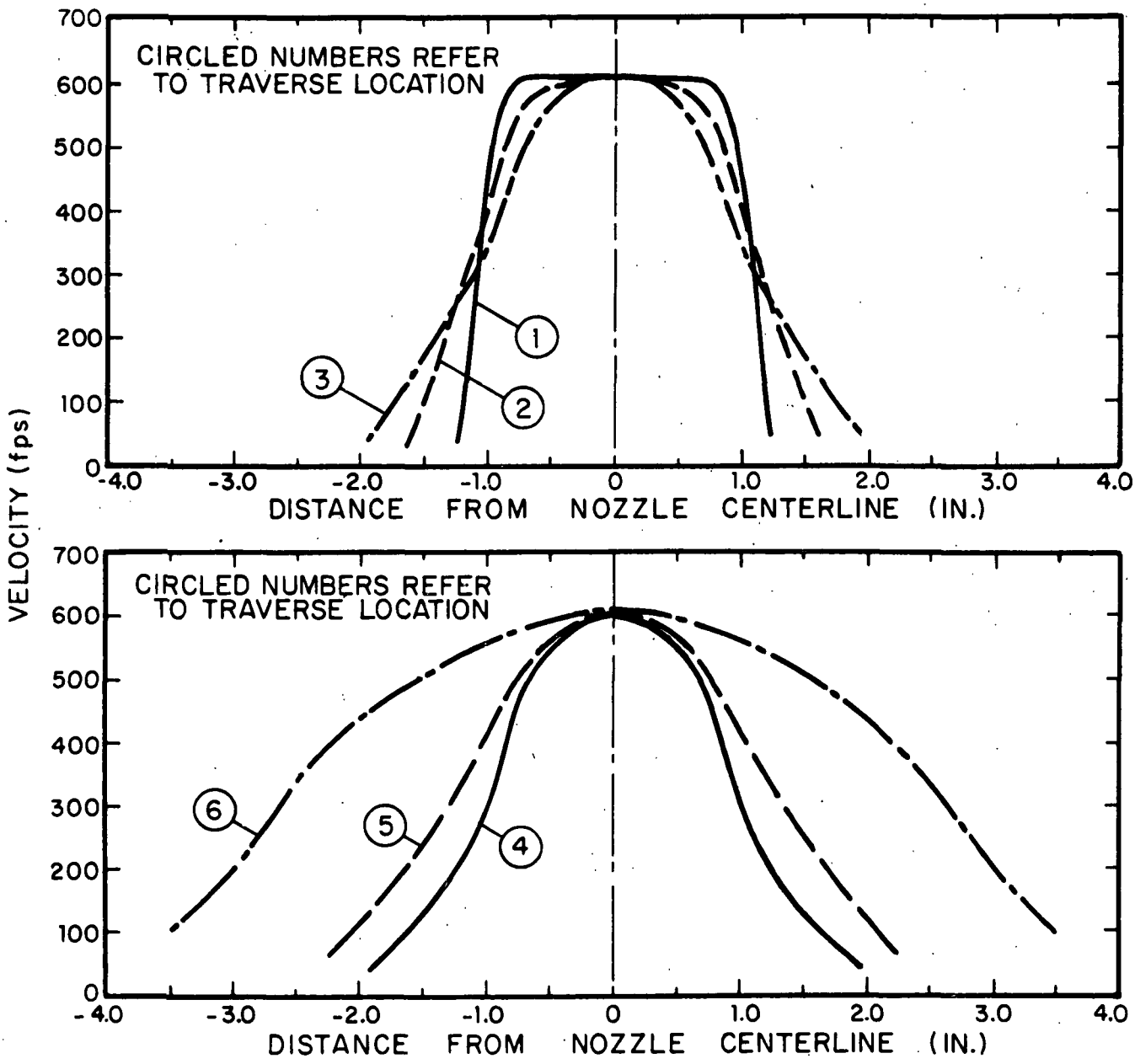

FIG. 18(b). MEASURED AXIAL VELOCITY PROFILES IN SPANWISE DIRECTION FOR THREE-FLAP EBF: TAKEOFF SETTING (see Figure 16 for gemoetry)

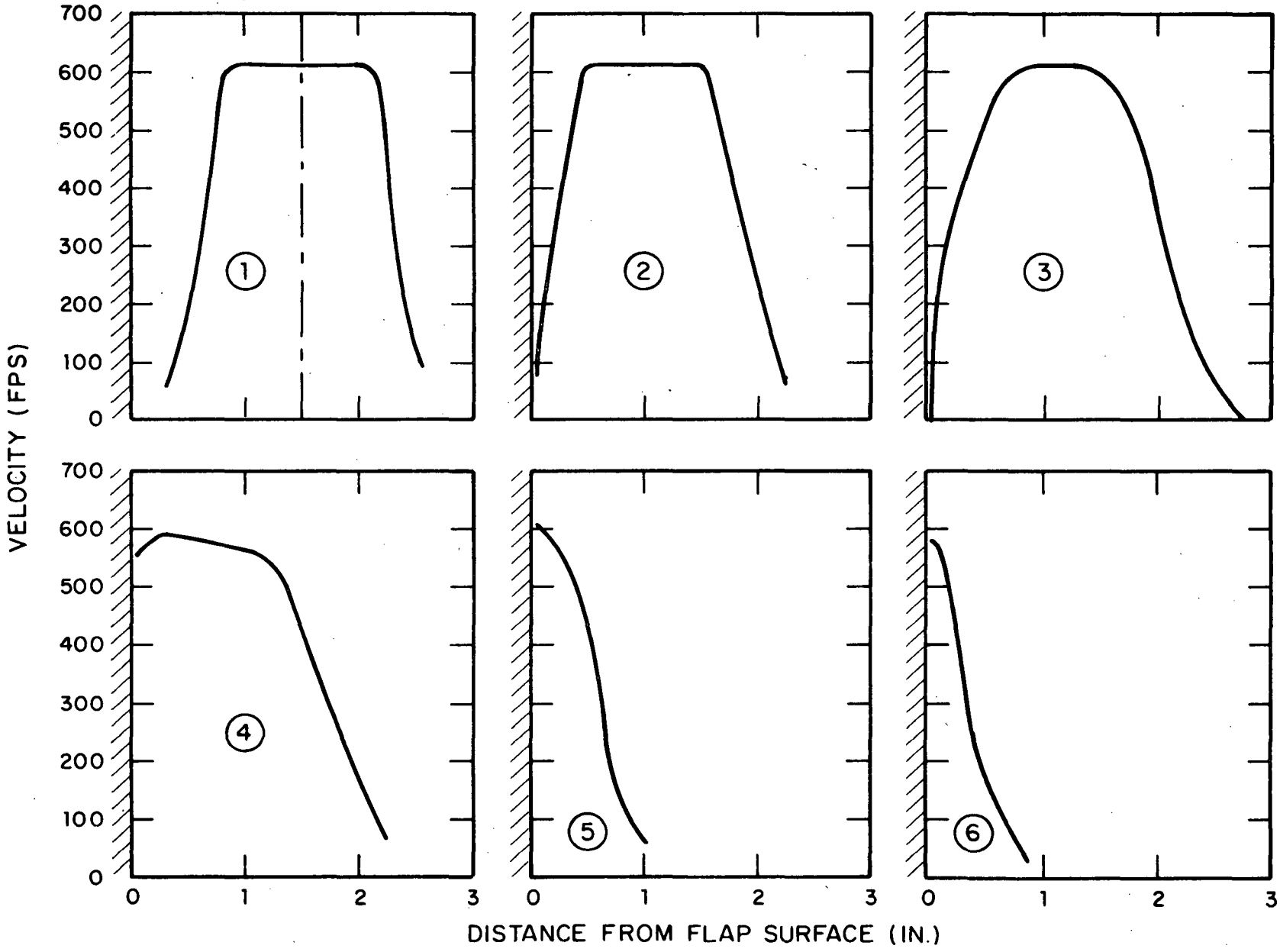

FIG. 19(a). MEASURED VELOCITY PROFILES NORMAL TO LOCAL FLAP SURFACE (APPROACH SETTING). (see Fig. 16 for traverse location and orientations.)

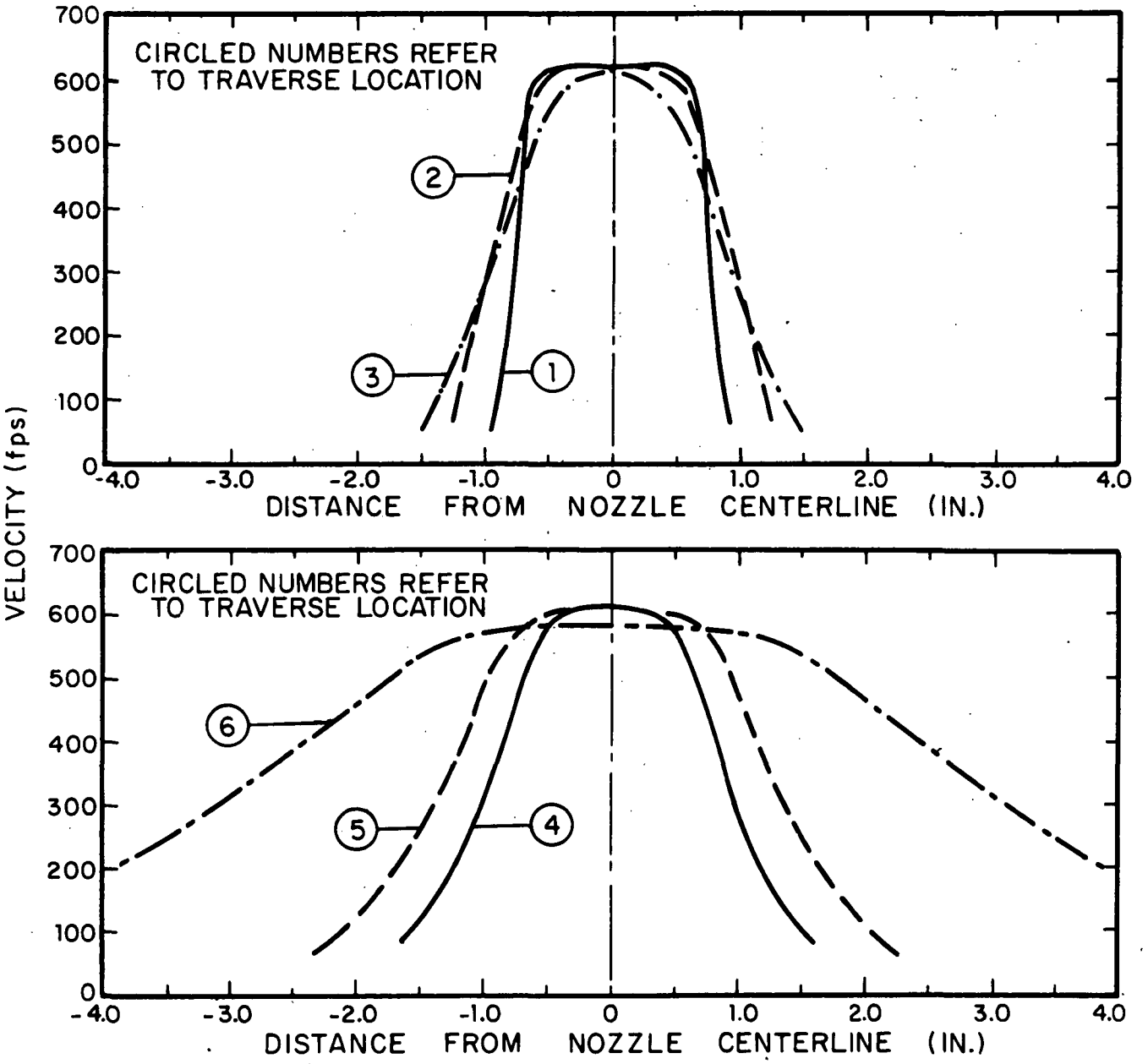

FIG. 19(b). MEASURED SPANWISE VELOCITY PROFILES FOR THREE-FLAP EBF AT APPROACH SETTING (see Figure 16 for Geometry).

deployed settings. Representative photographs are shown in Figures 20 and 21 for a model with twice the span of that used in other tests. Arrows on the photograph indicate the local flow direction.

The oil flow patterns for the takeoff flap setting (Figure 20(a) show large regions of spanwise flow and only a small region of axially-directly flow on flaps 1 and 2. From this evidence one might logically deduce that the only important sound producing regions on flaps 1 and 2 are near the flow centerline at the leading and trailing edges of these flaps (since the oil flow gives no information on velocity magnitudes, additional measurements should yield further information on important source areas). The flow at the leading and trailing edges of the third flap is seen to be largely axial over a large part of the span, thus leading one to deduce that a large widely distributed source region is found there. From Figure 21, similar observations may be made for the approach setting.

The velocity profile data indicate that the most extensive source region is apparently the leading and trailing edges of the third flap.

Surface pressure fluctuations. Measurements of surface pressures over the flap surfaces can give a strong indication of the possible extent of the sound-producing region and can also define those areas of the flaps contributing most significantly to the various parts of the sound spectrum. In this investigation, point pressure spectra were measured with a BBN 0.1-in. pressure sensor which was mounted flush to the lower surfaces of the flaps at the locations shown in Figure 22.

Since the incident flow field was expected to be weakly dependent upon Reynolds and Mach number in the range of interest, the fluctuating pressures at various points on the flaps should vary in constant proportion to the mean dynamic pressures regardless of the exit velocity. Similarly, the spectra of fluctuating pressures should shift toward high frequencies linearly with increasing exit velocity. Thus, once such scaling is established, detailed surveys of pressure spectra on the flaps can be carried out at one intermediate velocity.

The procedure for normalization of fluctuating pressure level (FPL) is as follows:

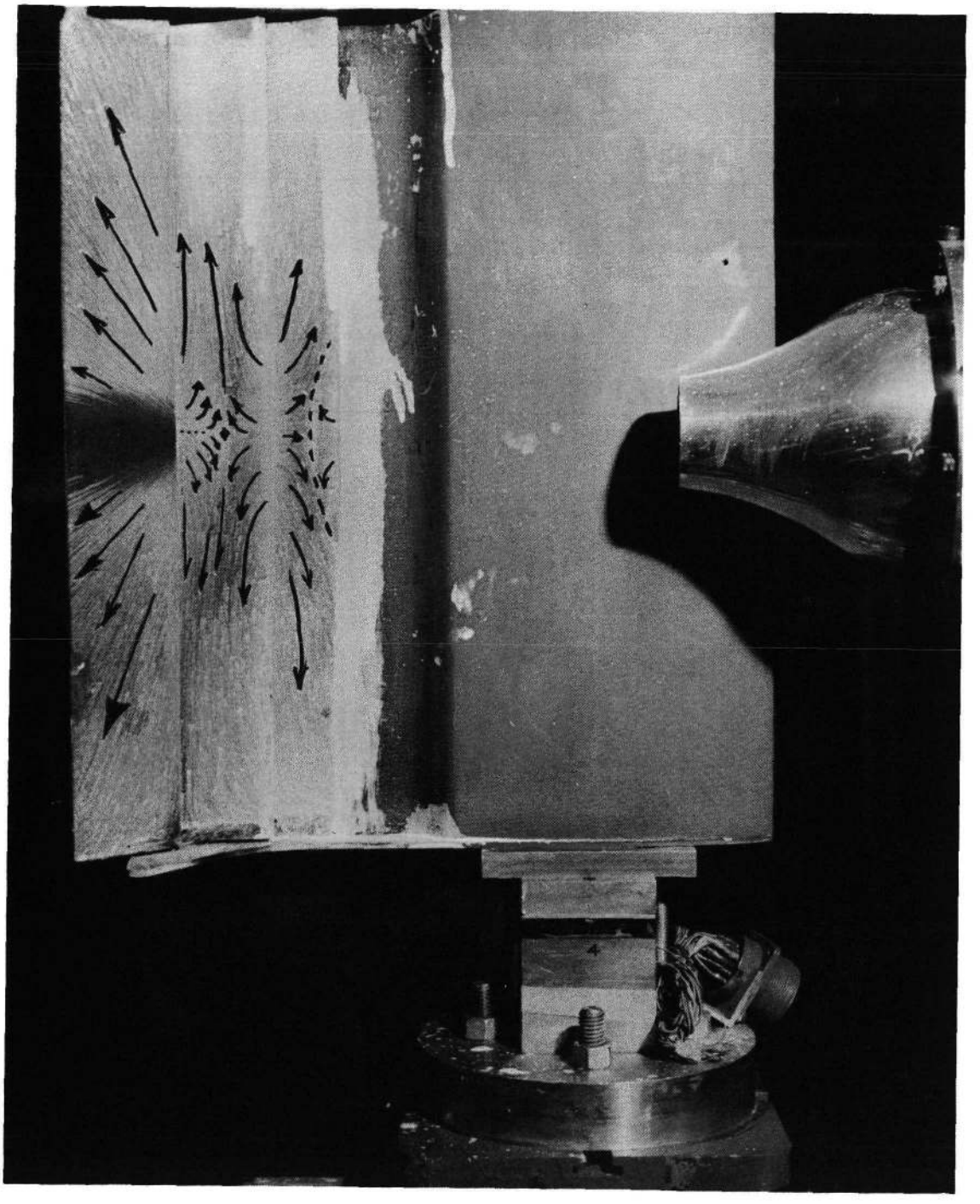

FIG. 20(a). FLOW VISUALIZATION OF LOWER SURFACE OF FLAPS: TAKEOFF SETTING (ARROWS INDICATE FLOW DIRECTION)

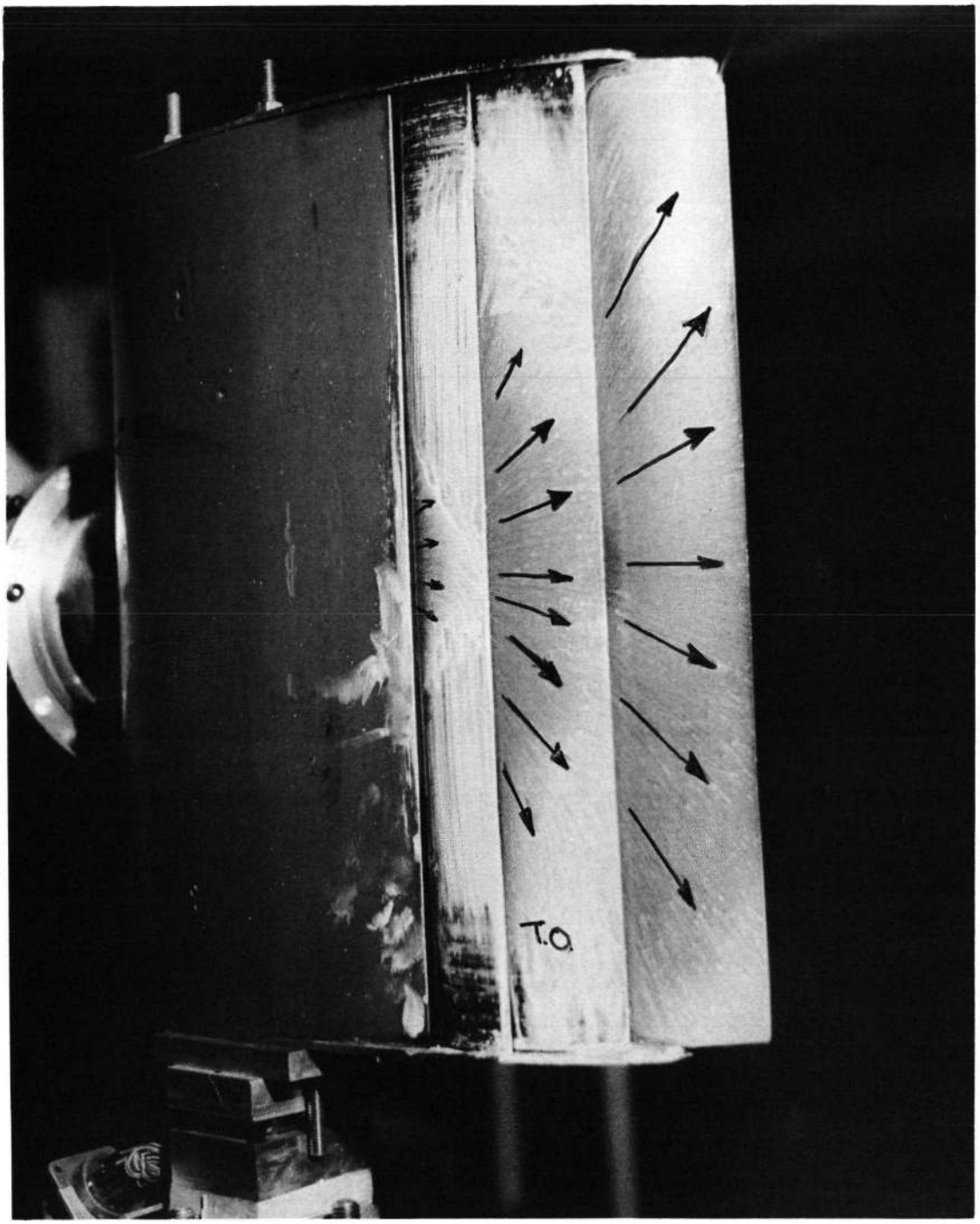

FIG. 20(b). FLOW VISUALIZATION OF UPPER SURFACE OF FLAPS: TAKEOFF SETTING (ARROWS INDICATE FLOW DIRECTION).

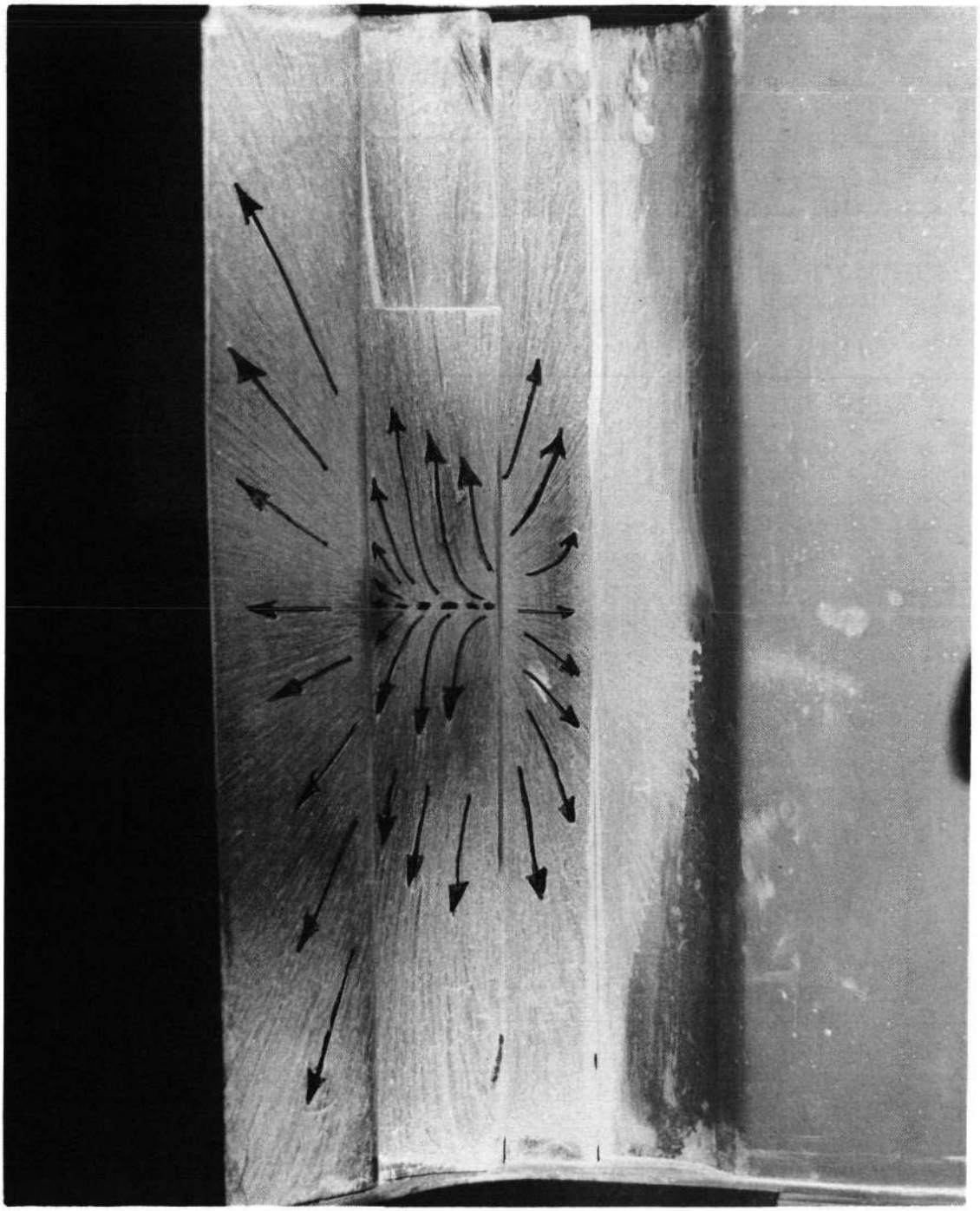

FIG. 21(a). FLOW VISUALIZATION OF LOWER SURFACE OF FLAPS: APPROACH SETTING (ARROWS INDICATE FLOW DIRECTION).

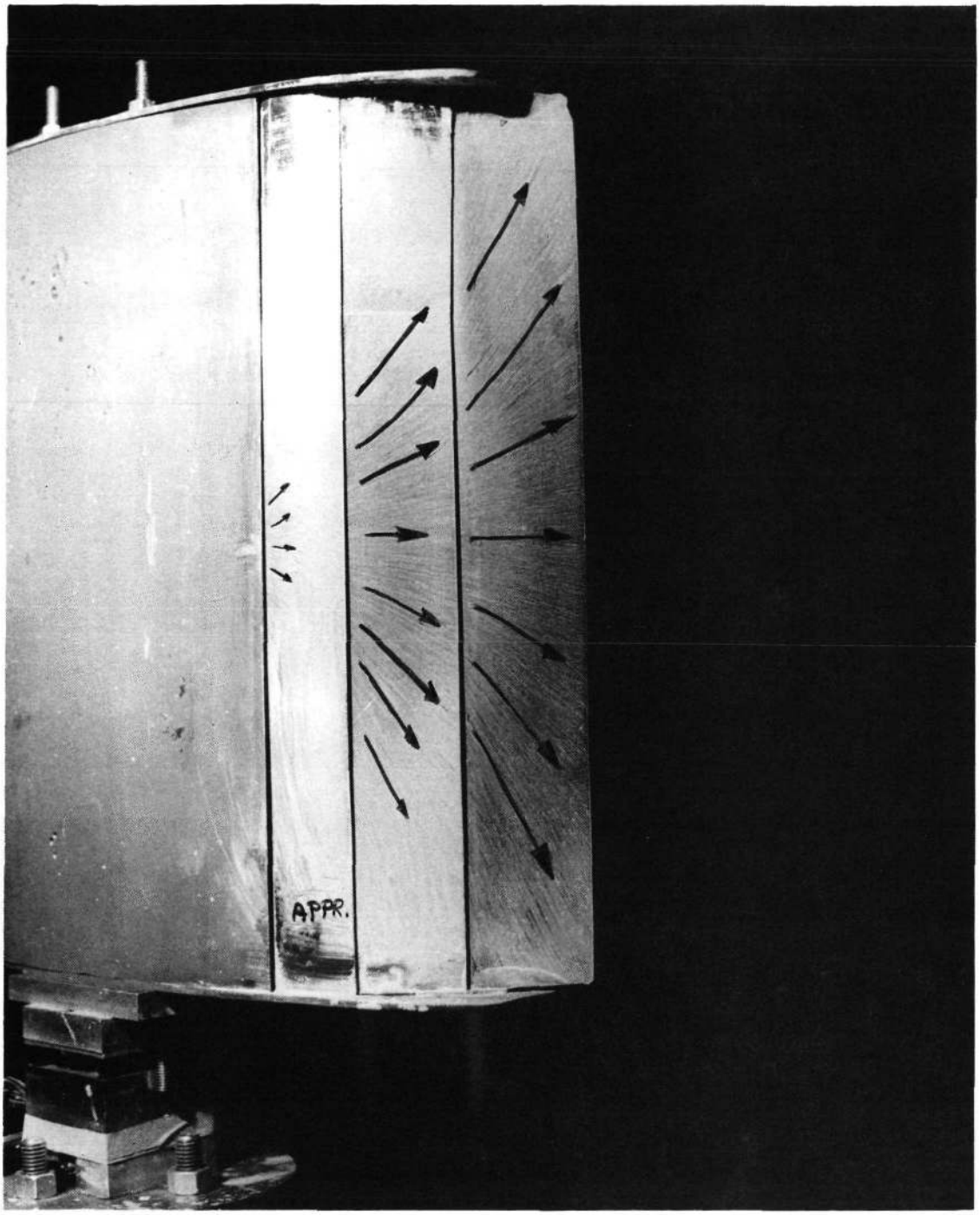

FIG. 21(b). FLOW VISUALIZATION OF UPPER SURFACE OF FLAPS APPROACH SETTING (ARROWS INDICATE FLOW DIRECTION).

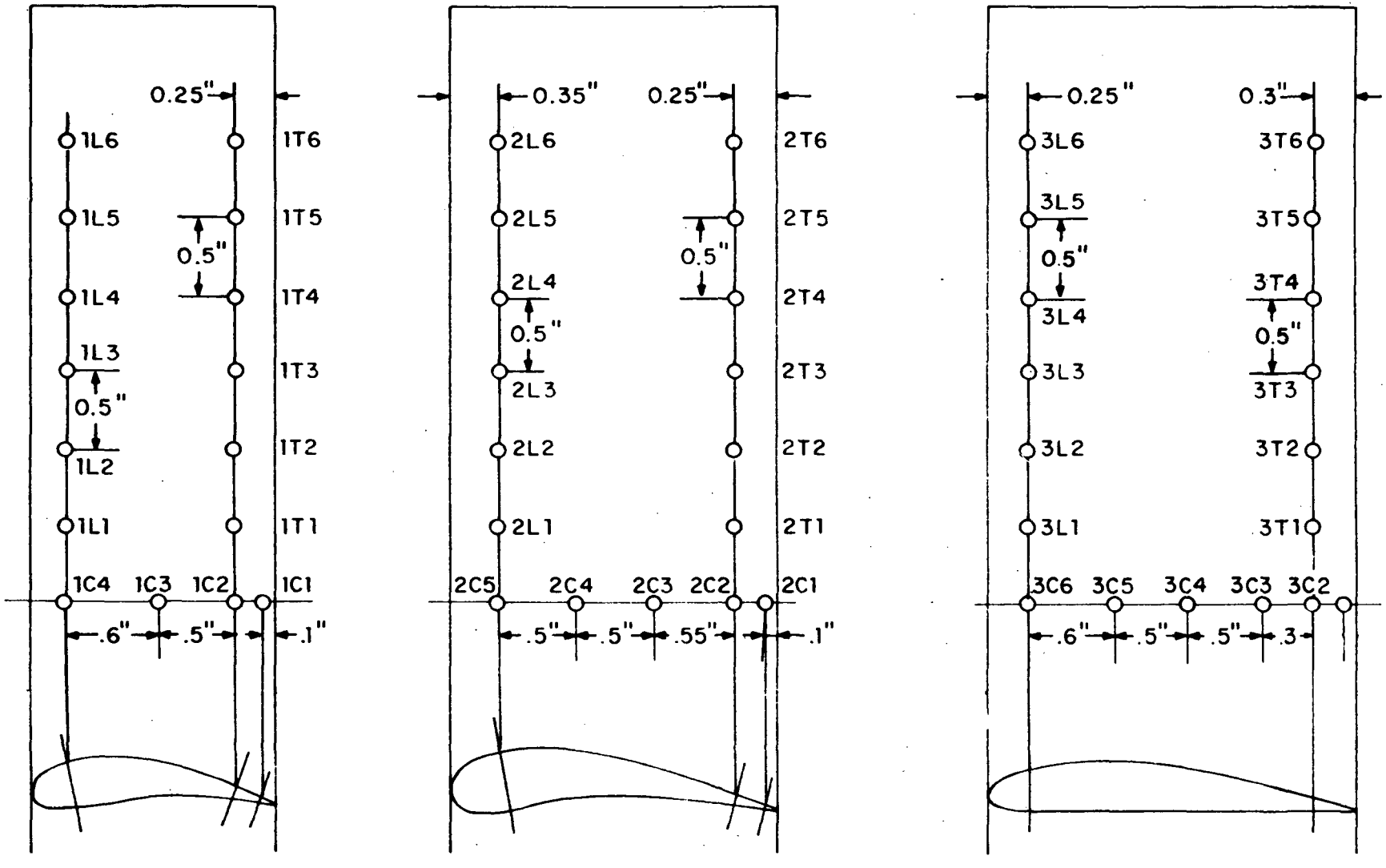

FIG. 22. SCHEMATIC OF SURFACE PRESSURE SENSOR LOCATIONS & DESIGNATIONS (1/15 SCALE EBF)

$$FPL_{norm} = 20 \log(p/q) = 20 \log(p/p_{ref}) + 20 \log p_{ref} + 20 \log q, \quad (19)$$

where $q = 1/2\ \rho U^2$.

For $p_{ref} = 2 \times 10^{-4}$ μbar one arrives at a simple engineering equation for the normalization:

$$FPL_{norm} = FPL_{measured} - 69.1 - 40 \log U \left[\frac{ft}{sec}\right]. \quad (20)$$

The validity of the above normalization is demonstrated in Figures 23 and 24.

Figure 23 duplicates the output of the one-third octave band analyzer for four different velocities. Figure 24 shows the same curves after they were normalized by use of Eq. 20.

The above data were taken at pressure-sensor location 3C6 when the flaps were in approach setting.

Overall "point" FPL for some representative locations on the flaps (approach flap setting) are shown in Table I.

TABLE I. TYPICAL FLUCTUATING PRESSURE LEVELS ON FLAPS

Pressure-Sensor Location	OAFPL for U_0 = 400 fps (dB re 0.0002 μbar)
1C3	155.7
2C3	139.8
3C3	150.7
1T6	143.0
2T6	143.4
3T6	147.3

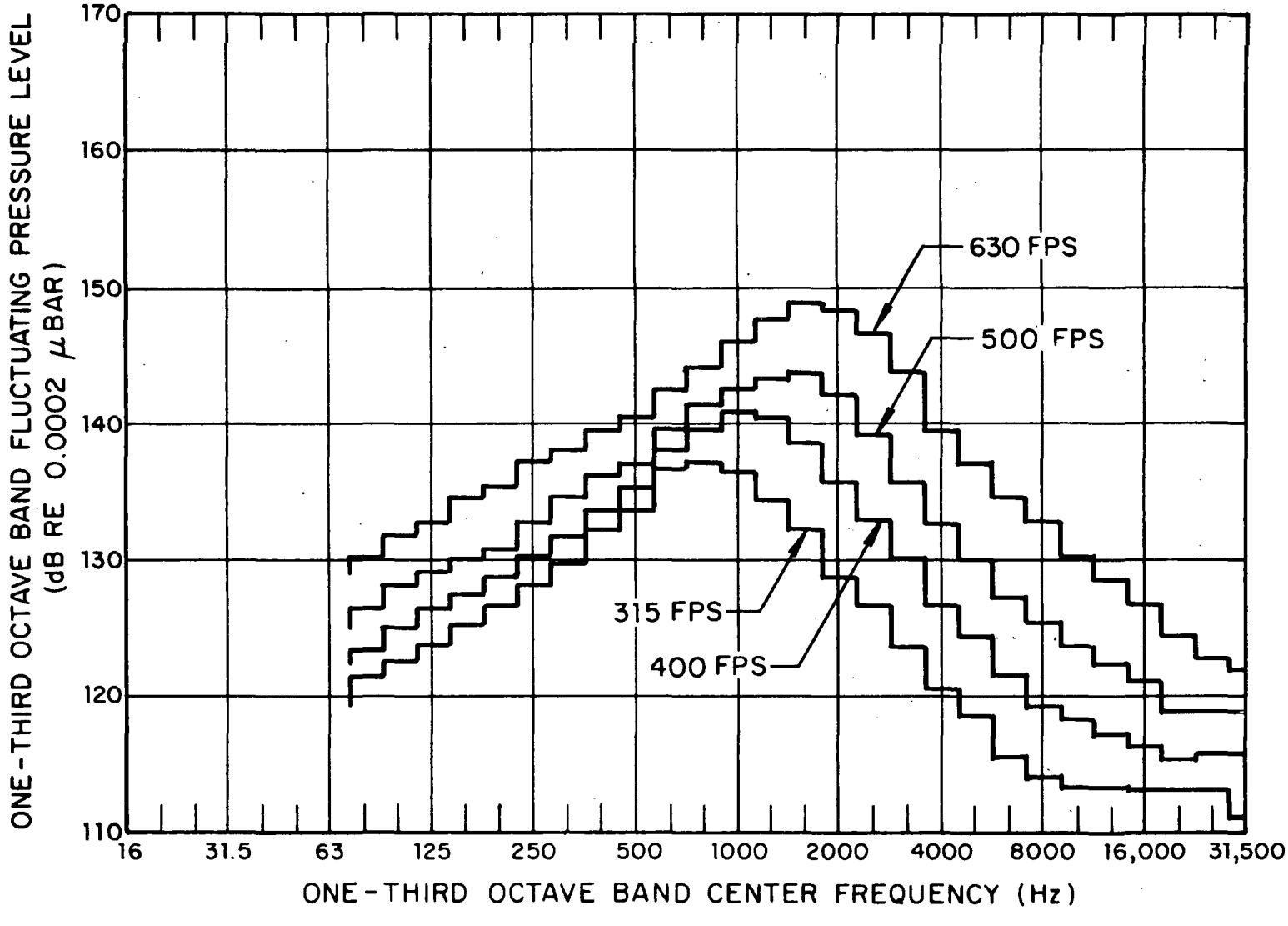

FIG. 23. TYPICAL ONE-THIRD OCTAVE BAND "POINT" PRESSURE SPECTRA vs VELOCITY: APPROACH FLAP SETTING.

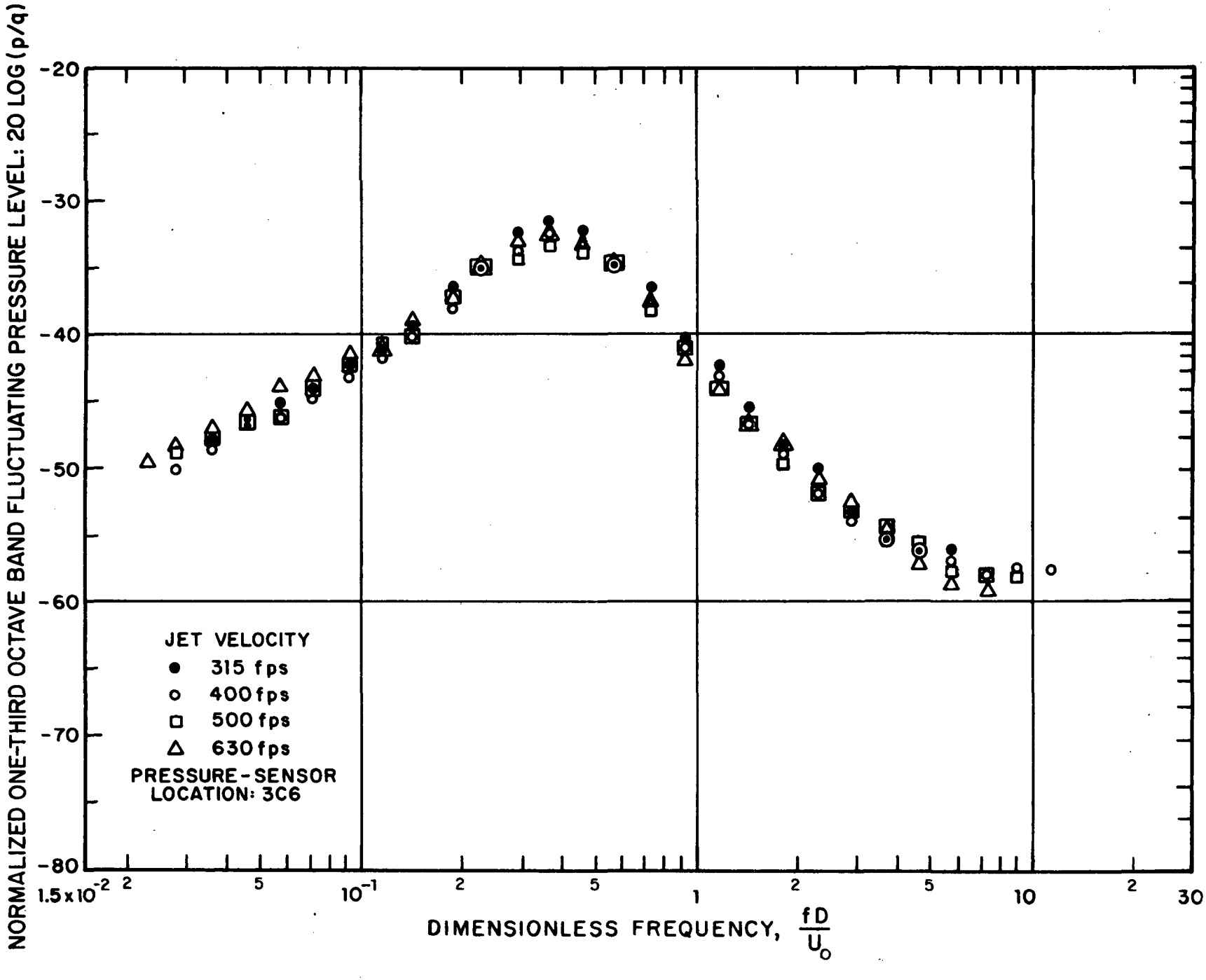

FIG. 24. NORMALIZED THIRD OCTAVE BAND "POINT" PRESSURE SPECTRA FOR DIFFERENT VELOCITIES: APPROACH FLAP SETTING.

The surface pressure data on all three flaps show a strong dependence on flap setting and location with respect to the center line of the flow. High levels were observed in all cases as shown in Figures B.1-B.18 (Appendix B).

For the takeoff flap setting (0°-20°-40°), the highest levels observed were near the trailing edges of the second (20°) flap at the leading edge of the third flap, and along a relatively large part of the trailing edge of the third (40°) flap. For the approach setting (15°-35°-50°), generally higher levels were noted and again the highest levels appeared near the trailing edges. On the first (15°) flap, the levels fell off quickly away from the flow centerline (Figures B.10-B.12). On the second (35°) flap, the highest levels were at the trailing edge but a significant distance from the centerline (Figures B.13-B.15). Considerably greater spanwise extent of high level pressure fluctuations exists on flap 2 than on flap 1.

Flap 3 (50°) is subjected to the highest pressure levels, and a very large span of the trailing edge was immersed in high level fluctuating pressures (Figures B.16-B.18).

Static lift, drag, and pitching moment. The static lift, drag, and moment resulting from deployment of the flaps were determined (without simulation of forward speed effects) using an eight-element six-degree-of-freedom strain gauge force balance (see Figure 2).

The coordinate system to which all measurements are referred is shown in Figure 25. The lift, drag, and pitching moment for the takeoff and approach flap settings are shown in Figures 26, 27, and 28. These curves show that lift and pitching moments vary in direct proportion to the dynamic pressure as expected; however, the drag increased at a rate slightly less than q_0A_0 the exit dynamic pressure times exit area. This data will be used in the next section as a basis for evaluating aerodynamic performance penalties associated with the modifications implemented for noise control purposes. (The pitching moment was normalized using the distance from the center of the force balance to the leading edge of the third flap - see Fig. 25 - and the usual q_0A_0).

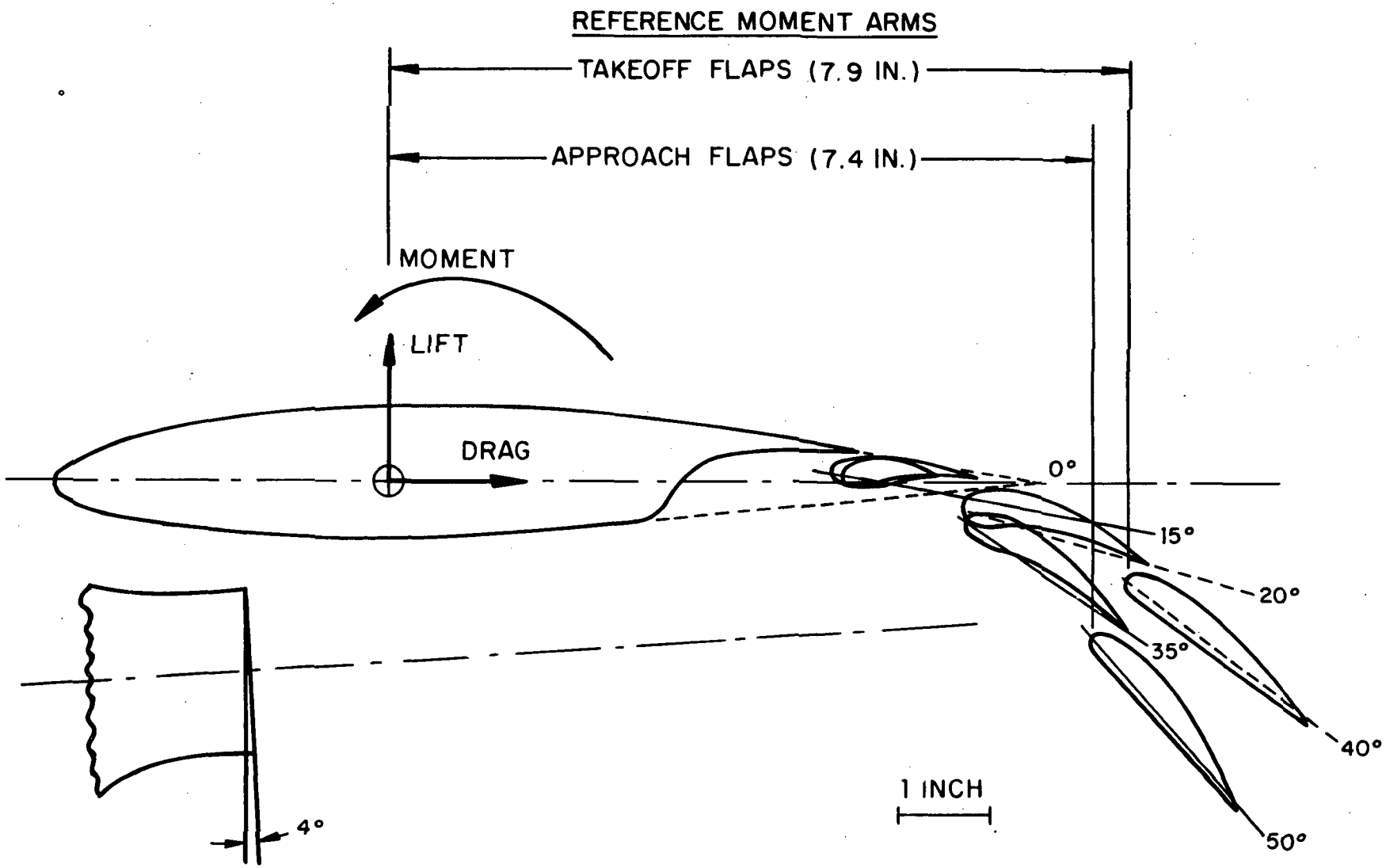

FIG. 25. LOCATION OF FORCE BALANCE AND DEFINITION OF REFERENCE QUANTITIES.

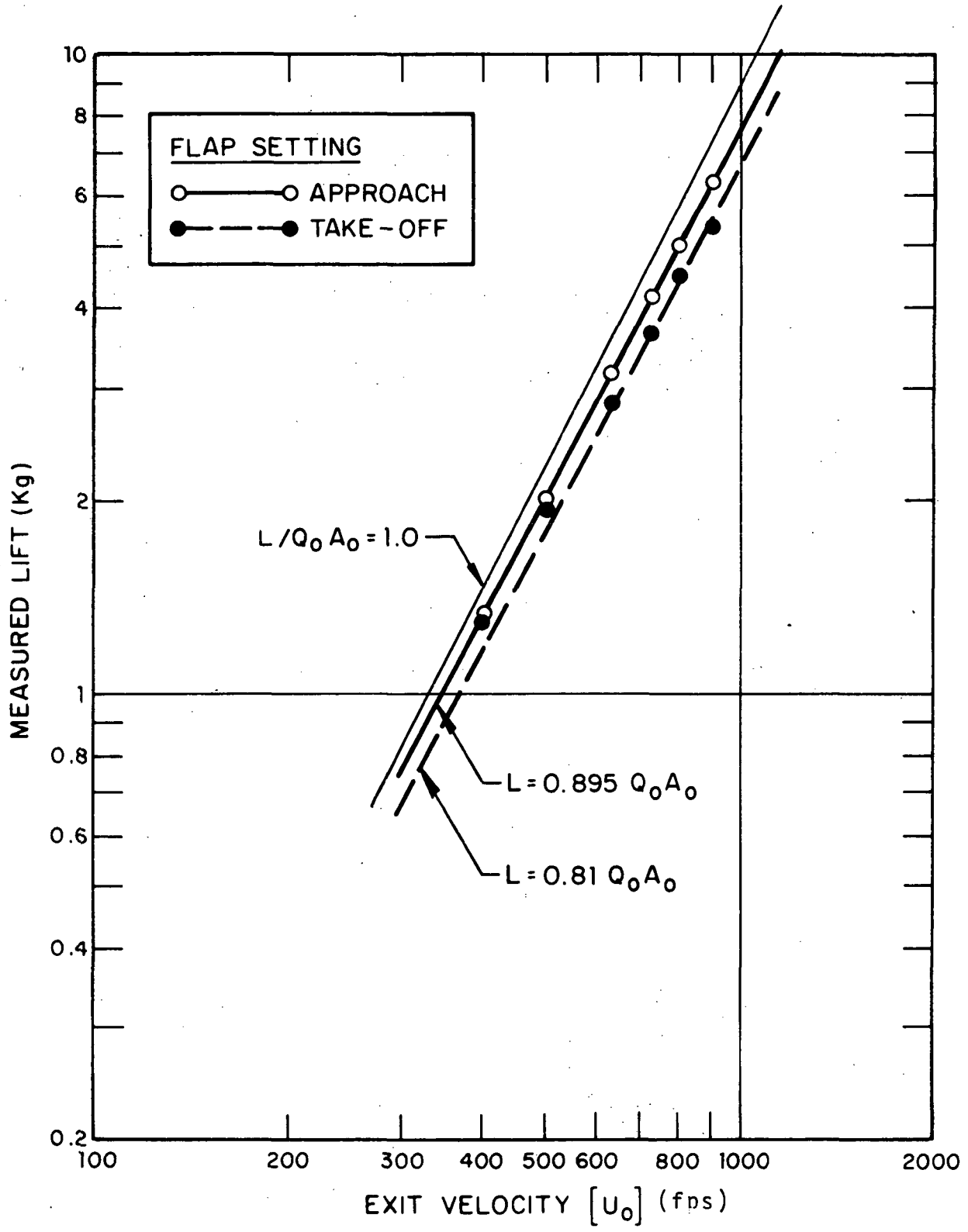

FIG. 26. MEASURED LIFT vs VELOCITY FOR UNMODIFIED FLAPS.

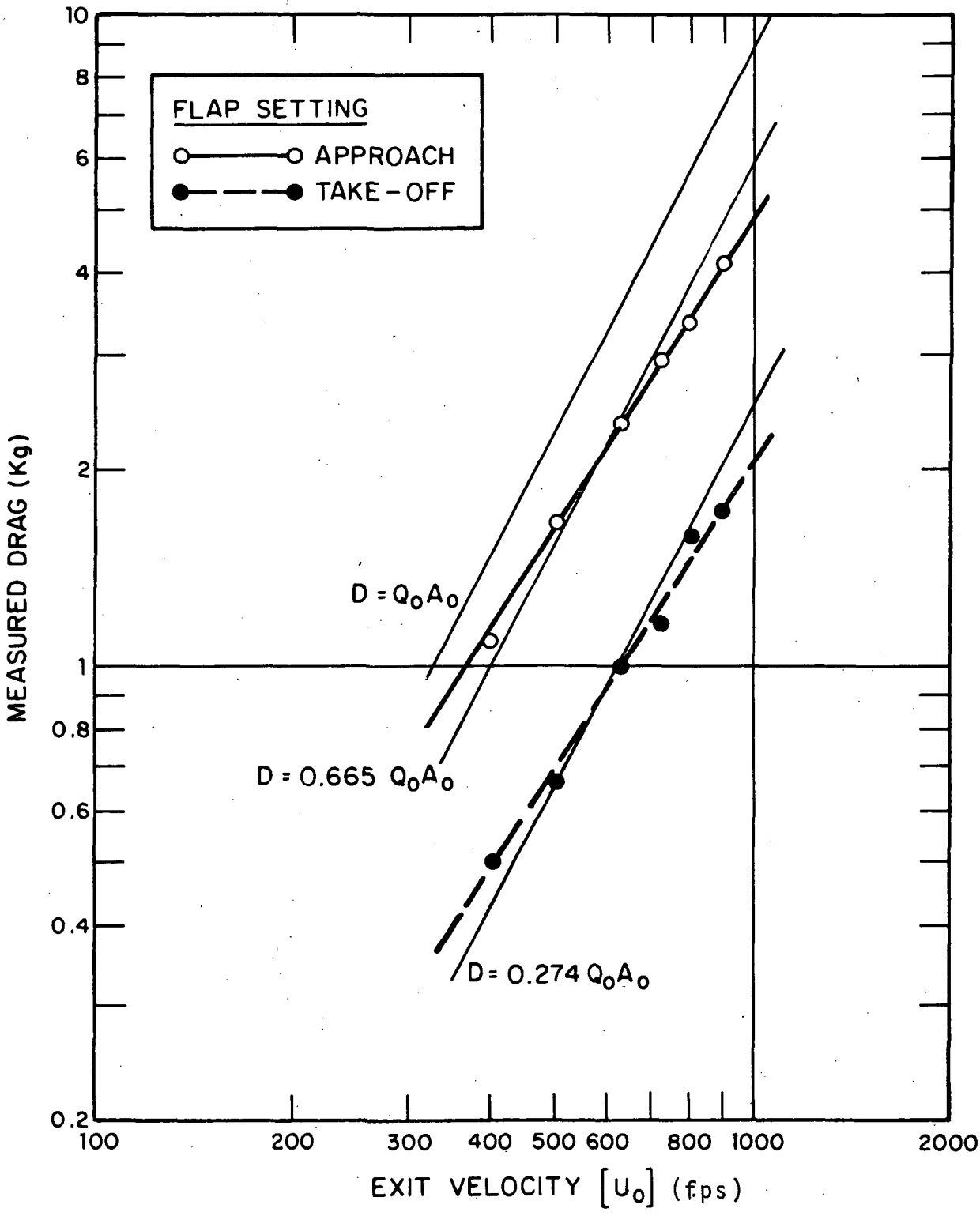

FIG. 27. MEASURED DRAG vs VELOCITY FOR UNMODIFIED FLAPS.

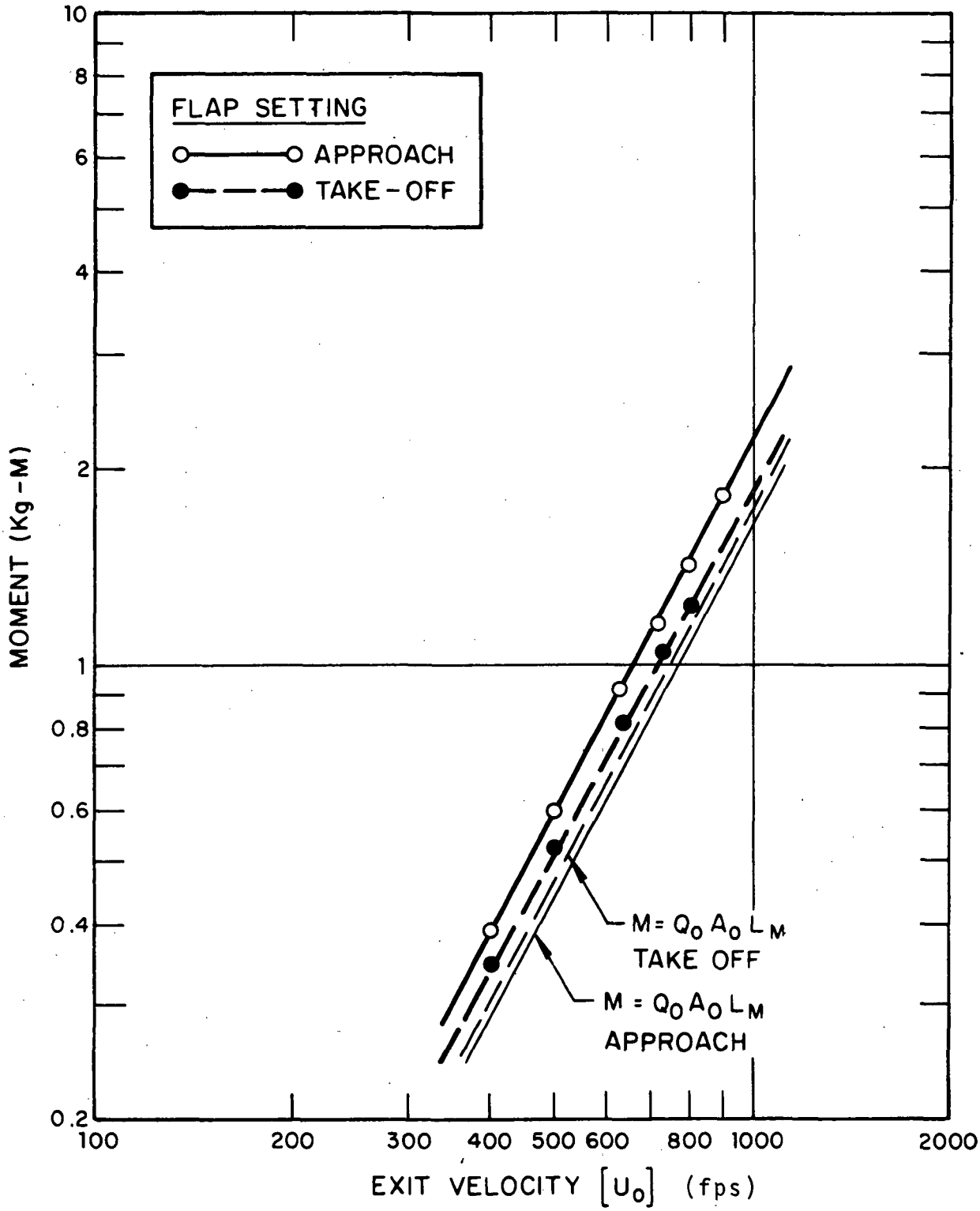

FIG. 28. MEASURED PITCHING MOMENT vs VELOCITY FOR UNMODIFIED FLAPS.

SUMMARY OF OBSERVED NOISE REDUCTIONS AND AERODYNAMIC PERFORMANCE PENALTIES ASSOCIATED WITH VARIABLE IMPEDANCE SURFACES

This section summarizes exploratory experiments to assess the feasibility of (1) using variable impedance surfaces to modify the acoustic transduction process associated with edge noise and (2) modifying the jet flow field with mesh grids (screens were used) to alter length scales and turbulence intensities.

Description of Hardware

The variable impedance concept relies heavily on the ability to treat the surfaces appropriately. In the time period available for this study, no materials having both spatially varying impedance and reasonable structural integrity were located. Therefore, a fiber metal sheet of uniform impedance was used and gross effects were obtained by either punching holes in the sheet, or by varying the air gap behind it. The material used has a flow resistance of approximately 10 to 15 Rayls and was approximately 0.030 in. thick. The material was either applied to the leading and trailing edges of the flaps (which were hollowed out to about 1/4-chord in each case) or deployed as a continuous sheet over the solid or "porous" flaps. These configurations are illustrated schematically in Figure 29.

The concept of reducing eddy scales and turbulence intensity with mesh grids placed in the jet was investigated for commercially available mesh screens - either "fine mesh" (15 meshes per inch, 70% open area) or "coarse mesh" (4 meshes per inch, 81% open area). The screen was deployed at a number of locations as shown in Figure 30.

Acoustic Data

The noise reduction achieved using both the variable impedance surface and the mesh grid techniques was found to be very sensitive to details of the various configurations. Figures 31 and 32 compare measured data at the 90° position for the takeoff flap setting for variable impedance surfaces and mesh grids respectively. Figures 33 and 34 present similar data for the approach flap setting. The noise reductions were found to be largely independent of observation angle as is illustrated by Figures 35 a-d.

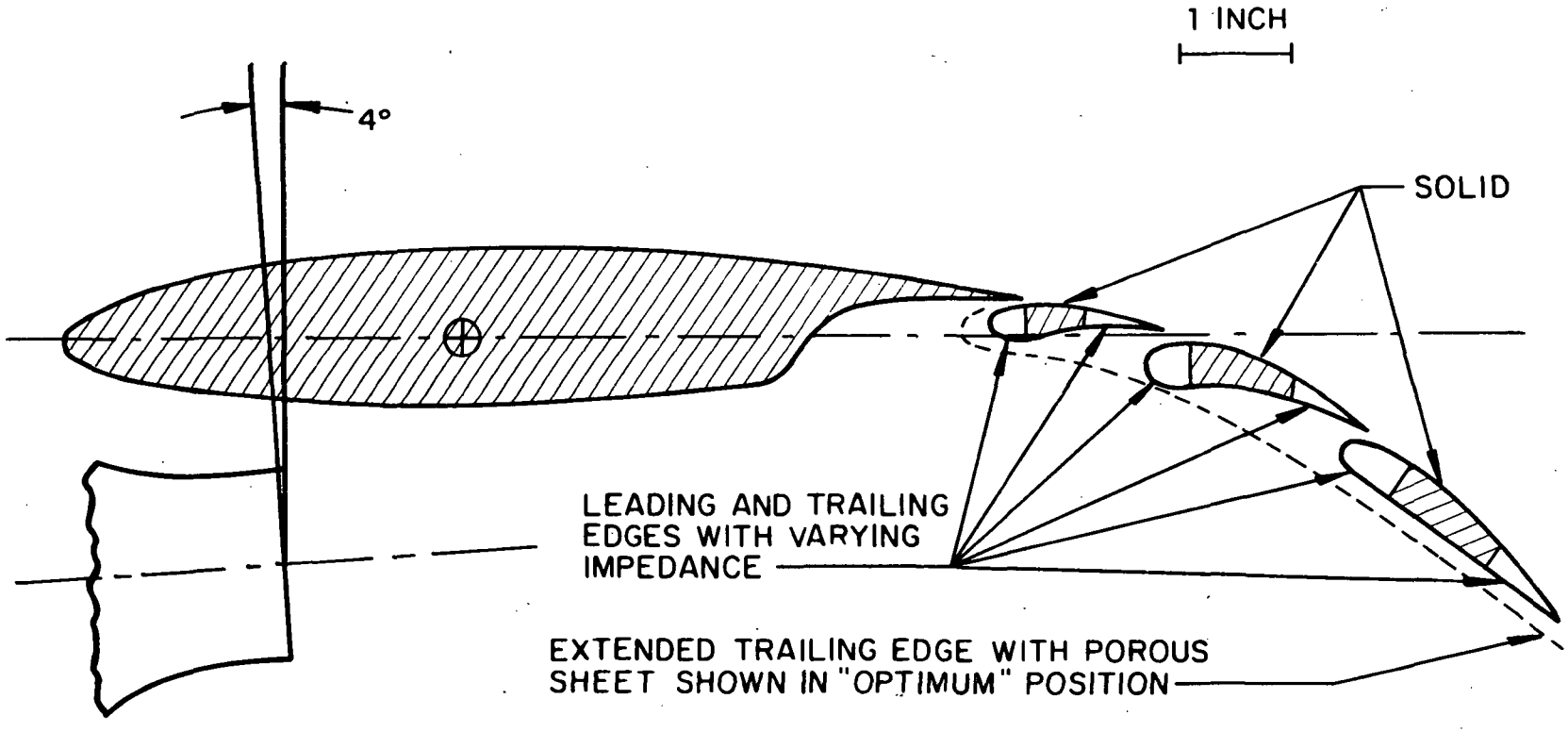

FIG. 29. SCHEMATIC OF DIFFERENT VARIABLE IMPEDANCE FLAP CONFIGURATIONS.

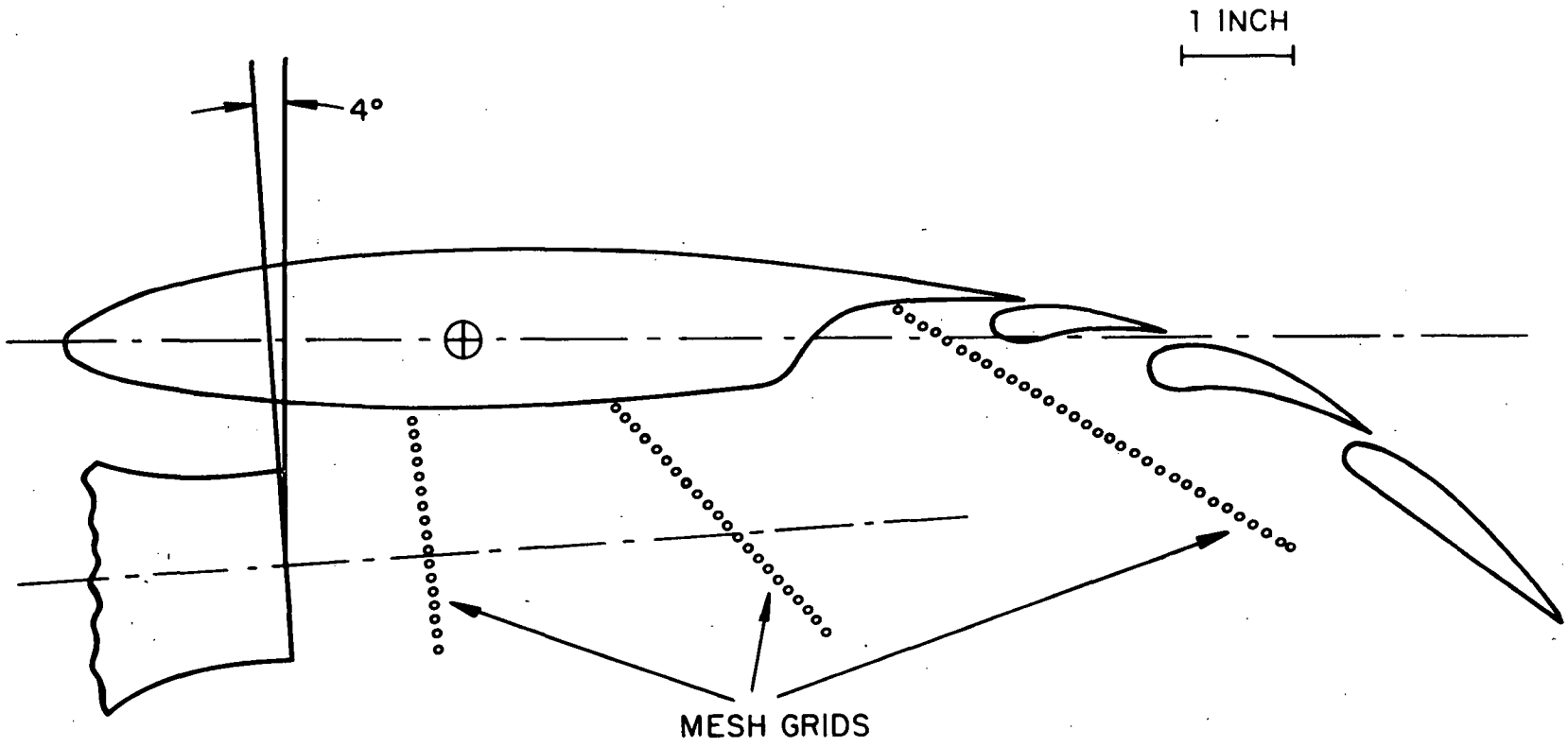

FIG. 30. LOCATION OF MESH GRIDS.

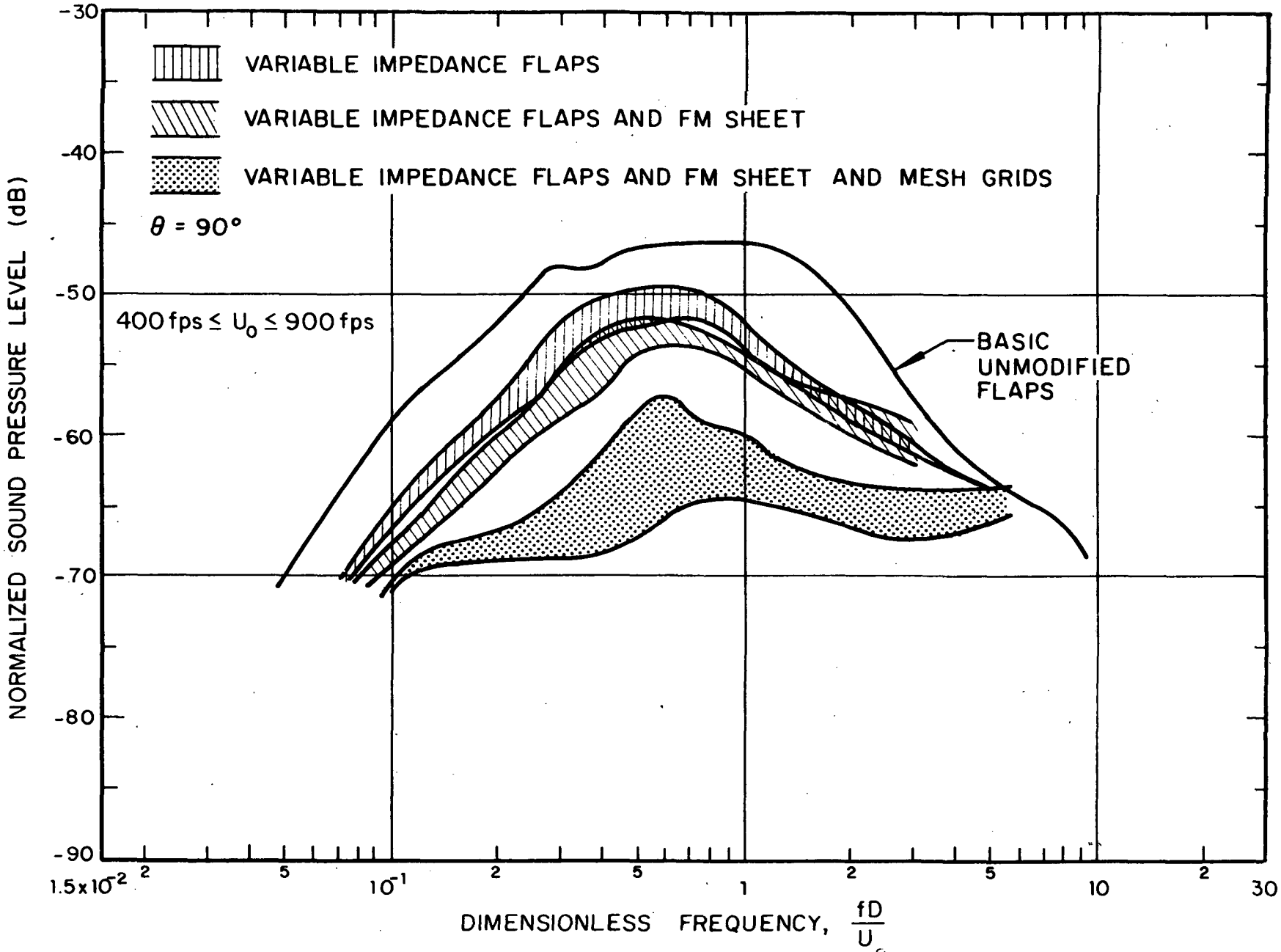

FIG. 31. COMPARISON OF NOISE RADIATION FROM BASIC FLAPS WITH SEVERAL VARIABLE IMPEDANCE FLAP CONFIGURATIONS: TAKEOFF SETTING.

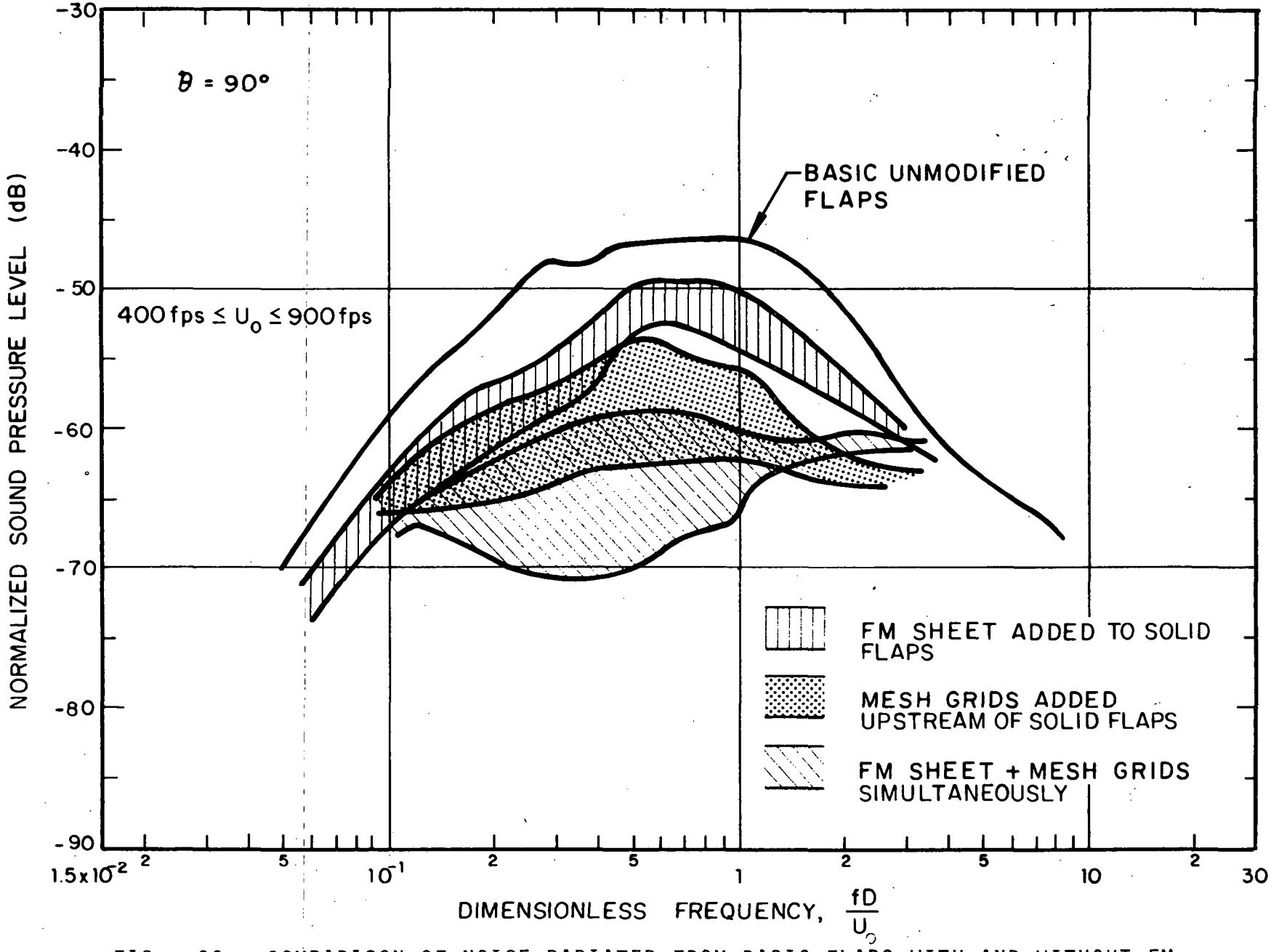

FIG. 32. COMPARISON OF NOISE RADIATED FROM BASIC FLAPS WITH AND WITHOUT FM SHEET AND MESH GRIDS: TAKEOFF SETTING.

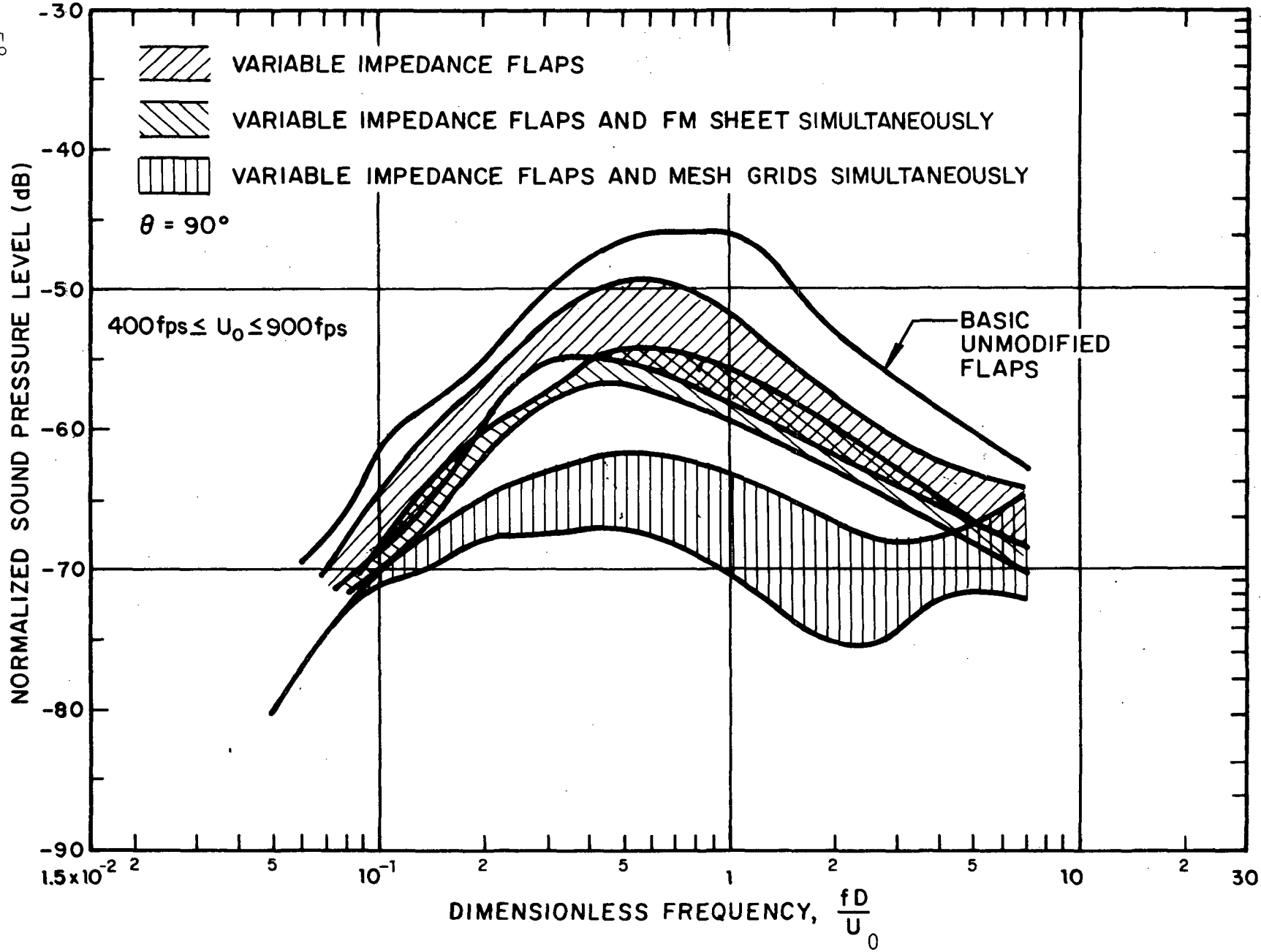

FIG. 33. COMPARISON OF NOISE RADIATED FROM BASIC FLAPS WITH SEVERAL VARIABLE IMPEDANCE FLAP CONFIGURATIONS: APPROACH SETTING.

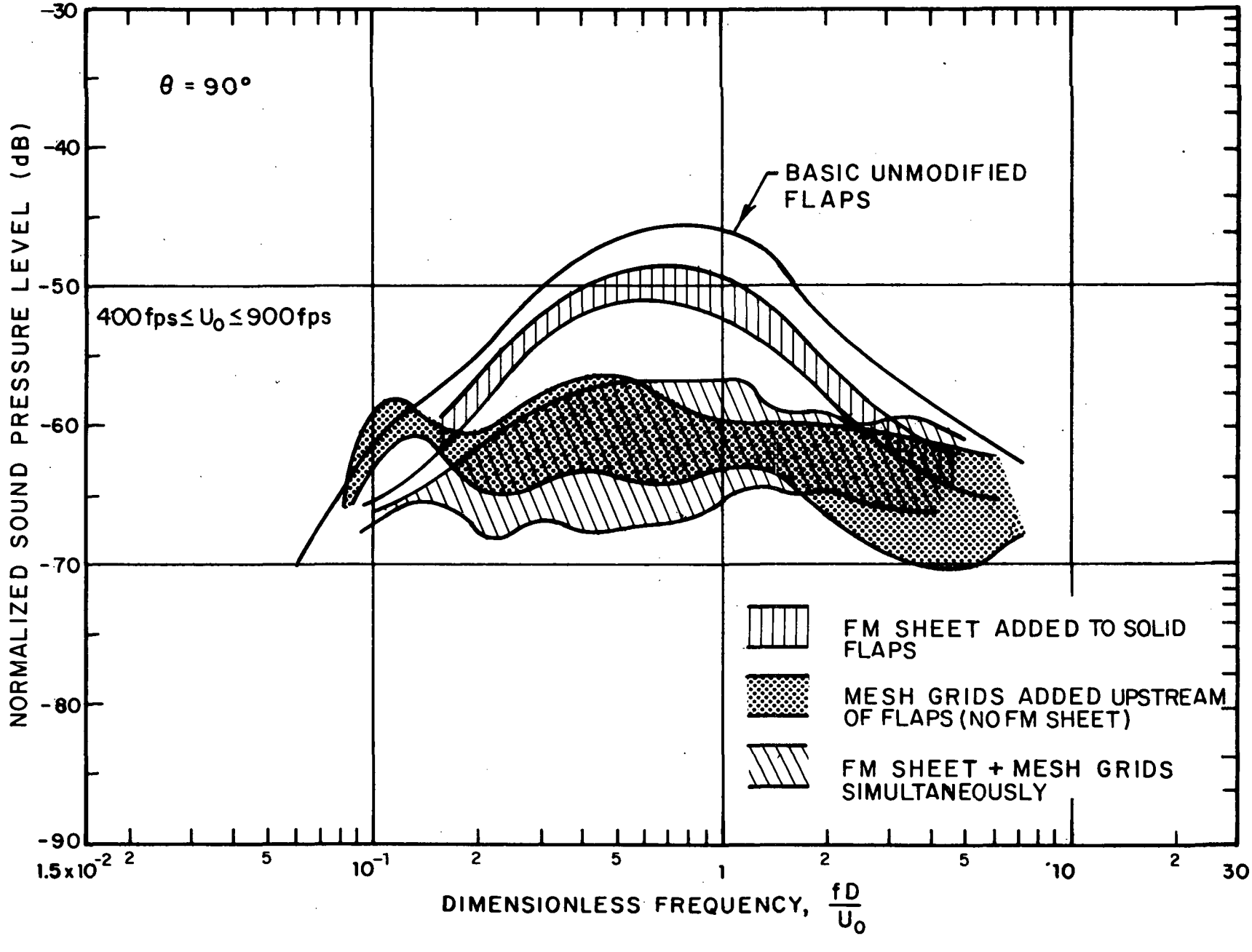

FIG. 34. COMPARISON OF NOISE RADIATED FROM BASIC FLAPS WITH AND WITHOUT MESH GRIDS AND FM SHEET: APPROACH SETTING

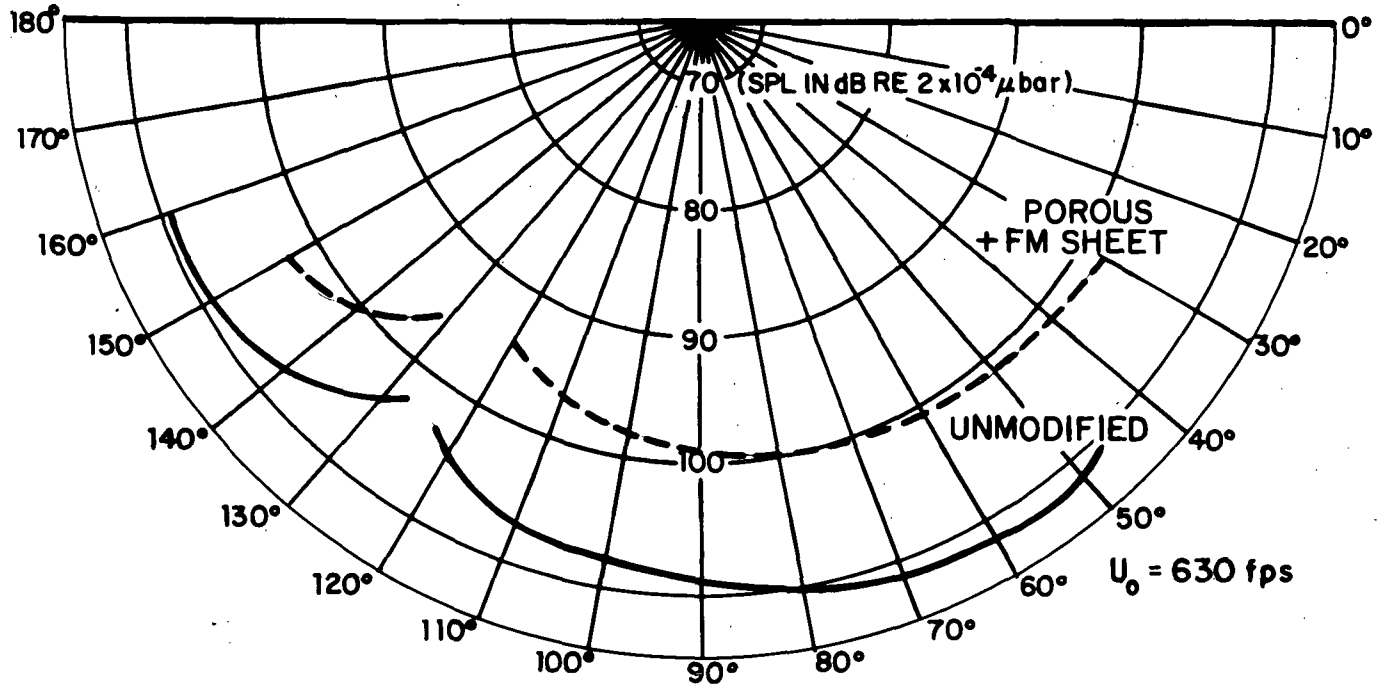

a) OVERALL SOUND PRESSURE LEVEL

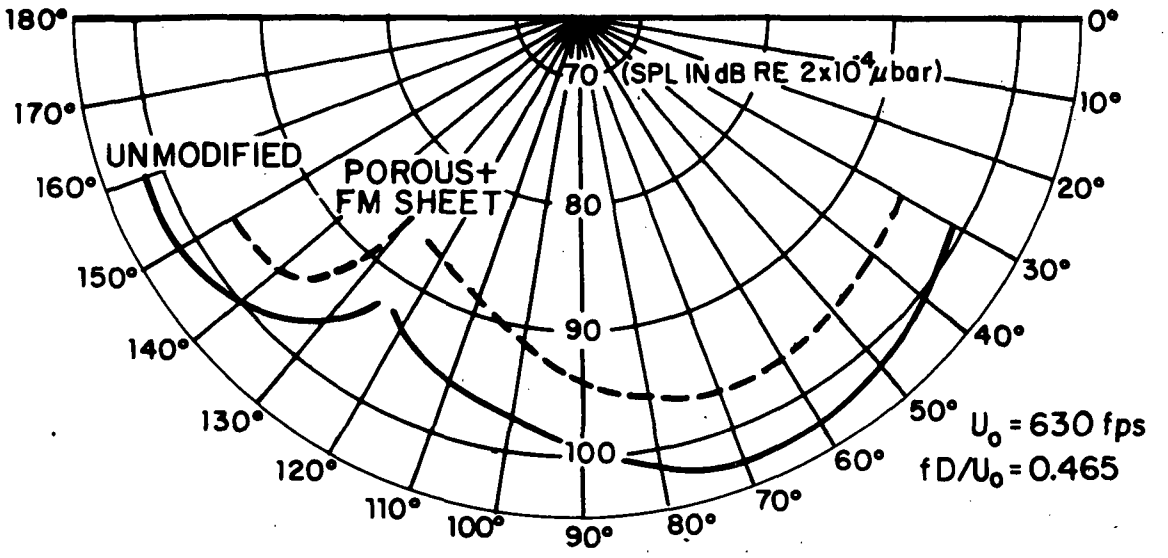

b) 2000 Hz THIRD OCTAVE BAND

FIG. 35. NOISE REDUCTION AS A FUNCTION OF OBSERVATION ANGLE: APPROACH FLAP SETTING.

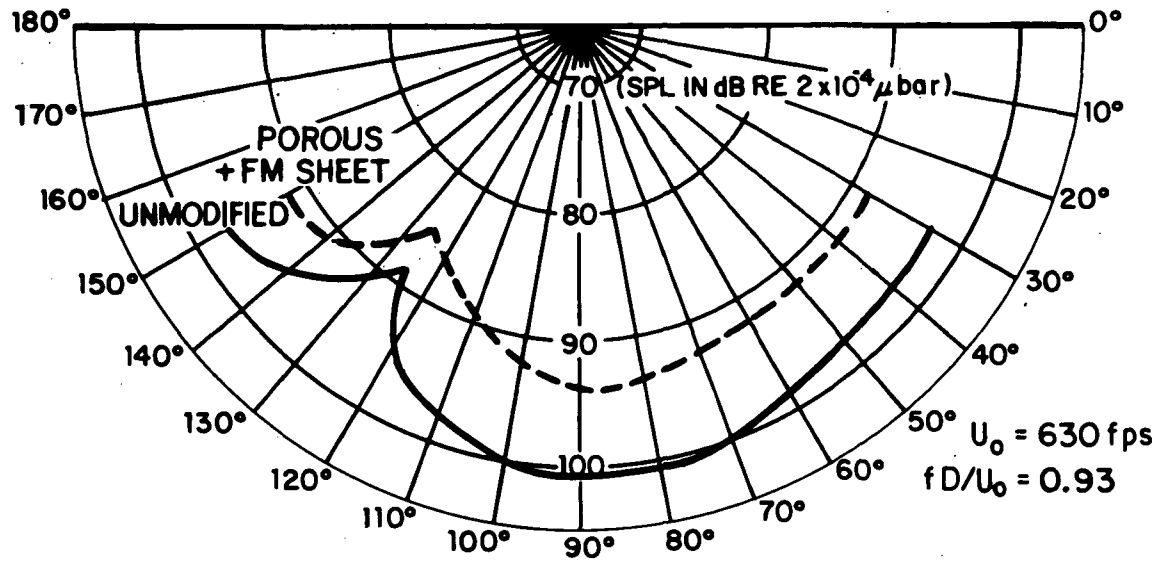

c) 4000 Hz THIRD OCTAVE BAND

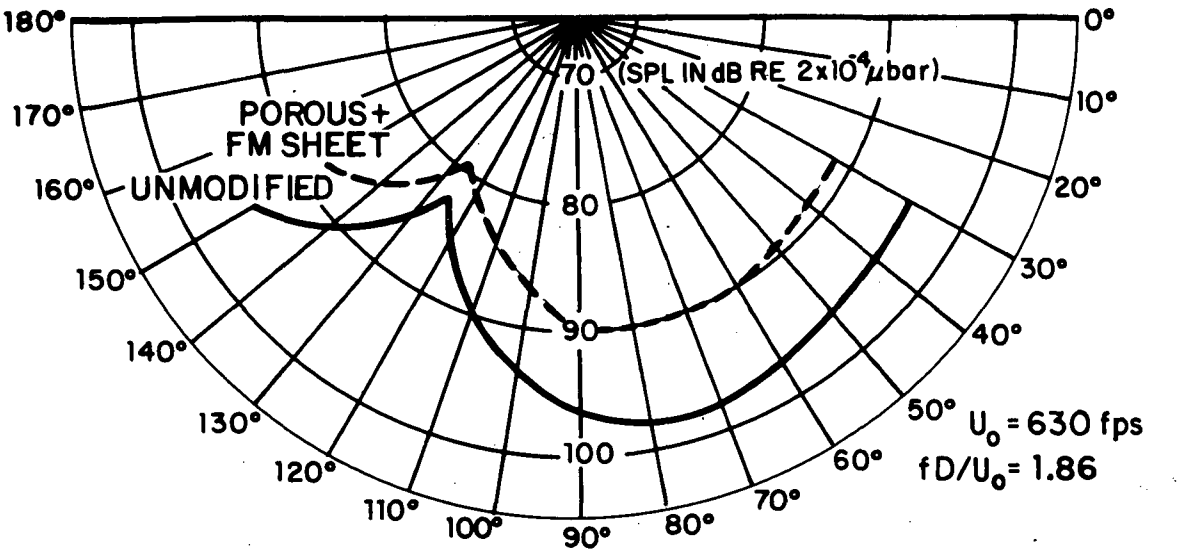

d) 8000 Hz THIRD OCTAVE BAND

FIG. 35. (Cont.) NOISE REDUCTION AS A FUNCTION OF OBSERVATION ANGLE: APPROACH FLAP SETTING.

Aerodynamic Data

Lift and drag were measured for the modified flaps and compared with the unmodified flaps in Tables II and III. The aerodynamic losses observed indicate trends only, since materials limitations and lack of information on the predominant sources have yet to be overcome.

TABLE II

ACOUSTIC AND AERODYNAMIC COMPARISONS

TAKE-OFF FLAP SETTING - RANKING BY LIFT AND DRAG

Configuration	Lift Factor (fraction of nominal unmodified flap value)	Drag Factor	Representative[a] noise reduction @ St=1 (dB)
Solid Flaps	1	1	0
Solid + Coarse mesh grid (1 Layer)	0.86	1.42	7
Solid + FM[b] Sheet	0.84	1.8	7-12
Solid + Fine mesh grid	0.79	2.10	10-15
Solid + Coarse mesh grid (2 layers)	0.74	2.04	8.5
Porous Flaps	0.72	2.0	6-8
Porous Flaps + FM Sheet	0.72	2.0	8-10
Solid + FM Sheet + Coarse mesh grid	0.71	2.7	11
Solid + coarse mesh grid (3 Layers)	0.68	2.4	--
Solid + FM + Fine mesh grid	0.66	2.8	14-18
Porous + Fine mesh grid	0.615	2.82	18-20

[a]Noise Reductions were often found to be sensitive to very small changes in configuration, whereas little effect of these changes was noted in lift and drag.

[b]FM = Fibermetal Sheet (10 Rayl)

TABLE III

ACOUSTIC AND AERODYNAMIC COMPARISONS

APPROACH FLAP SETTING - RANKING BY LIFT AND DRAG

Configuration	Lift Factor (fraction of nominal unmodified flap value)	Drag Factor	Representative[a] noise reduction @ St=1 (dB)
Solid	1	1	0
Solid + Coarse mesh grid (1 Layer)	0.84	1.17	7
Solid + Fine mesh grid	0.79	1.28	9
Solid + FM[b] Sheet	0.77	1.46	6
Solid + Coarse mesh grid (2 Layers)	0.72	1.32	8
Porous Flaps + FM Sheet	0.685	1.45	12
Solid + FM + Coarse mesh grid	0.65	1.57	10
Porous Flaps	0.64	1.43	6-8
Solid + Coarse mesh grid (3 Layers)	0.63	1.42	14
Solid + FM Sheet + Coarse mesh grid (2 Layers)	0.59	1.66	15
Porous Flaps + FM Sheet + Fine mesh grid	0.57	1.75	20-22
Solid + Coarse mesh grid (4 Layers)	0.55	1.56	18

[a]Noise Reductions were often found to be sensitive to very small changes in configuration, whereas little effect of these changes was noted in lift and drag.

[b]FM = Fibermetal Sheet (10 Rayl)

SUMMARY AND CONCLUSIONS

1. Dipole-like sound from jet interaction with the flaps and their edges dominates the sound output from a subsonic jet/deployed flap system.

2. Point surface pressure measurements show that for the configuration studied, the trailing edge of the second flap and leading and trailing edges of the third flap appear to have the highest source strengths; the trailing edge of the third flap is important in all cases.

3. Analytical similarity models of the sound sources suggest that varying the surface impedance of the flaps spatially and breaking up the jet will reduce the sound output of all flap noise sources, even when no reduction of local mean velocity is made.

4. Experimental results using flaps with porous leading and trailing edges or a porous sheet over the entire flap surfaces showed noise reductions of about 10 dB. Performance penalties were substantial in these pilot tests; however, further work at larger scale would enable one to more readily configure the edges with the desired spatial impedance gradient. Also, this study used available materials which were far from optimum acoustically and aerodynamically. All these factors point out that the aerodynamic penalties noted in this gross preliminary survey should not yet be cause for despair as refinements should retain or increase the present noise reductions and reduce aerodynamic losses.

5. Experimental results using mesh grids to break up the jet showed about 10 dB noise reduction without prohibitive performance penalties. Clever implementation of this concept could conceivably give the same or more noise reduction with very small performance penalities.

REFERENCES

1. Goodykoontz, J.H.; Olsen, W.A.; and Dorsch, R.G.: Preliminary Tests of the Mixer Nozzle Concept for Reducing Blown Flap Noise. NASA TMX-67936, 1971.

2. Goodykoontz, J.H.; Dorsch, R.G.; and Groesbeck, D.E.: Mixer Nozzle-Externally Blown Flap Noise Tests. NASA TMX-68021, February 1972.

3. Lasagna, P.L.; and Putnam, T.W.: Externally Blown Flap Impingement Noise. Presented at the NASA Ames STOL Technology Conference (Moffett Field, California), October 17-19, 1972.

4. Hayden, R.E.: Sound Generation by Turbulent Wall Jet Flow over a Trailing Edge. M.S. Thesis, Purdue Univ., 1969.

5. Hayden, R.E.; and Chanaud, R.C.: Sound Generation by Turbulent Wall Jet Flow over a Trailing Edge. Paper FF-10, Spring Meeting of the Acoust. Soc. Am. (Atlantic City, N.J.), 1970.

6. Chanaud, R.C.; and Hayden, R.E.: Edge Sound Produced by Two Turbulent Wall Jets. Paper FF-11, Spring Meeting of the Acoust. Soc. Am. (Atlantic City, N.J.), 1970.

7. Curle, N.: The Influence of Solid Boundaries upon Aerodynamic Sound. Proc. Roy. Soc. (London), A231, 1955.

8. Dorsch, R.G.; Kreim, W.J.; and Olsen, W.A.: Externally Blown Flap Noise. AIAA Paper No. 72-129, January 1972.

APPENDIX A

SUMMARY OF A PILOT EXPERIMENTAL STUDY ON LEADING EDGE NOISE FROM JET IMPINGEMENT ON A SEMI-INFINITE WEDGE

To supplement the similarity model for leading edge noise developed earlier in this text, a brief experimental investigation was conducted on a large wedge (compared to a wavelength) and subsonic jet from a round nozzle (diameter 0.25 in. to 0.75 in.). The experimental arrangement is shown in Figure A.1. The nozzle velocity and position with respect to the leading edge were variable. The entire frame was rotatable about an axis corresponding to the leading edge for the purpose of making directivity measurements with a fixed far-field microphone. The experiments were conducted in a small anechoic room whose lower cutoff frequency was about 300 Hz.

Sound pressure spectra were measured for various nozzle velocities and positions and for different leading edge configurations. Recalling the theoretical developments presented earlier, one expects two distinct features of the leading edge noise source: (1) a $6th$ power dependence on mean velocity at a constant value of Strouhal number; (2) a cardioid-like directivity pattern with a maximum along the plane of the surface and a null in the plane of the surface "upstream" of the edge (see Figure 5). Furthermore, it is expected that the sound spectra and levels produced at the leading edge reflect characteristics of the local inflow; thus, we expect a variation in level and spectral content when the position of the edge is varied relative to a given nozzle exit plane.

Basic Sound Field Characteristics

It was found that the sound spectra along a given azimuth normalize using the dimensional arguments presented earlier (Eq. 14). A typical normalized spectrum for a 0.5-in. diameter nozzle and a sharp leading edge positioned at X/D = 7.5 is shown in Figure A.2. For the range of exit velocities studied (400 fps to 900 fps), variations from the curve shown were ±1 dB.

The directivity was measured using both the wedge shown in Figure A.1 and a flat plate with a sharpened leading edge. Both cases substantially verified the "theoretical" directivity plots of Figure 5, except where some convective refraction of the sound was expected along the axis of the flow. The data for the flat

plate are presented in Figure A.3. Effects of source area finiteness and secondary sound sources are evident in Figures A.3(b) and A.3(c), but the basic curves show good agreement with the predicted patterns.

The effect of the position of the edge relative to the nozzle was strong as is demonstrated in Figure A.4. One could use this curve to predict the effect of moving a nozzle away from or toward a flap.

Effects of Modified Leading Edge

Two significant modifications of the basic sharp, rigid, leading edge structure are of interest — leading edge roundness and a nonrigid (variable impedance) structure. Figure A.5 shows that the effect of increasing leading edge radius is to reduce the radiated sound. Figure A.6 shows that replacing the entire tip of the wedge with one made of low-impedance fibermetal (10 Rayl flow resistance) is to reduce dramatically the radiated sound (in all directions).

Thus, the leading edge is now verified to be a potent source of sound when placed in a turbulent inflow. The observed sound field characteristics tend to support the distributed, "half-baffled" dipole model developed earlier. The noise reduction achieved with the porous tip is consistent with the variable impedance concept.

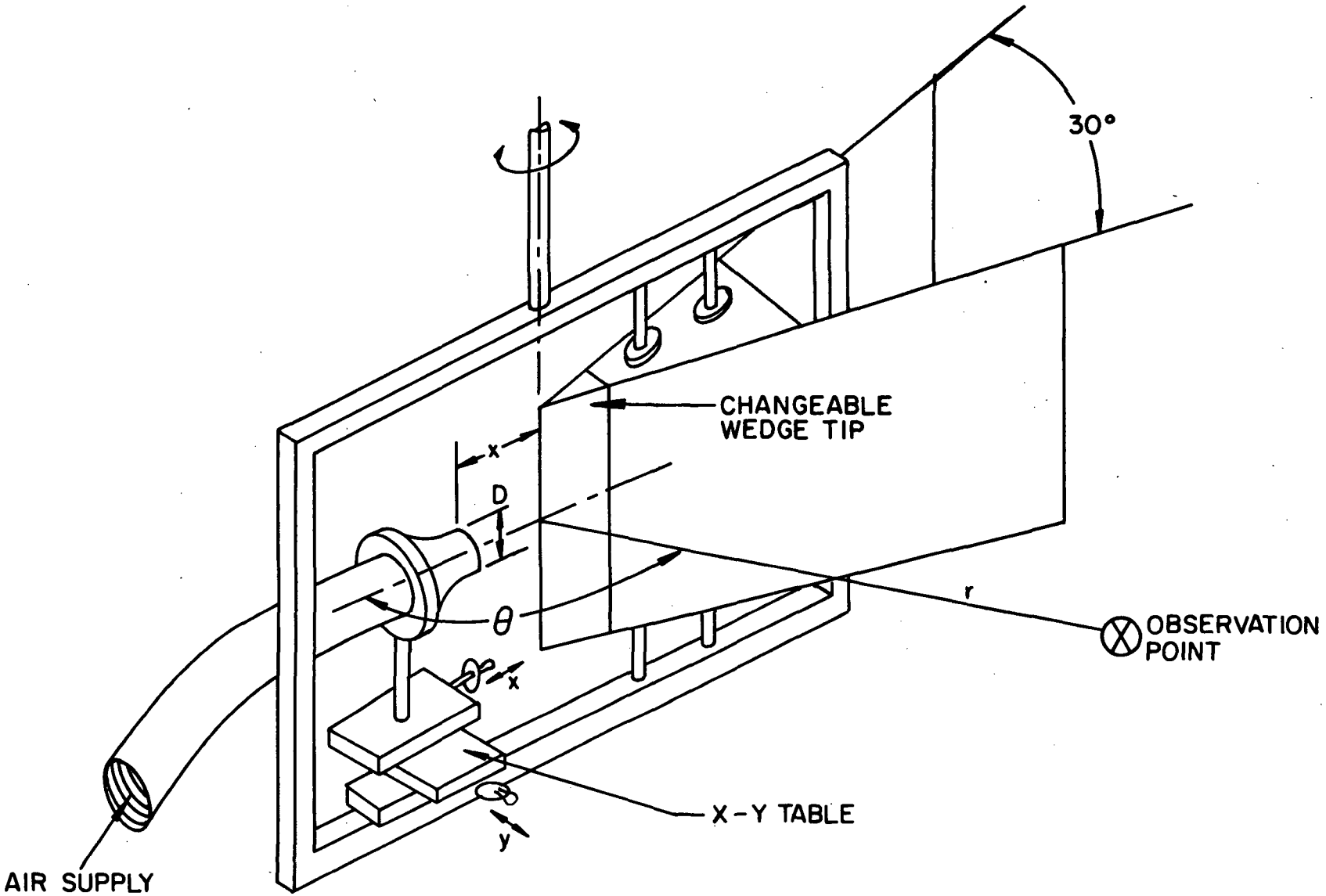

FIG. A.1. EXPERIMENTAL ARRANGEMENT AND COORDINATE SYSTEM FOR LEADING EDGE NOISE STUDY

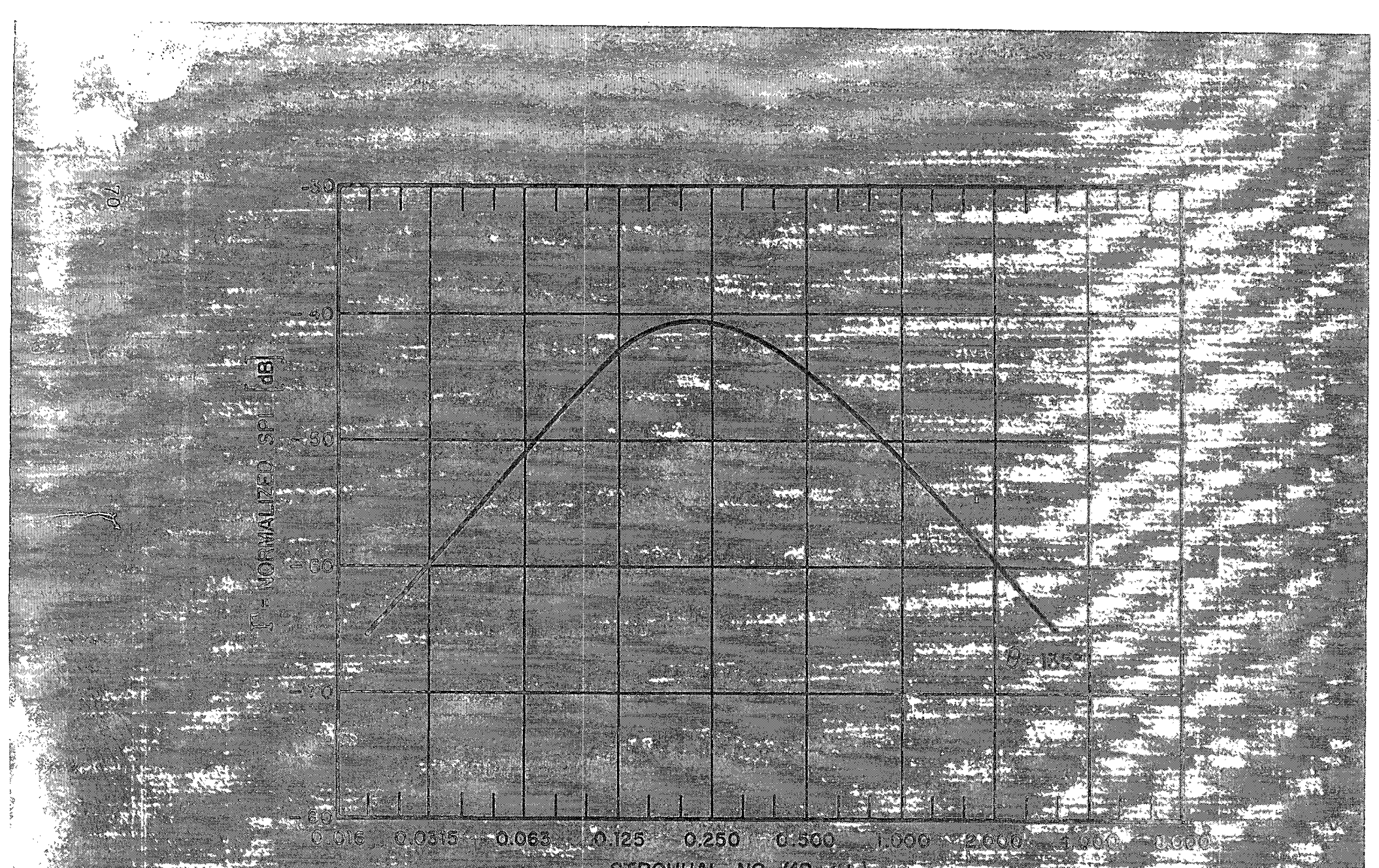

FIG. A.2. NORMALIZED SPECTRUM OF LEADING EDGE NOISE (SHARP EDGE, x/d = 7.5)

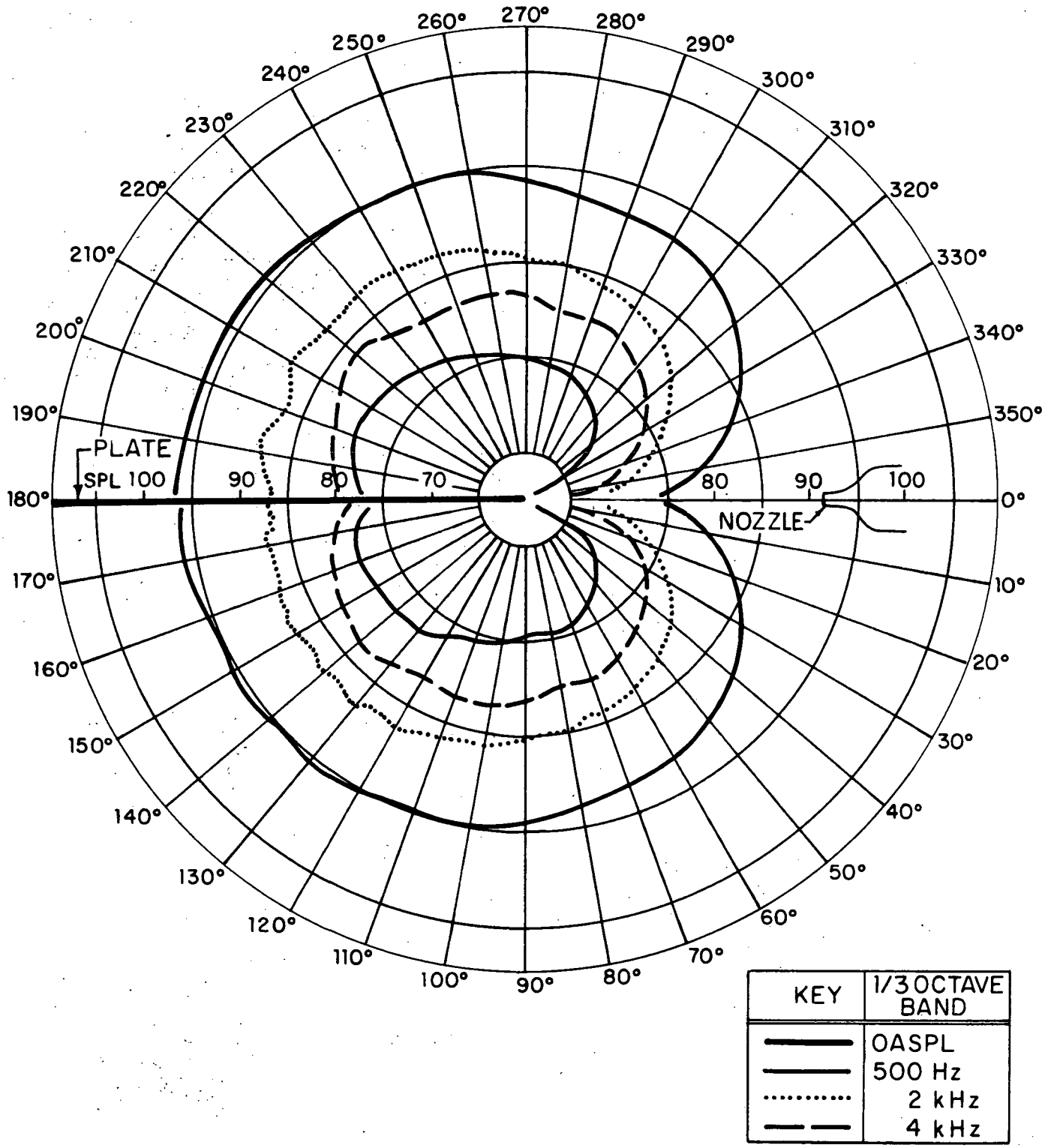

FIG. A.3(a). MEASURED DIRECTIVITY OF LEADING EDGE SOURCE IN PLANE NORMAL TO SURFACE PASSING THROUGH JET AXIS

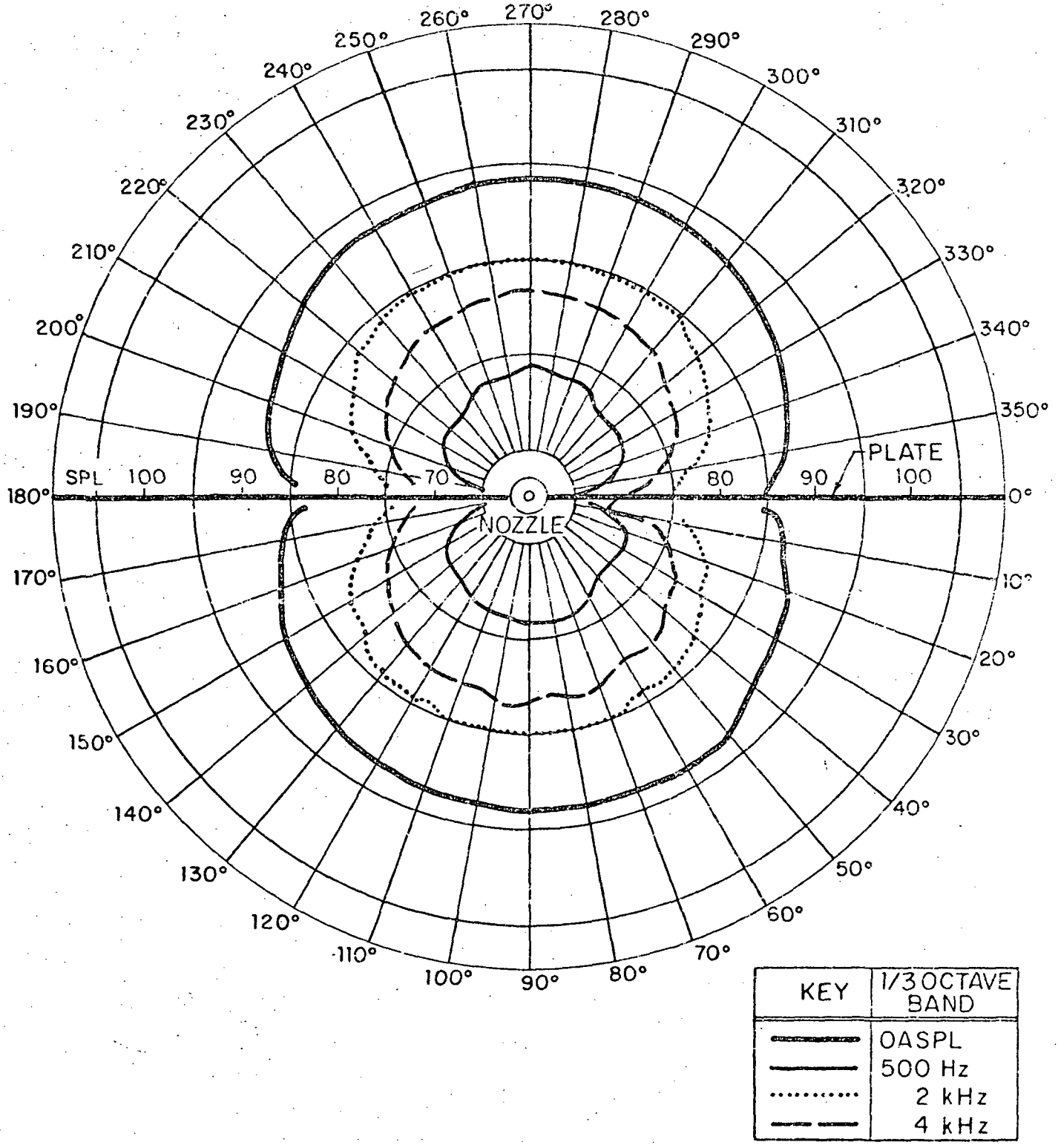

FIG. A.3(b). MEASURED DIRECTIVITY OF LEADING EDGE SOURCE IN PLANE NORMAL TO EDGE AND JET AXIS

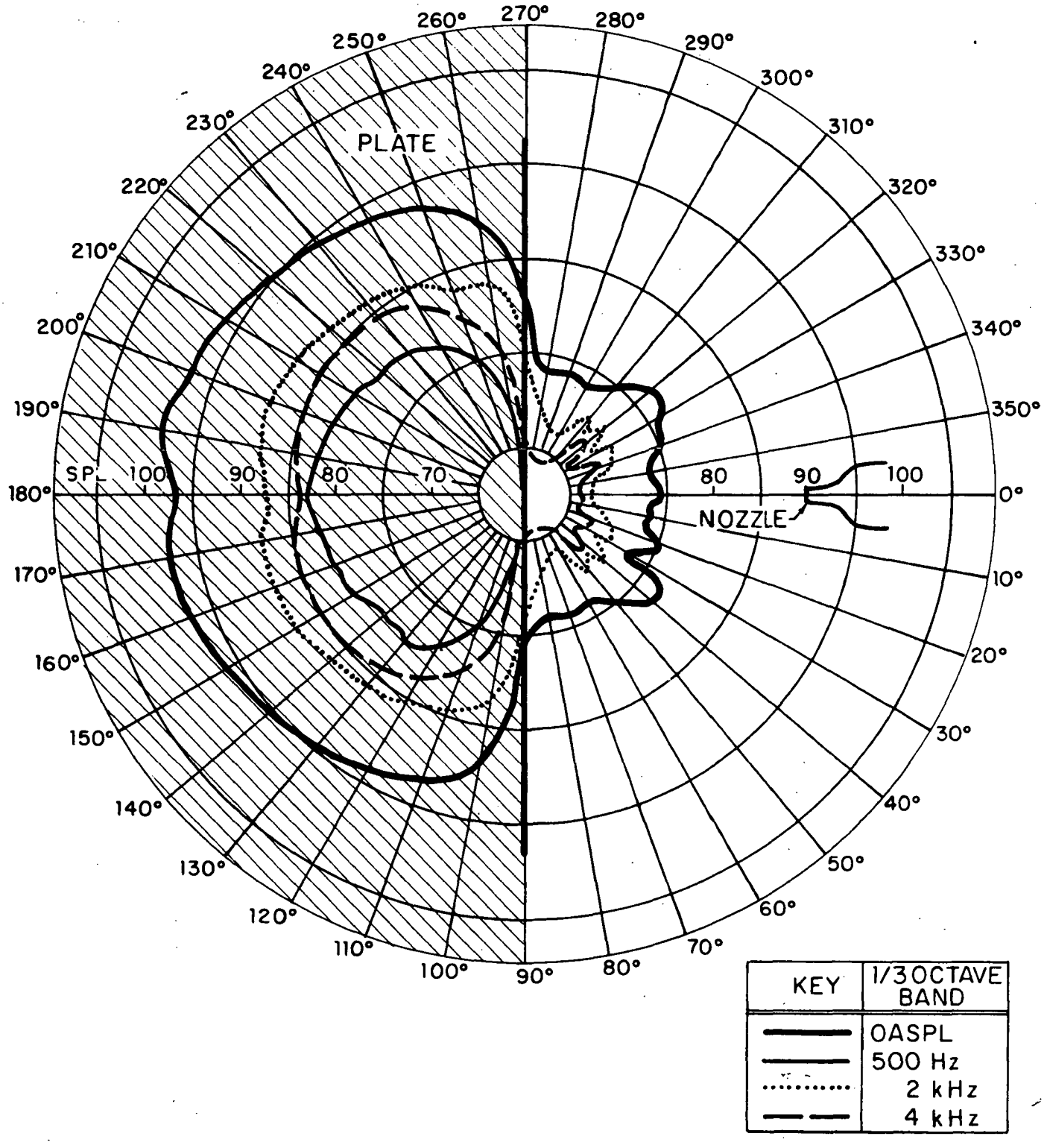

FIG. A.3(c). MEASURED DIRECTIVITY IN PLANE OF SURFACE

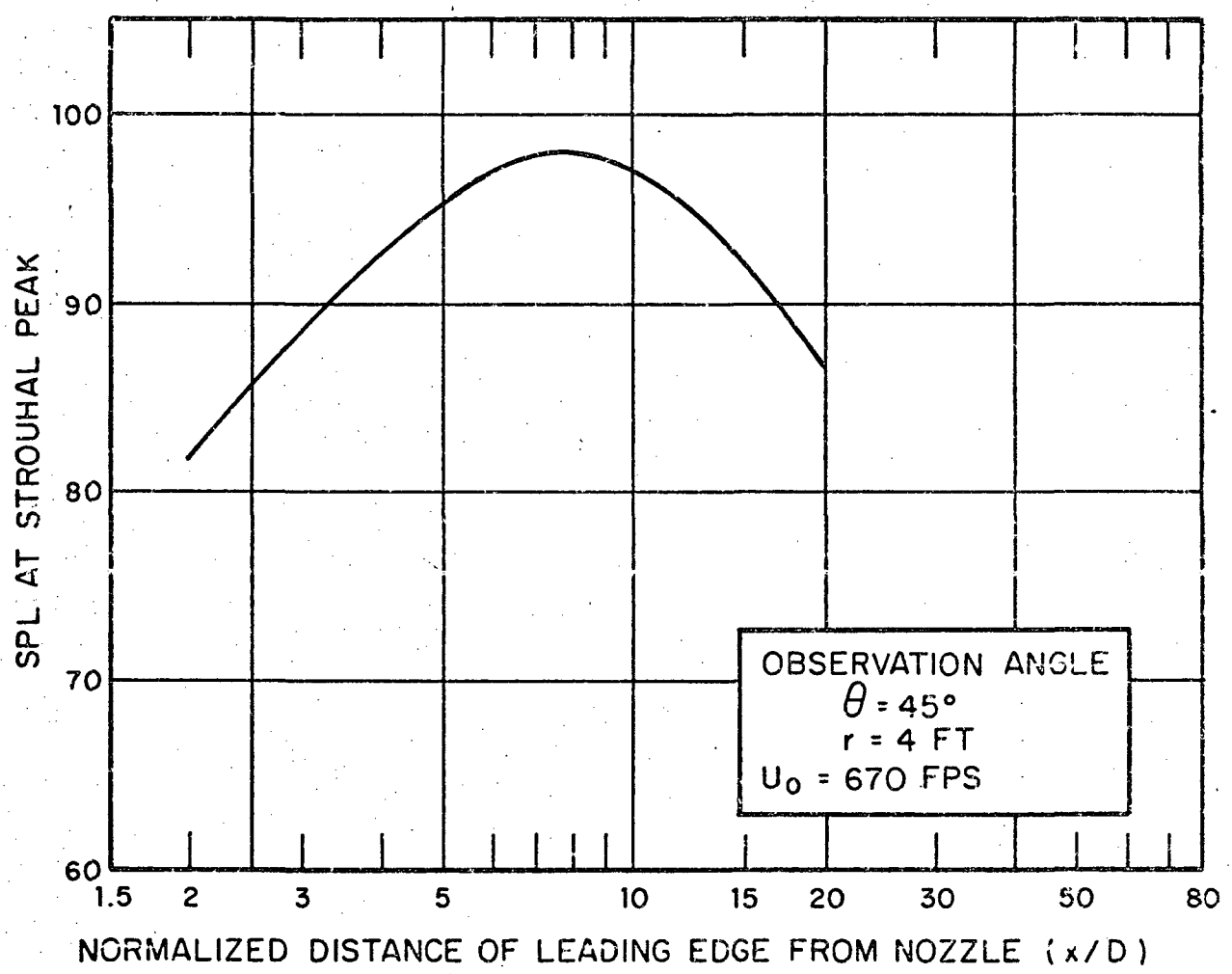

FIG. A.4. VARIATION OF PEAK SPL WITH DISTANCE FROM JET EXIT

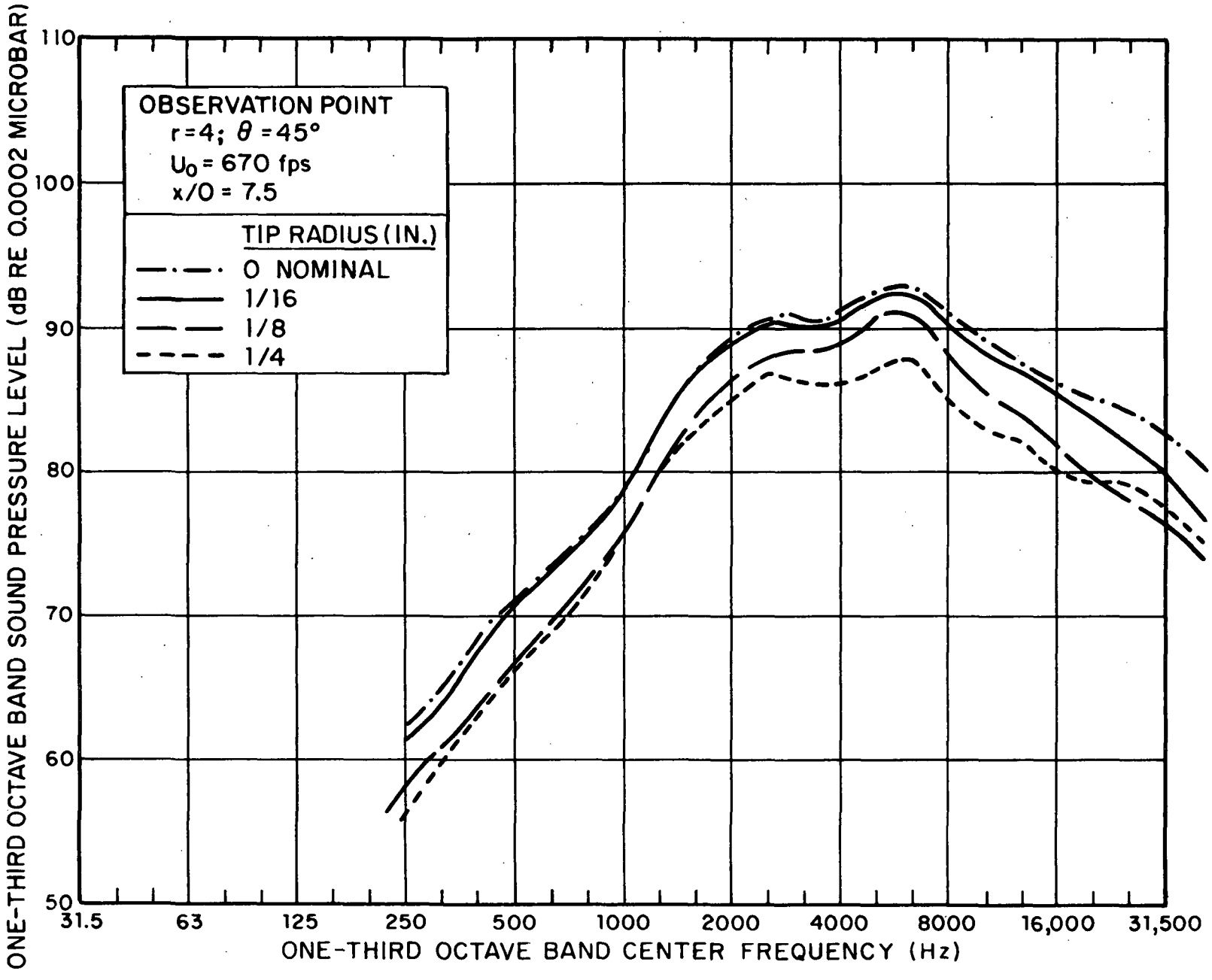

FIG. A.5. EFFECT OF LEADING EDGE RADIUS ON SOUND GENERATION

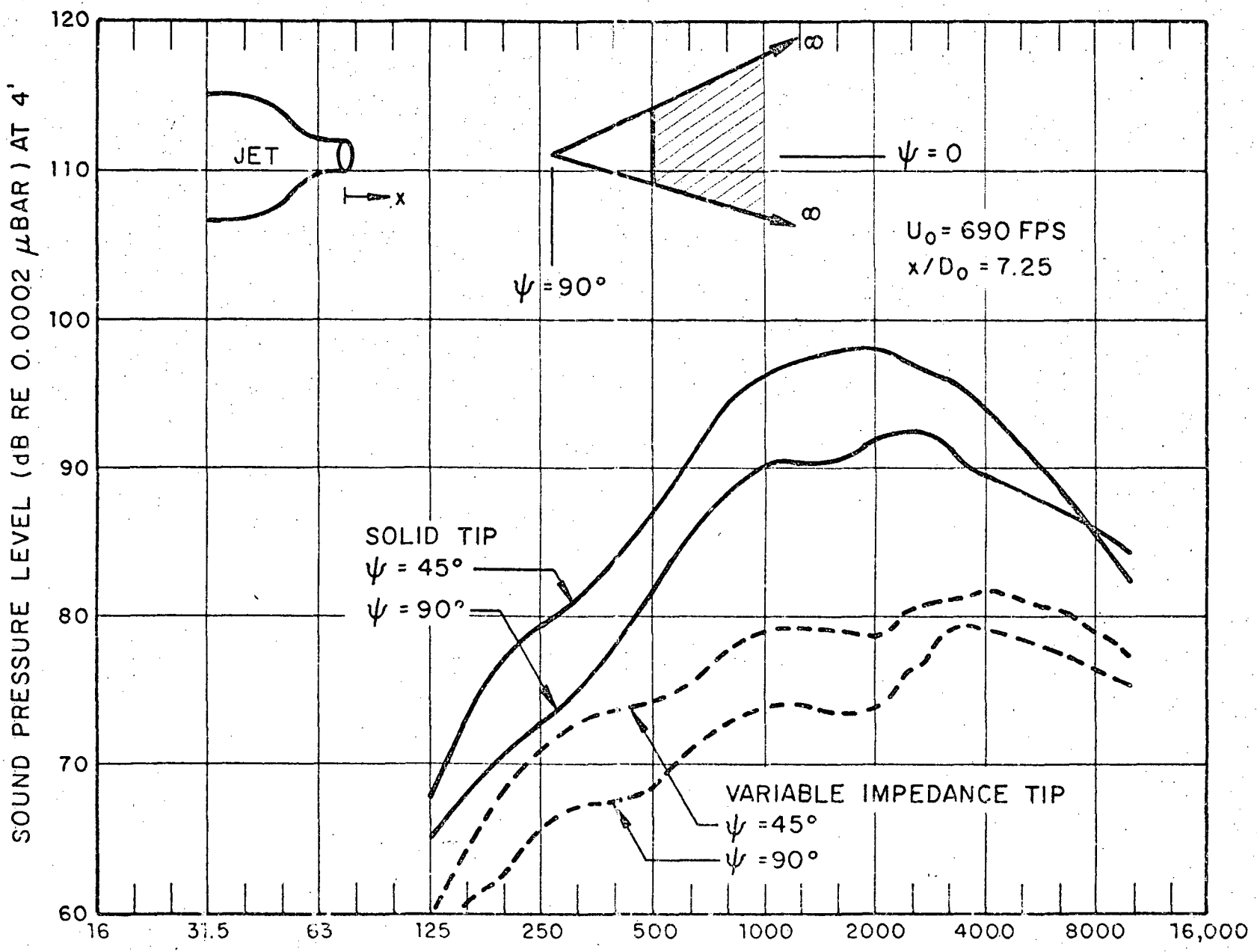

FIG. A.6. MEASURED REDUCTION IN LEADING EDGE NOISE USING VARIABLE IMPEDANCE TIP

APPENDIX B

SUMMARY OF SURFACE PRESSURE SPECTRA ON FLAPS

(See Fig. 22 for Layout)

Figures B.1 – B.9; Takeoff Flap Setting

Figures B.10– B.18; Approach Flap Setting

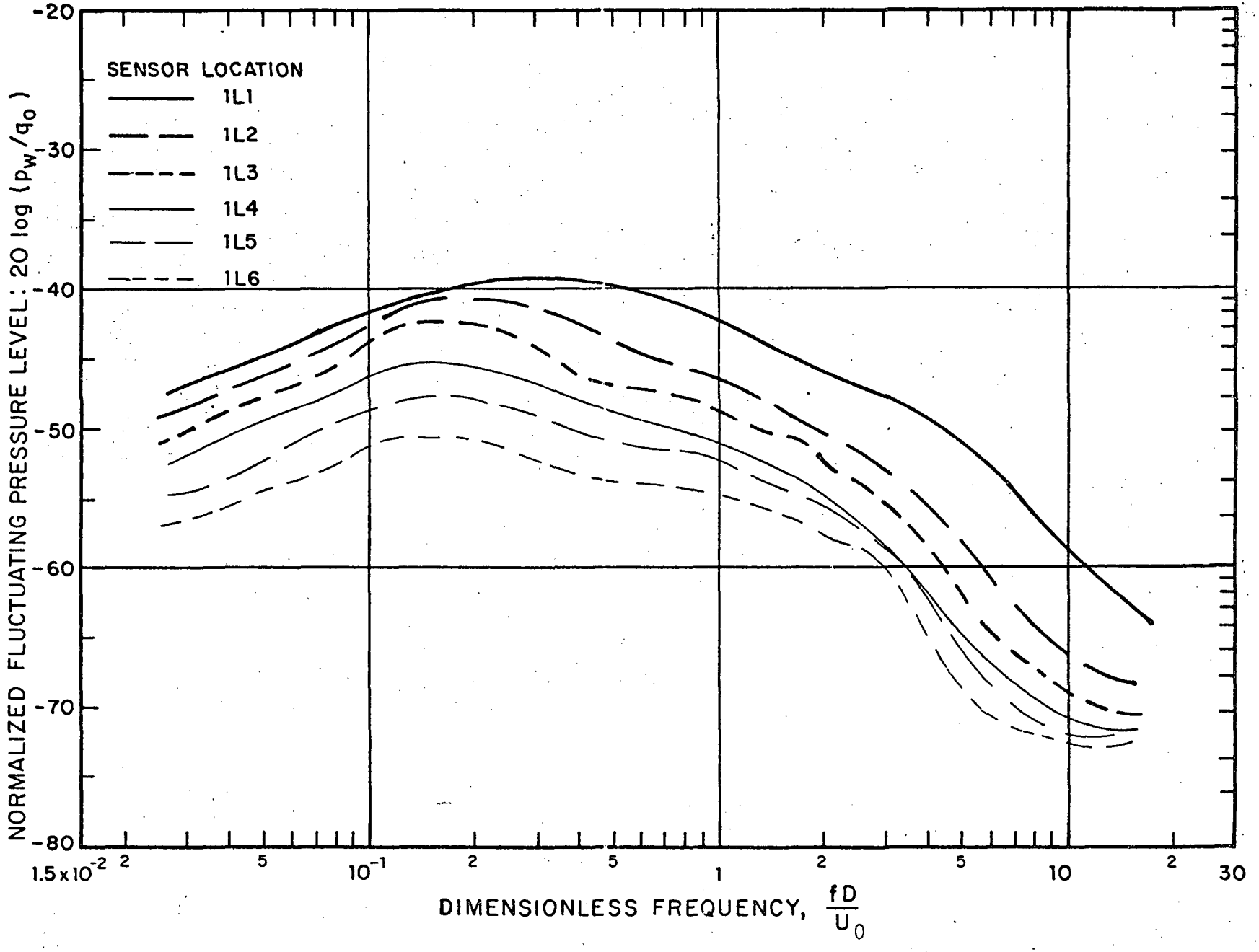

FIG. B.1. NORMALIZED "POINT" PRESSURE SPECTRA ON LOWER SURFACE OF FIRST FLAP TAKEOFF SETTING.

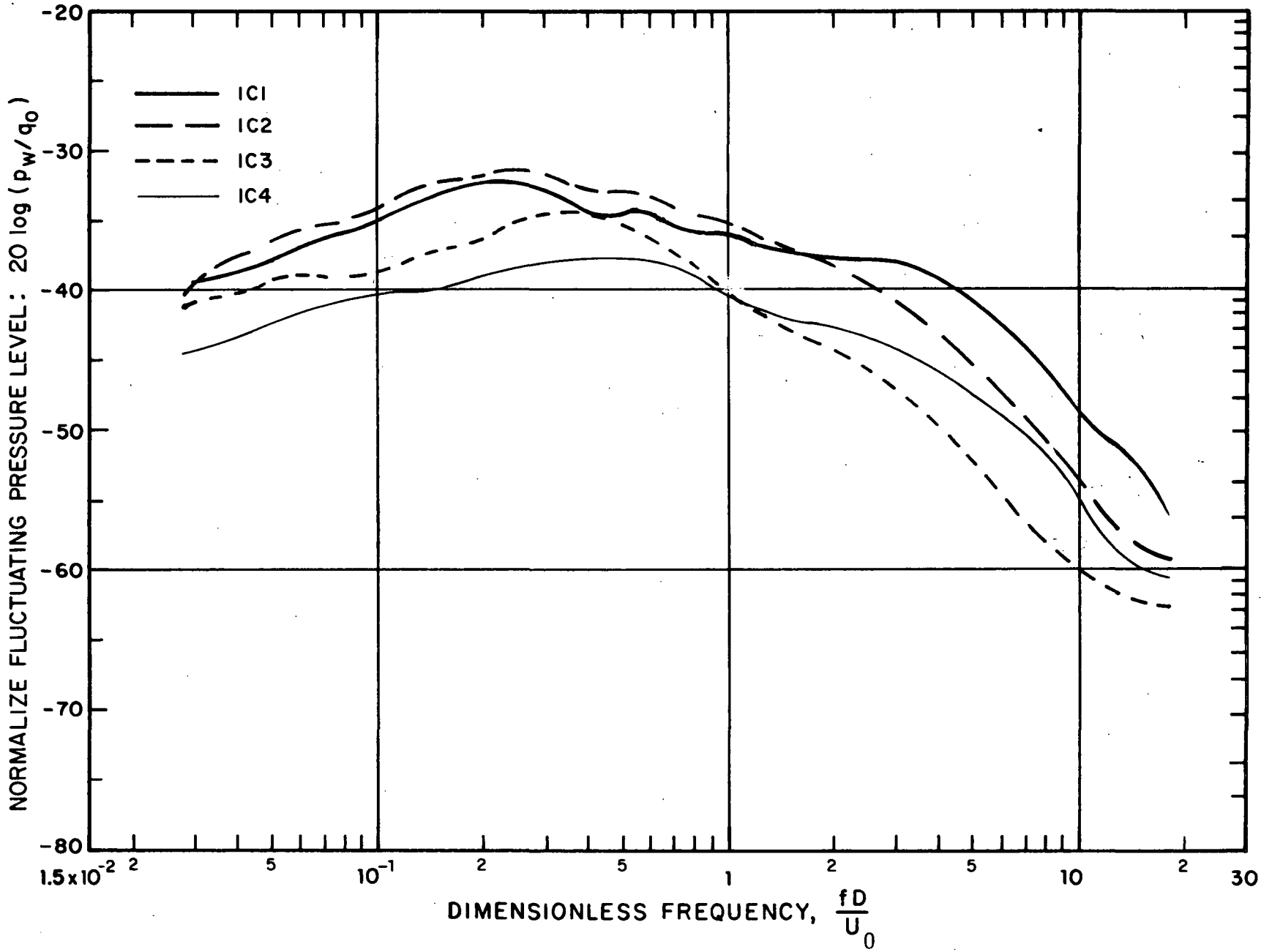

FIG. B.2. NORMALIZED "POINT" PRESSURE SPECTRA ON LOWER SURFACE OF FIRST FLAP TAKEOFF SETTING.

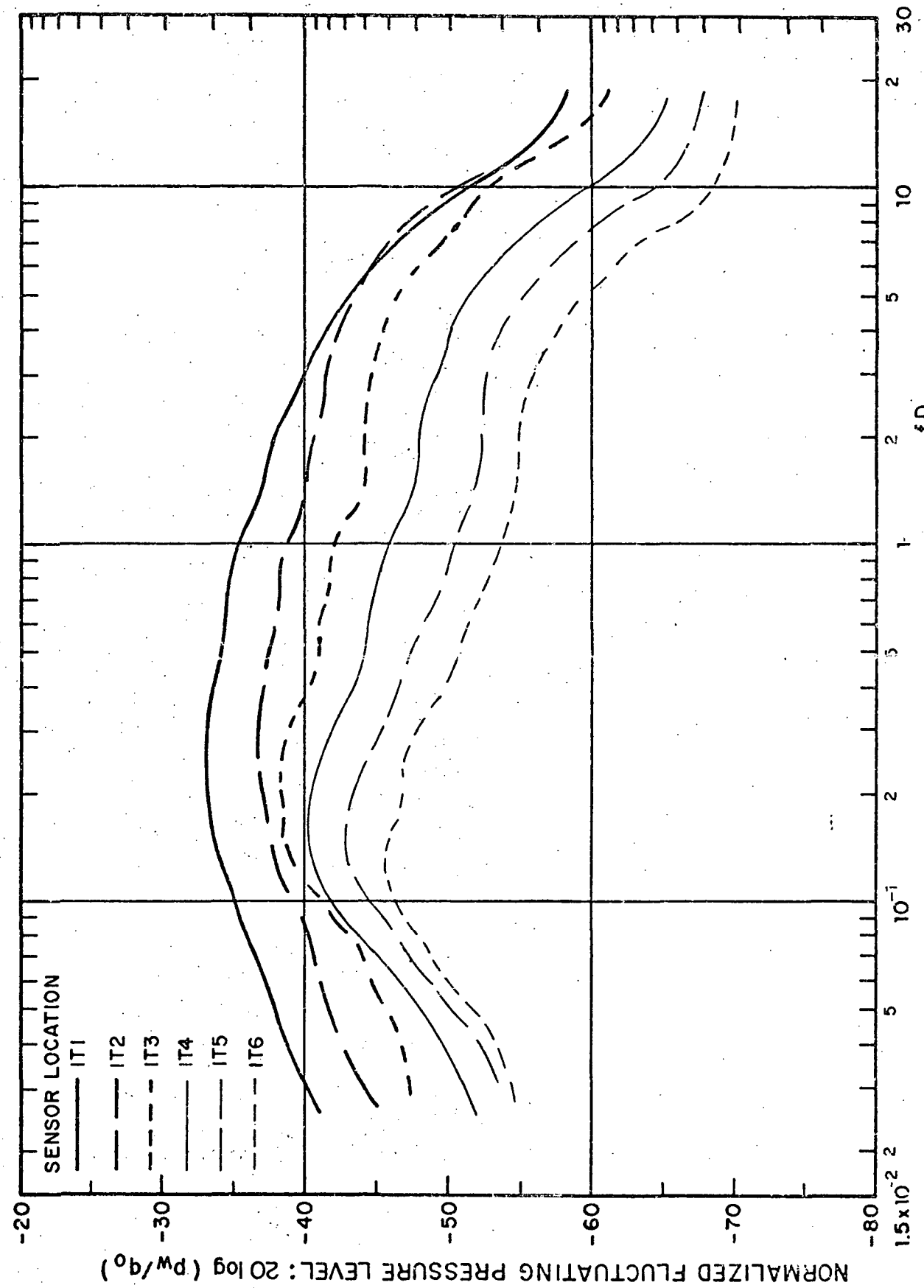

FIG. B.3. NORMALIZED "POINT" PRESSURE SPECTRA ON LOWER SURFACE OF FIRST FLAP TAKEOFF SETTING.

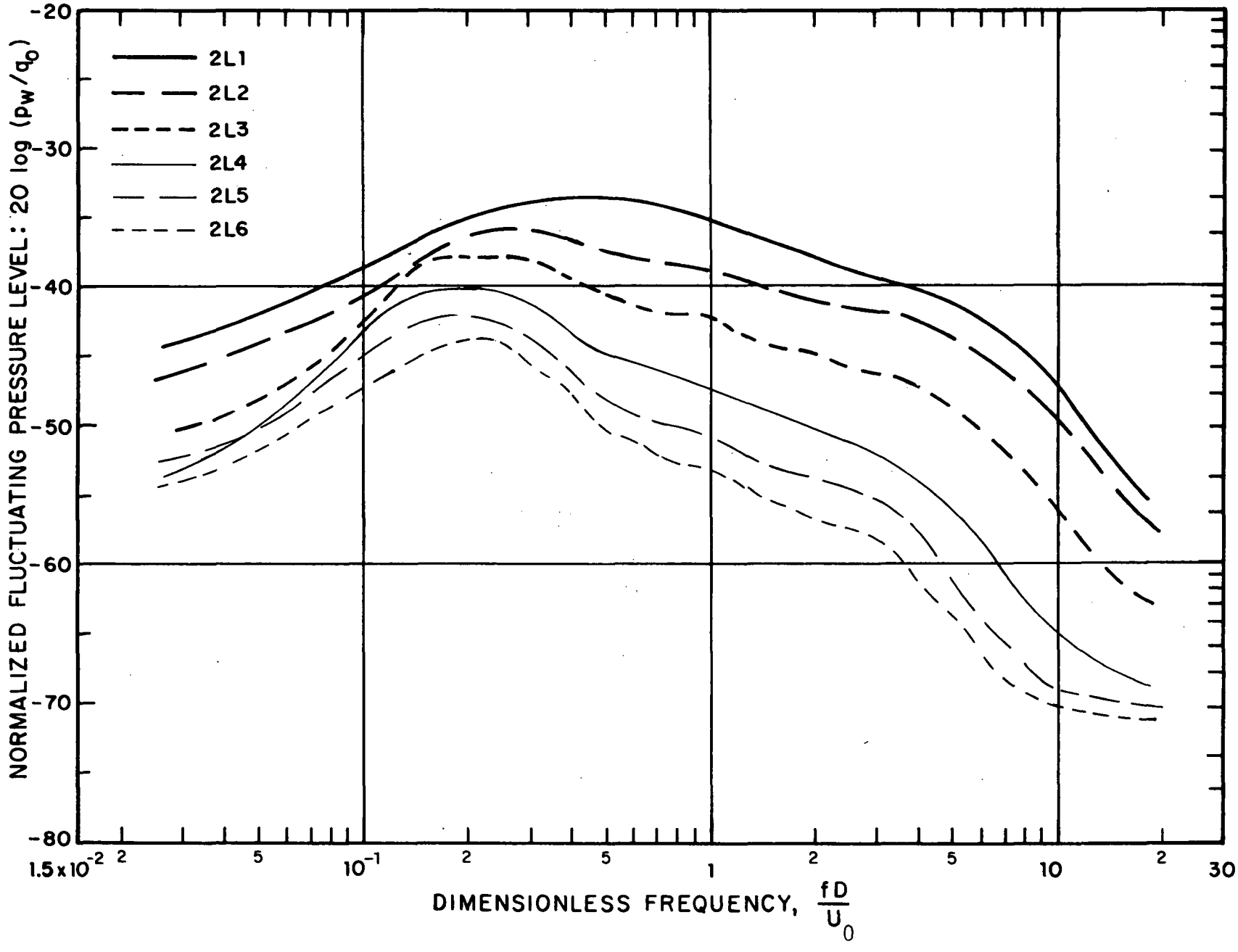

FIG. B.4. NORMALIZED "POINT" PRESSURE SPECTRA ON LOWER SURFACE ON SECOND FLAP TAKEOFF SETTING.

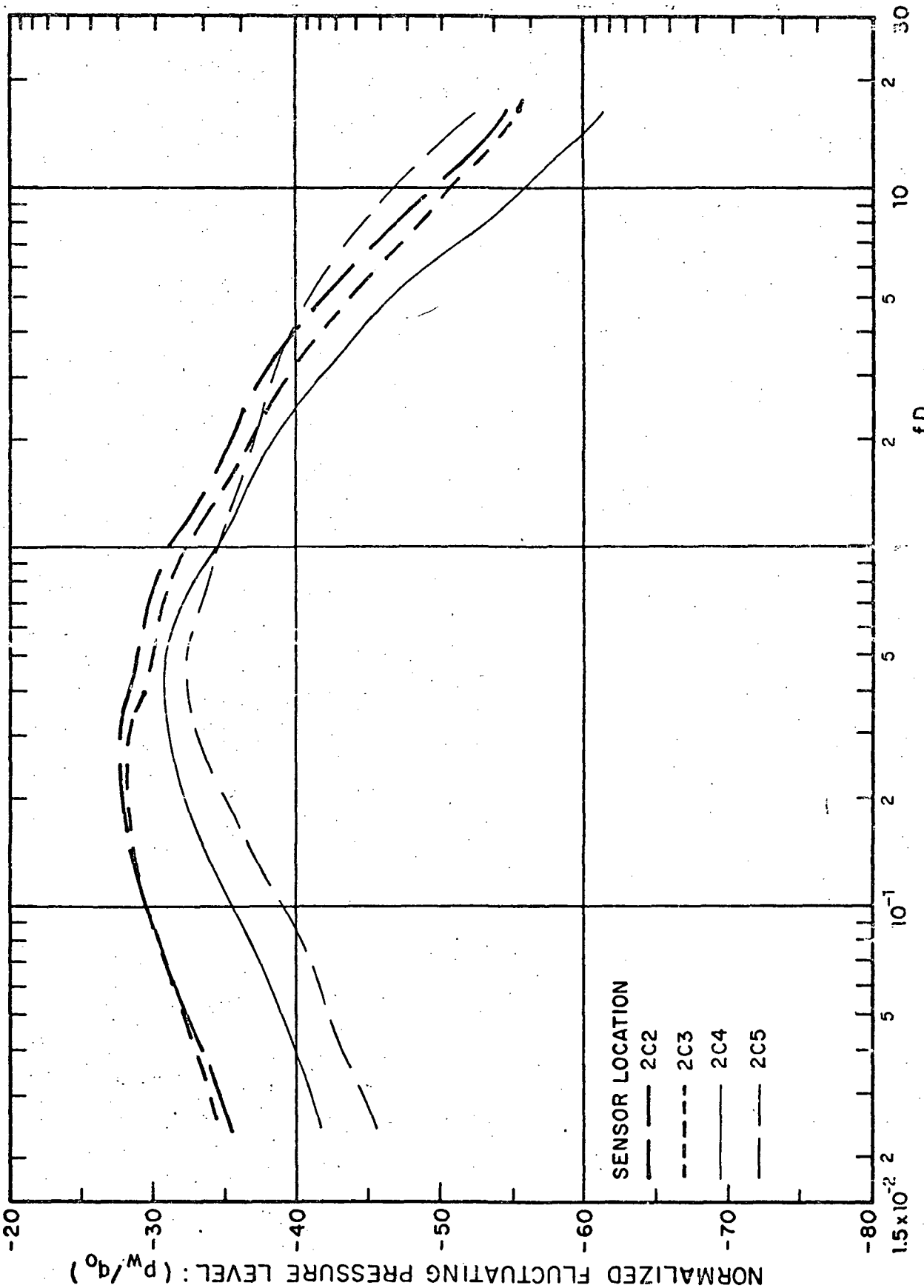

FIG. B.5. NORMALIZED "POINT" PRESSURE SPECTRA ON LOWER SURFACE OF SECOND FLAP TAKEOFF SETTING.

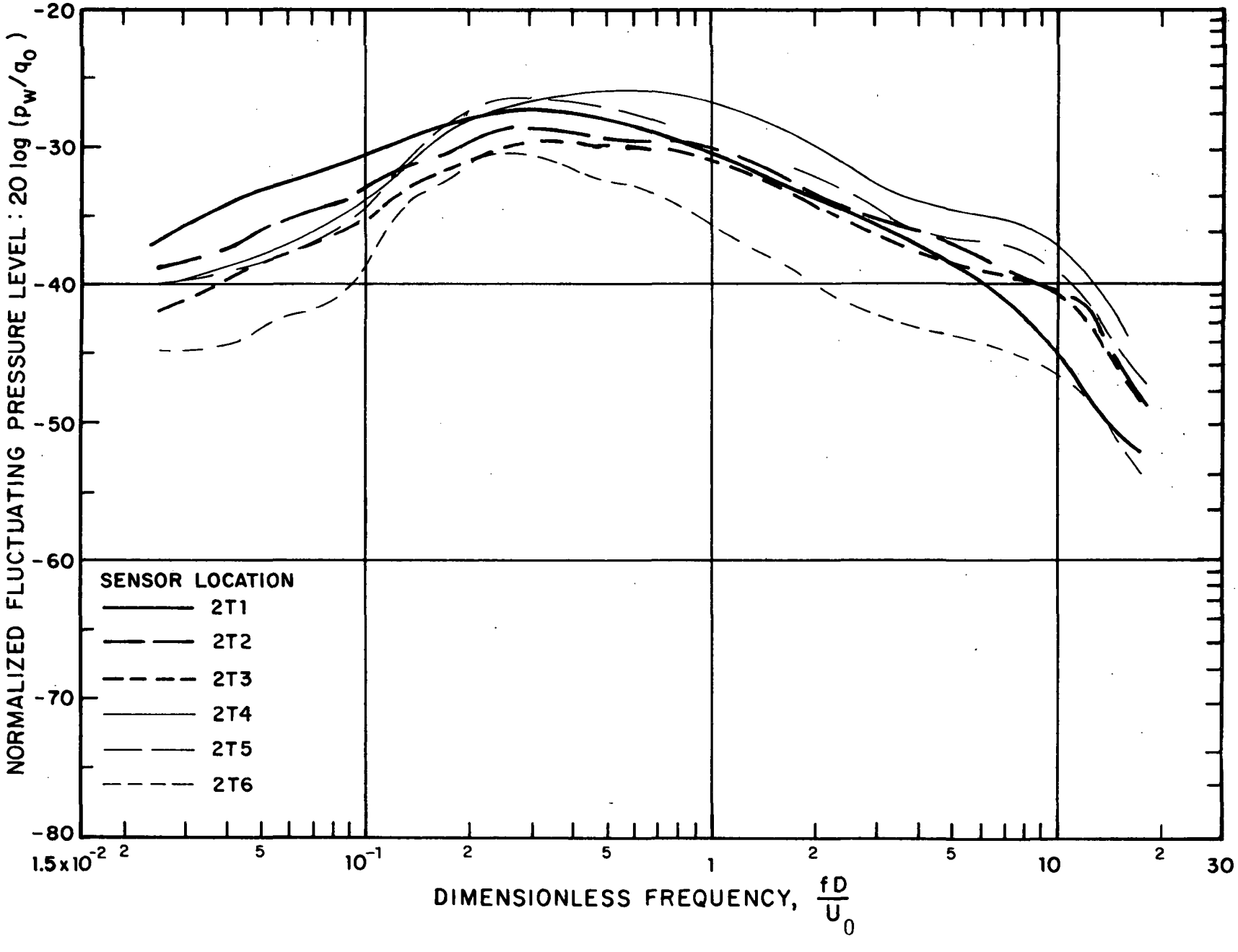

FIG. B.6. NORMALIZED "POINT" PRESSURE SPECTRA ON LOWER SURFACE OF SECOND FLAP TAKEOFF SETTING.

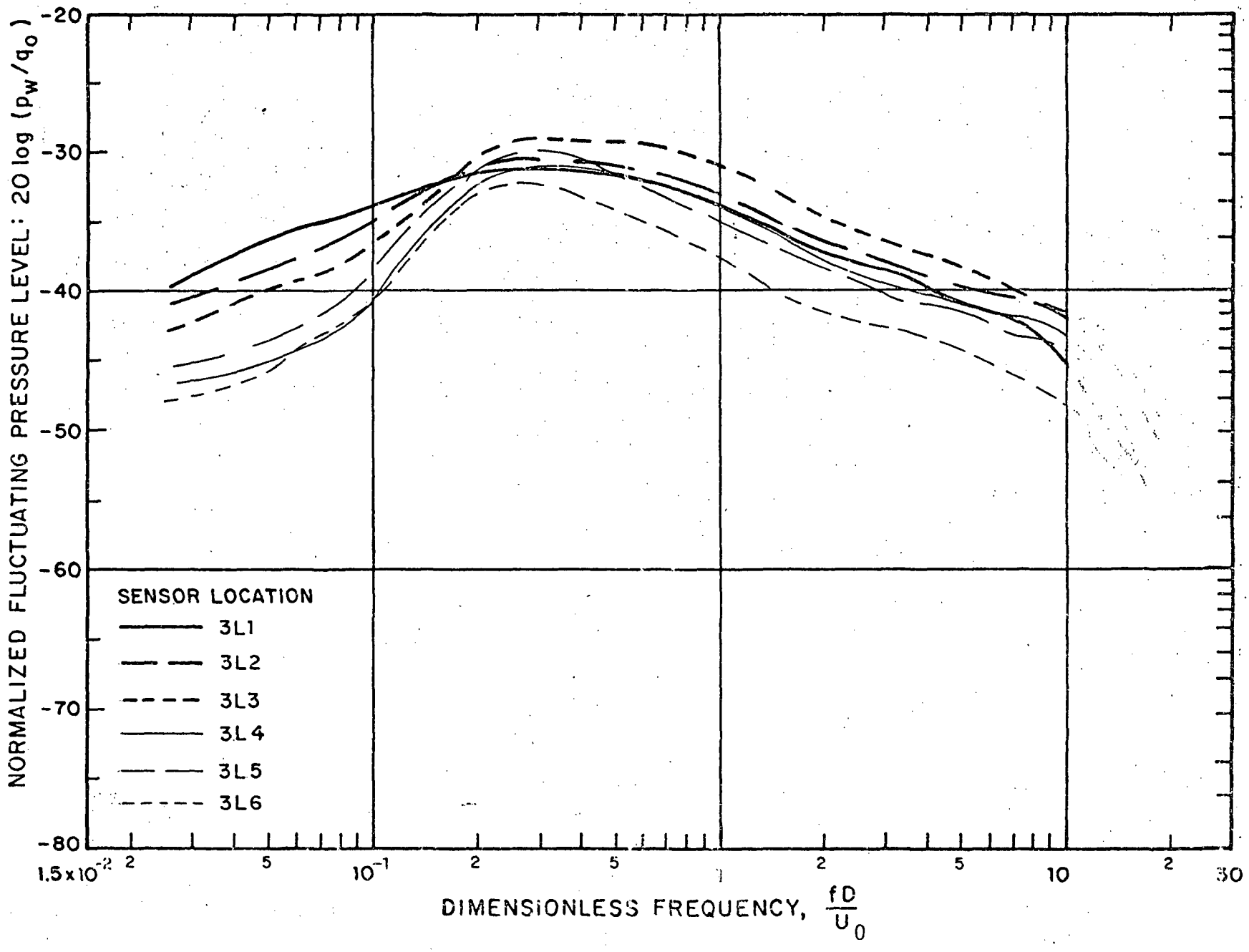

FIG. B.7. NORMALIZED "POINT" PRESSURE SPECTRA ON LOWER SURFACE OF THIRD FLAP TAKEOFF SETTING.

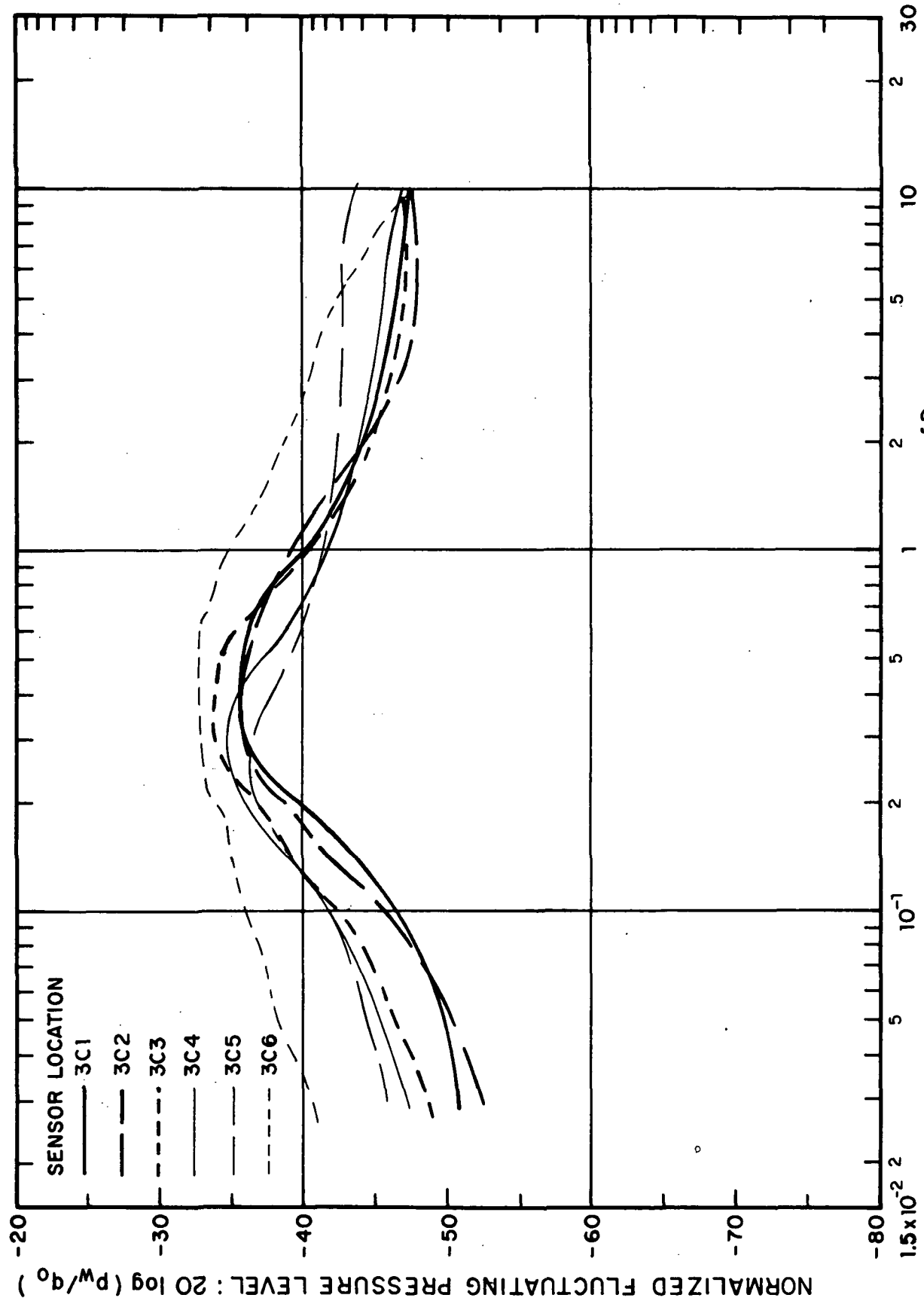

FIG. B.8. NORMALIZED "POINT" PRESSURE SPECTRA ON LOWER SURFACE OF THIRD FLAP TAKEOFF SETTING.

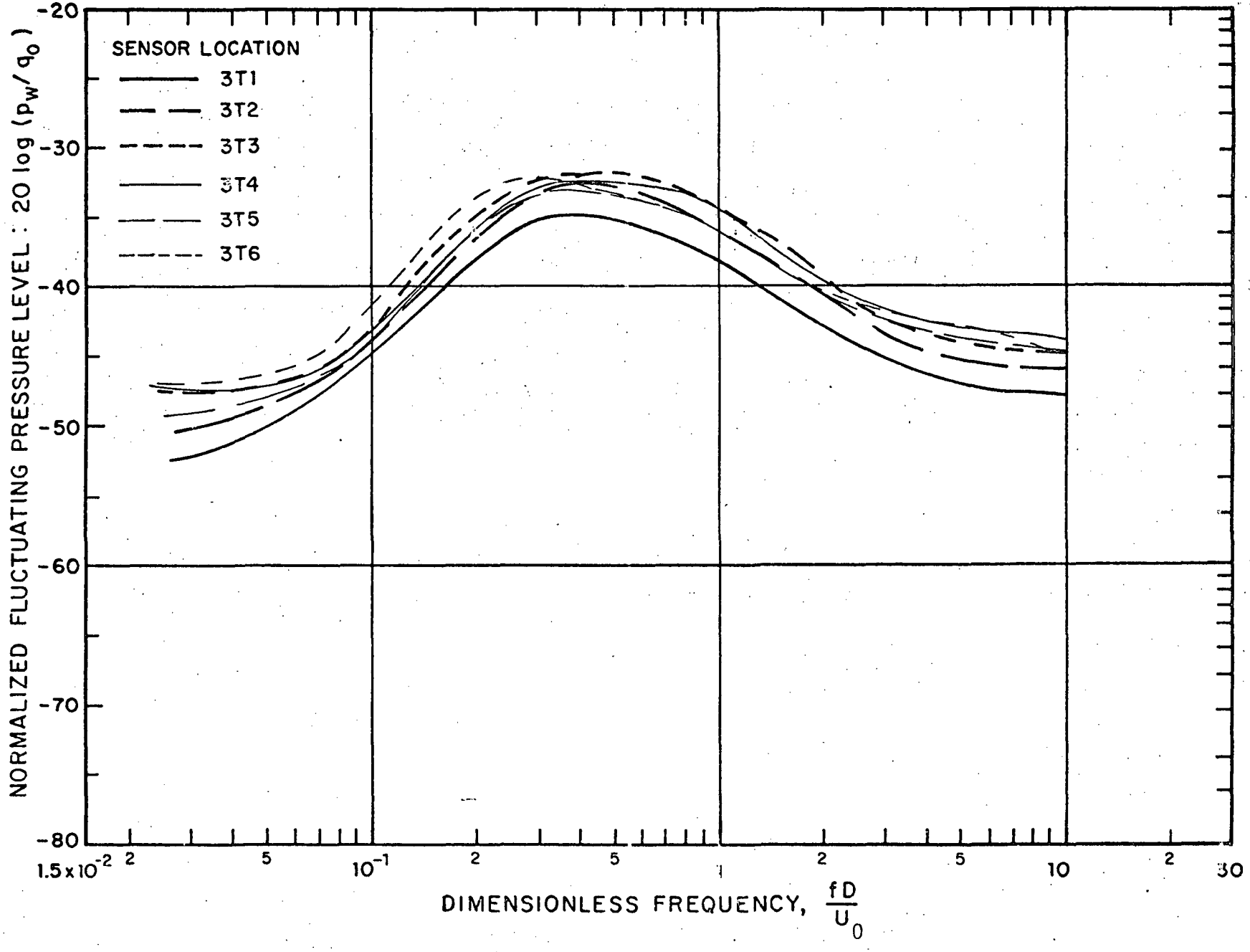

FIG. B.9. NORMALIZED "POINT" PRESSURE SPECTRA ON LOWER SURFACE OF THIRD FLAP TAKEOFF SETTING.

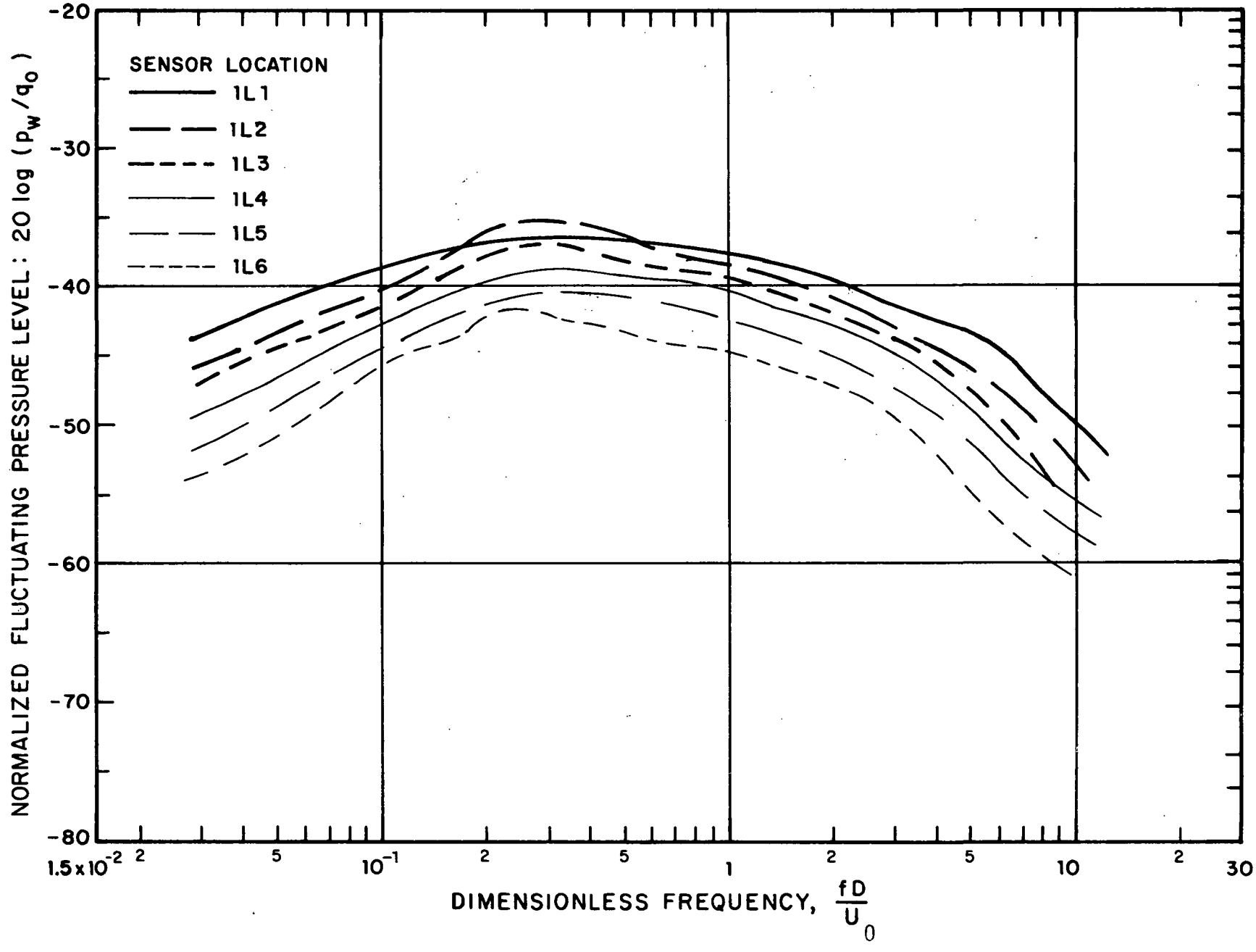

FIG. B.10. NORMALIZED "POINT" PRESSURE SPECTRA ON LOWER SURFACE OF FIRST FLAP APPROACH SETTING.

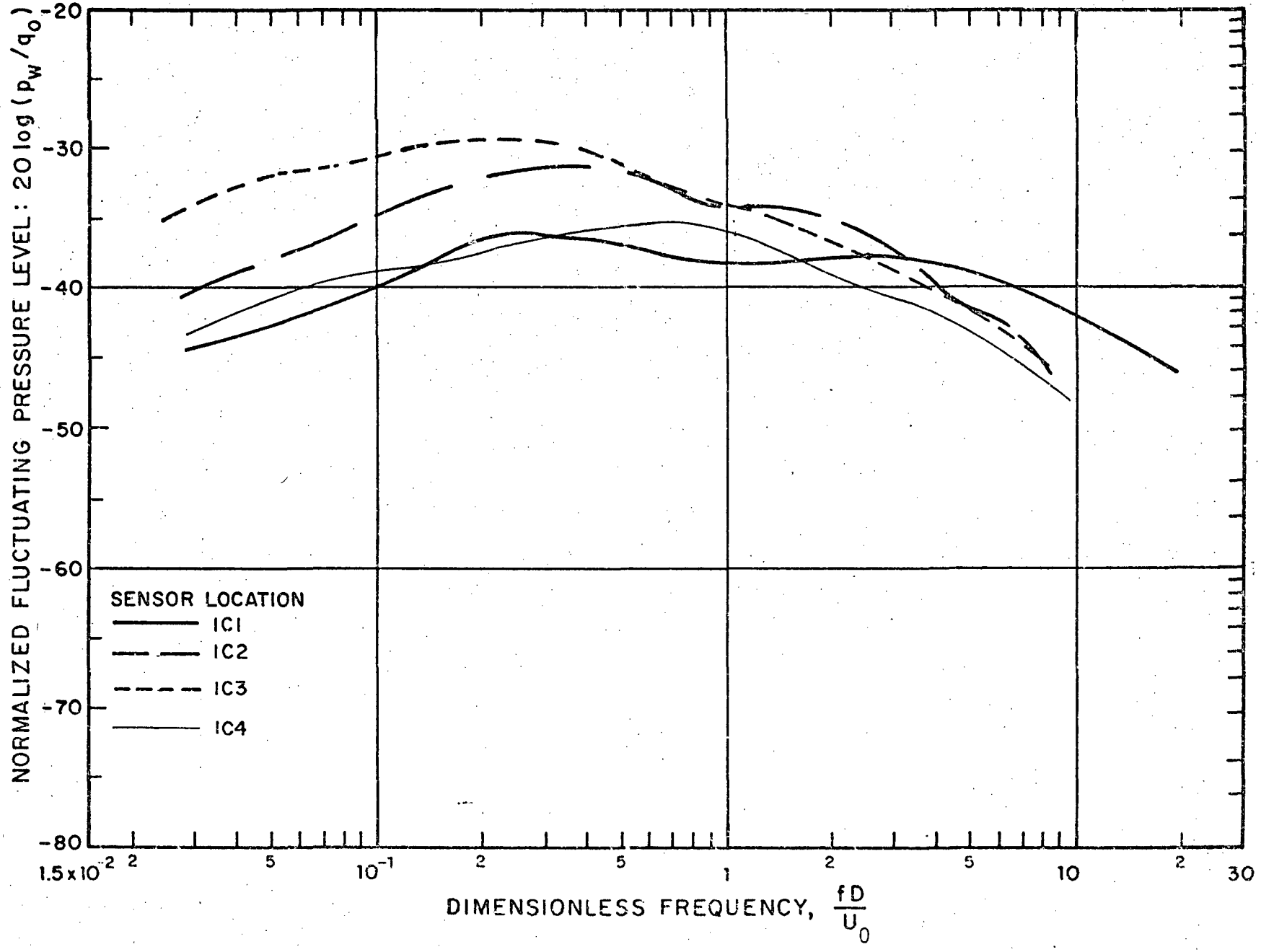

FIG. B.11. NORMALIZED "POINT" PRESSURE SPECTRA ON LOWER SURFACE OF FIRST FLAP APPROACH SETTING.

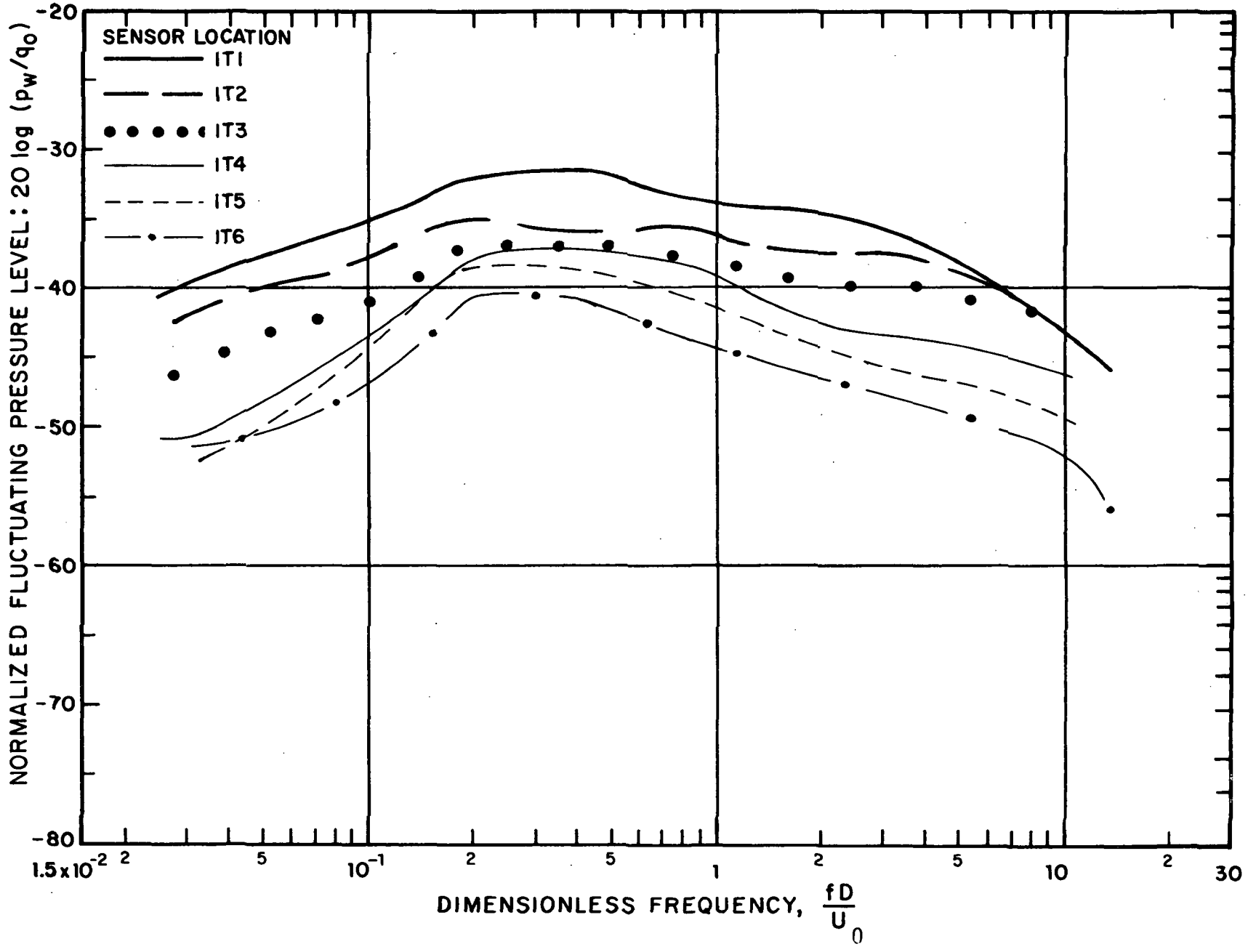

FIG. B.12. NORMALIZED "POINT" PRESSURE SPECTRA ON LOWER SURFACE OF FIRST FLAP APPROACH SETTING.

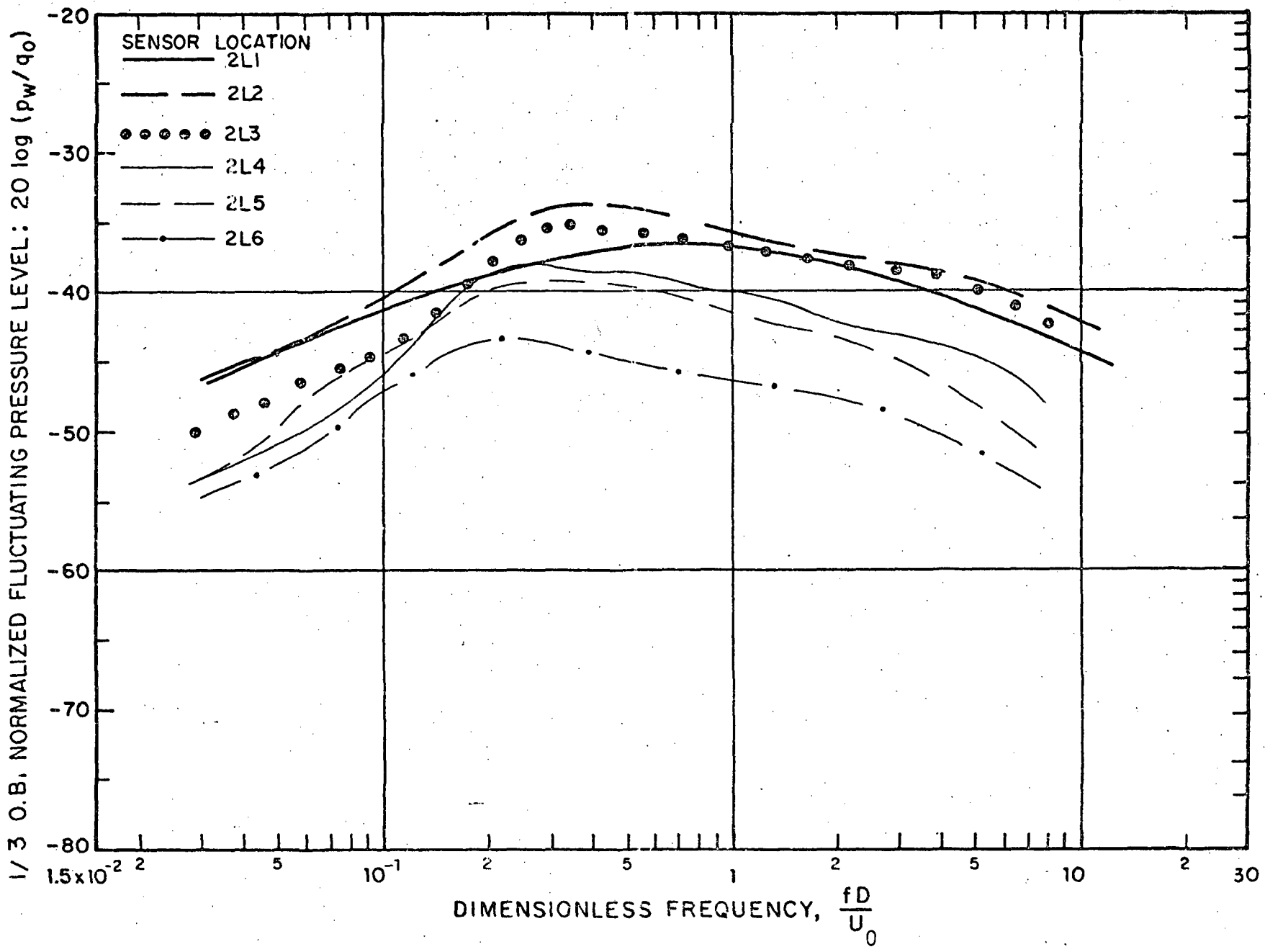

FIG. B.13. NORMALIZED "POINT" PRESSURE SPECTRA ON LOWER SURFACE OF SECOND FLAP APPROACH SETTING.

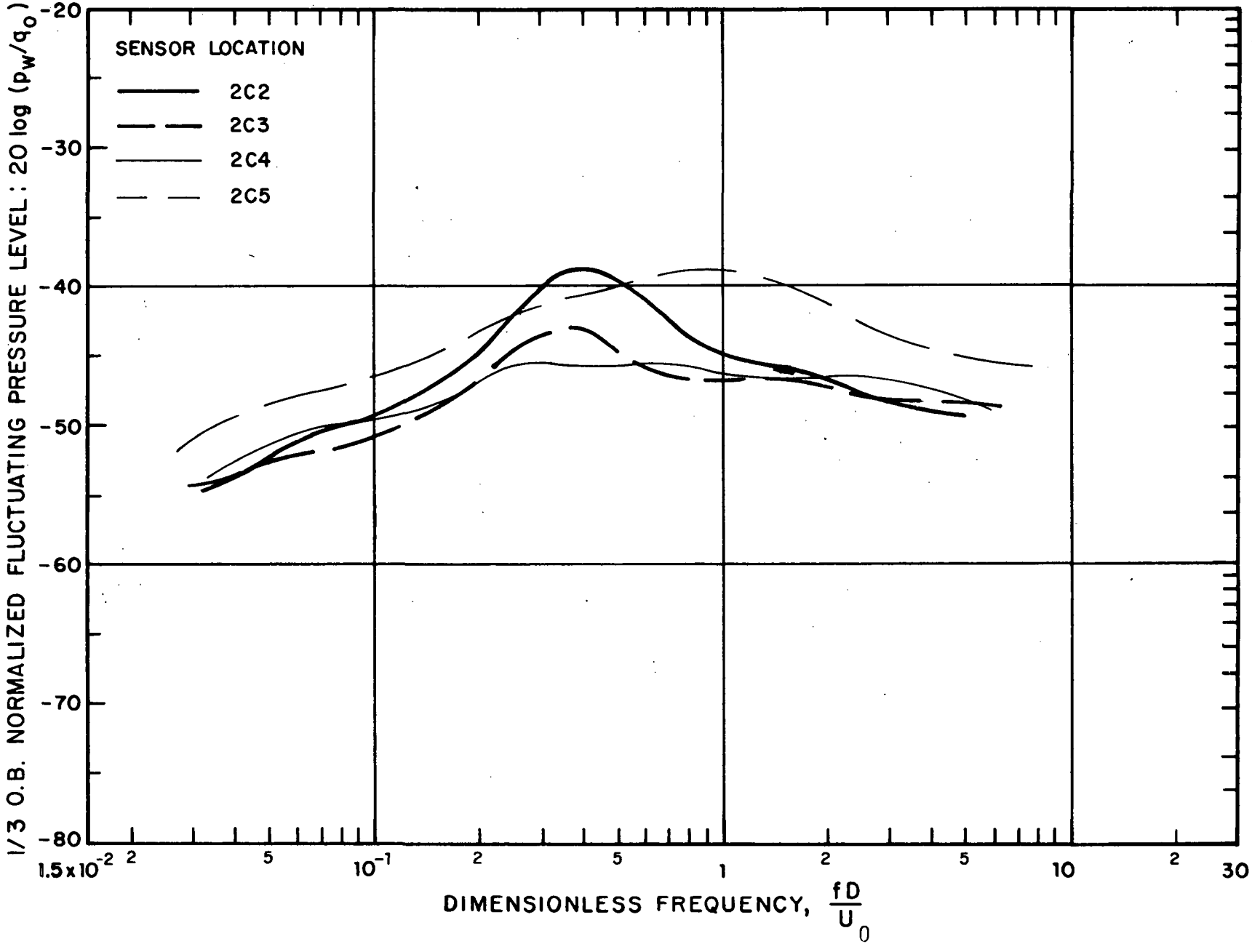

FIG. B.14. NORMALIZED "POINT" PRESSURE SPECTRA ON LOWER SURFACE OF SECOND FLAP APPROACH SETTING.

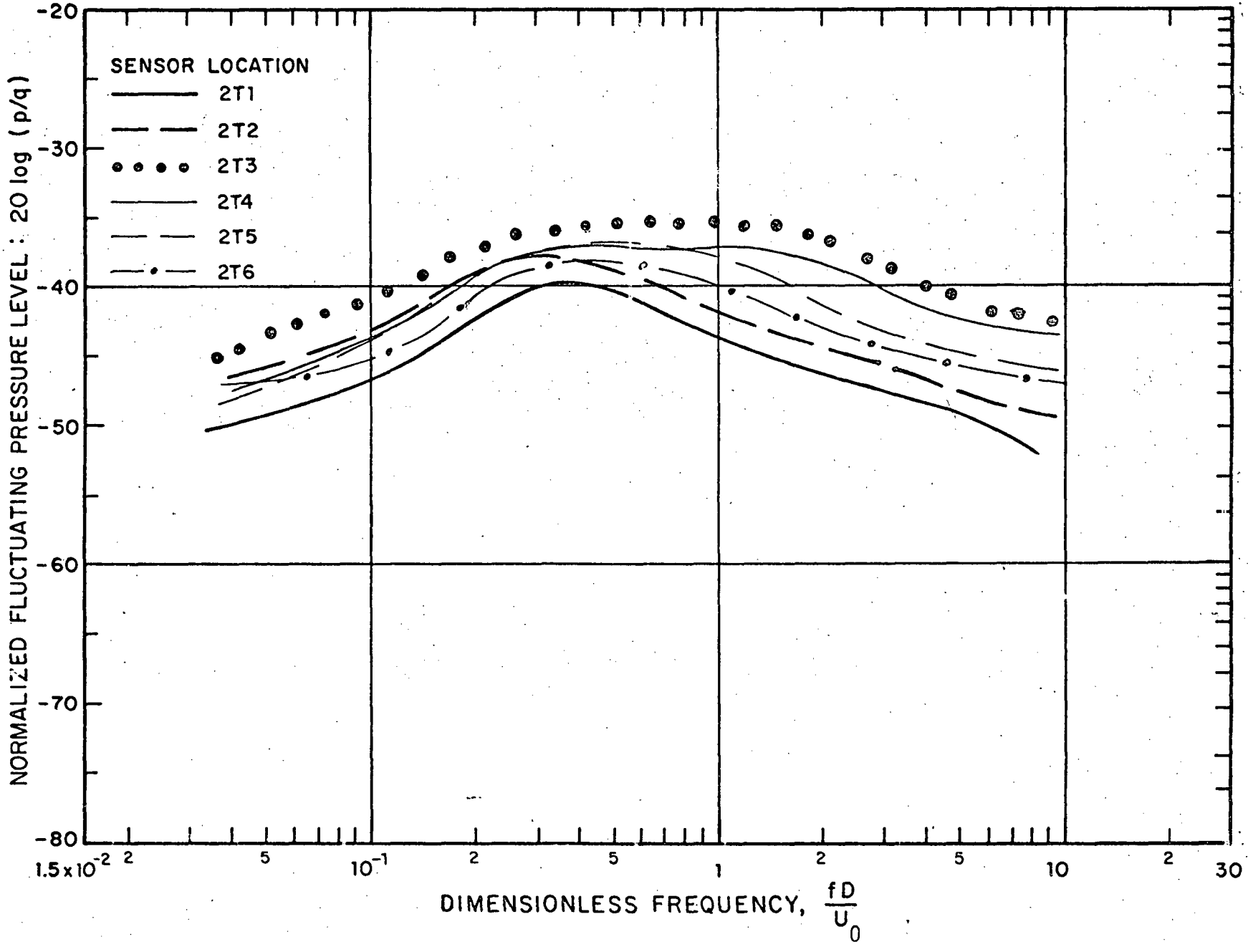

FIG. B.15. NORMALIZED "POINT" PRESSURE SPECTRA ON LOWER SURFACE OF SECOND FLAP APPROACH SETTING.

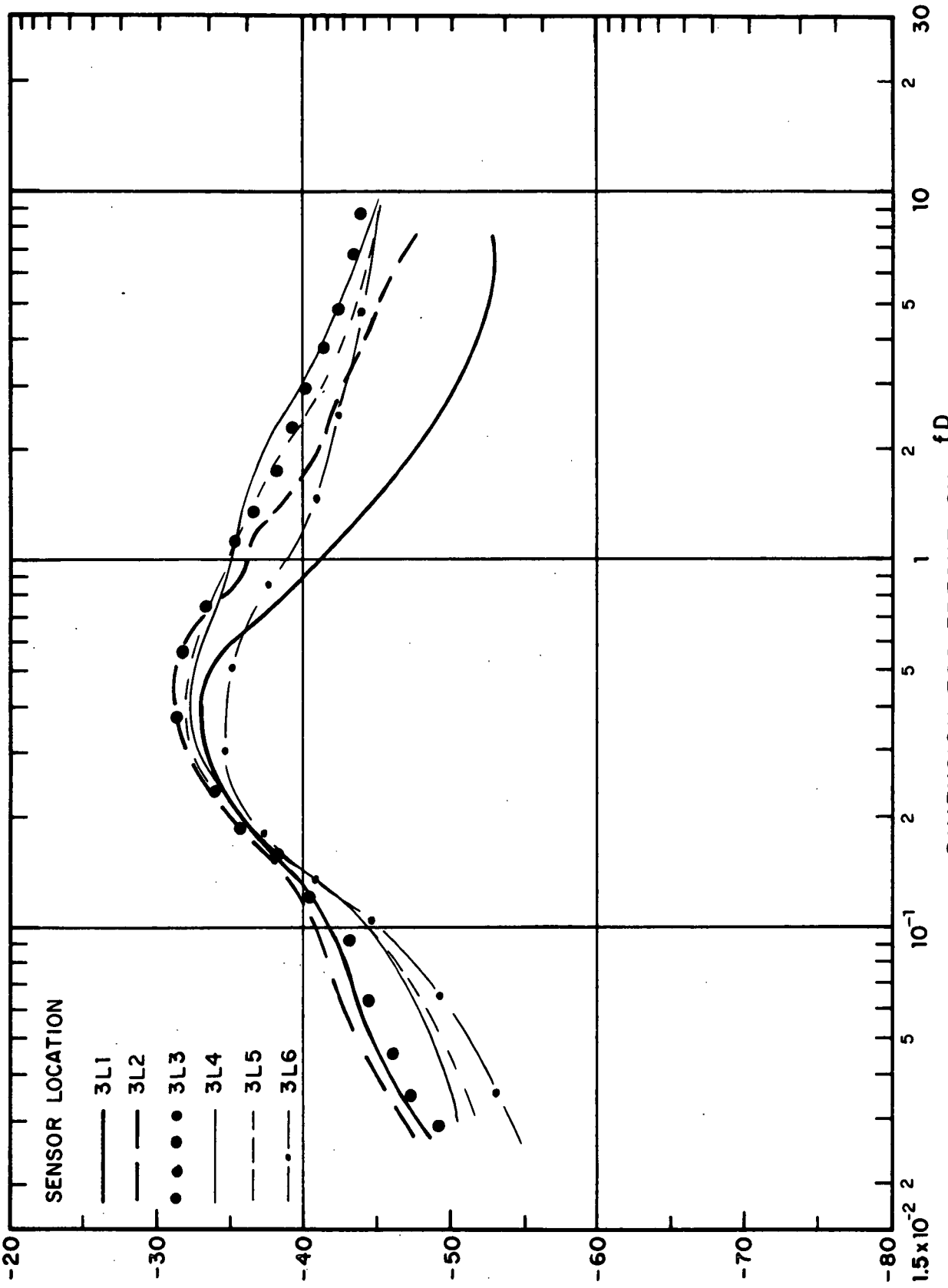

FIG. B.16. NORMALIZED "POINT" PRESSURE SPECTRA ON LOWER SURFACE OF THIRD FLAP APPROACH SETTING.

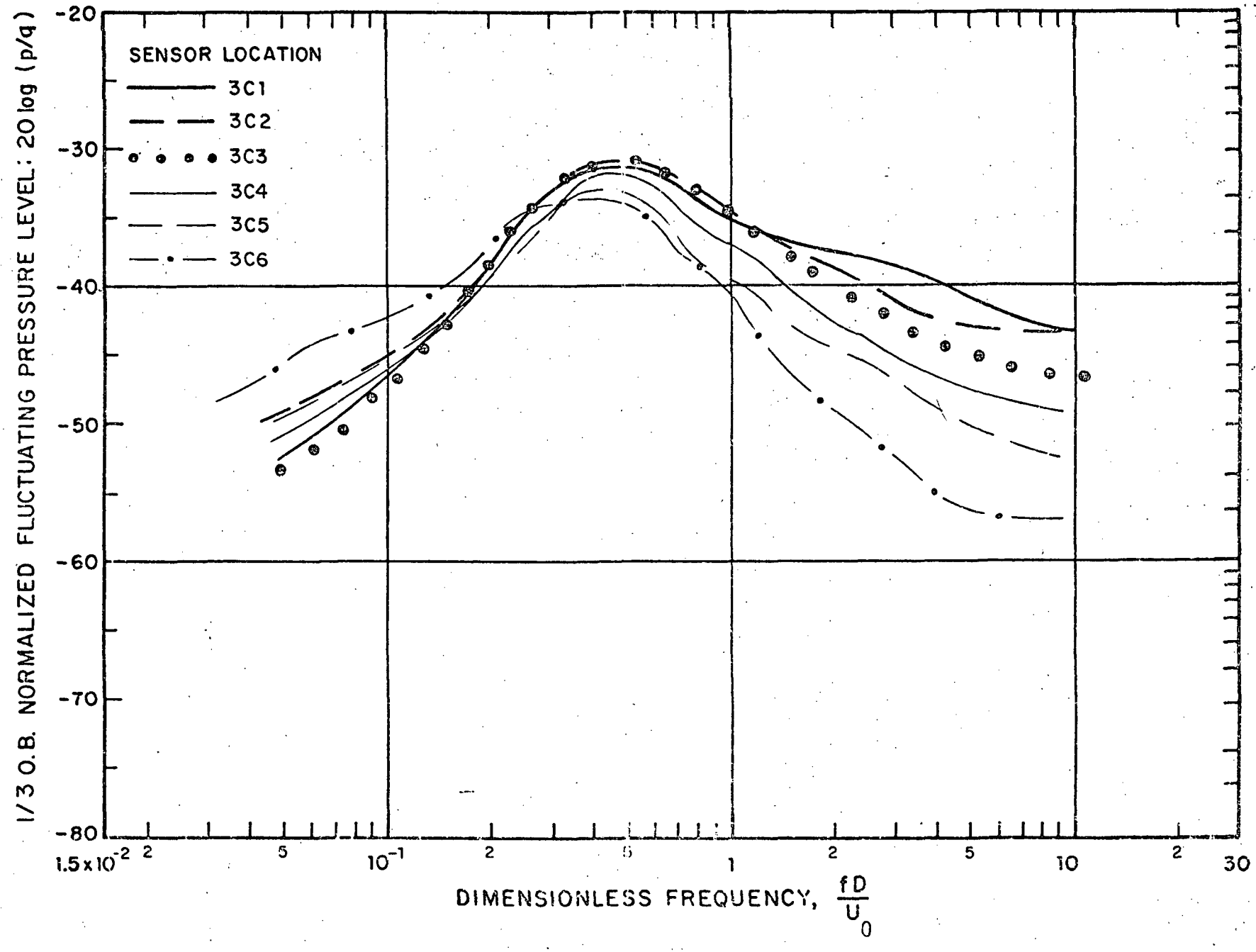

FIG. B.17. NORMALIZED "POINT" PRESSURE SPECTRA ON LOWER SURFACE OF THIRD FLAP APPROACH SETTING.

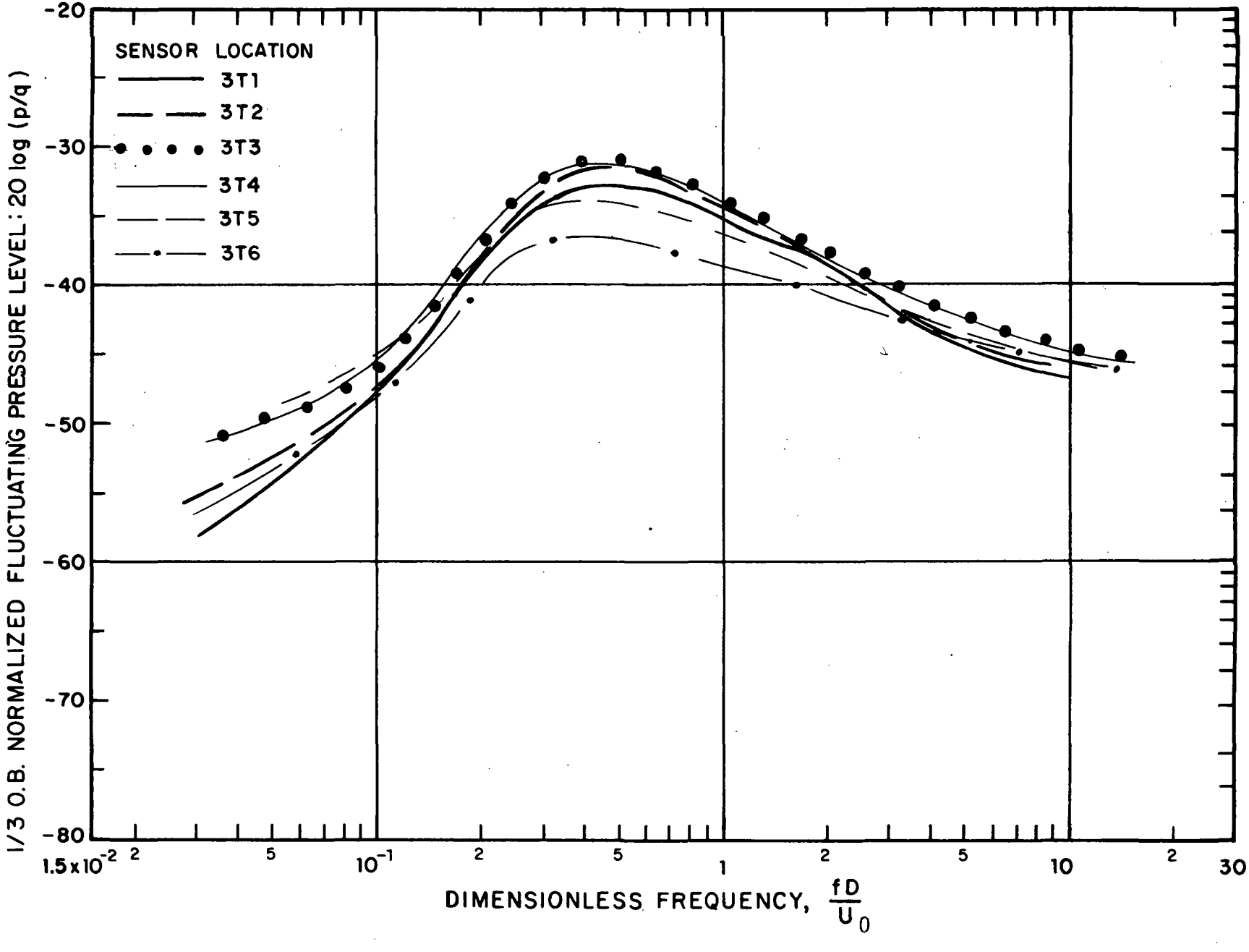

FIG. B.18. NORMALIZED "POINT" PRESSURE SPECTRA ON LOWER SURFACE OF THIRD FLAP APPROACH SETTING.